Protein Interactions With Model Phospholipid Monolayers

At The Air-Liquid Interface

Kevin Maurice Maloney

B.S. Chemistry, Worcester Polytechnic Institute, 1990

A dissertation submitted to the faculty of the

Oregon Graduate Institute of Science & Technology

in partial fulfillment of the

requirements for the degree

Doctor of Philosophy

in

Chemistry

January 1995

The dissertation "Protein Interactions with Model Phospholipid Monolayers at the Air-Liquid Interace" by Kevin M. Maloney has been examined and approved by the following Examination Committee:

David W. Grainger
Associate Professor, Colorado State University
Thesis Advisor

Jo-Ann Sanders Loehr
Professor, Oregon Graduate Institute of Science & Technology

Stephen B. Hall
Oregon Health Sciences University

Viola Vogel
Assistant Professor, University of Washington

ACKNOWLEDGMENTS

DEDICATION

In memory of Karen Janice Maloney

TABLE OF CONTENTS

LIST OF TABLES

LIST OF FIGURES

ABSTRACT

Protein Interactions With Model Phospholipid Monolayers at the Air-Liquid Interface

Kevin M. Maloney, Ph.D.
Supervising Professor: Dr. David W. Grainger

Molecular recognition of chemistry at organized interfaces often leads to interfacial self-assembly. Because many have evolved natural functions for membrane recognition, proteins are logical components to probe both interfacial reactivity and the self-organization of large molecules. In this study, phospholipase A_2 (PLA_2) and lung surfactant have been investigated with physical methods to determine the influence of interfacial properties on protein self-assembly and membrane organization. Biomembrane models at the air-water interface were used to alter the interfacial chemistry responsible for organization. Protein-membrane interactions were analyzed using monolayer film balance techniques and fluorescence microscopy at the air-water interface. Results show that macromolecules such as biopolymers will form large two-dimensional aggregates under conditions which favor specific protein binding and assembly.

PLA$_2$ was observed to form large two-dimensional domains during phospholipid hydrolysis. PLA_2-catalyzed phospholipid hydrolysis produces lyso-lipid and free fatty acid reaction products. PLA_2 self-assembly in model lipid monolayer systems results from interfacial fatty acid reaction product lateral phase separation. PLA_2 self-assembly occurred only under conditions where fatty acid phase separation was observed: the presence of Ca^{2+} and alkaline pH. PLA_2 self-assembly was mimicked using a water-soluble cationic dye as a protein analog. Results from mimicry studies indicate that, in addition to phase-separated fatty acids, chiral lipids also play an important role in determining self-assembled protein structural morphology.

Lung surfactant monolayers comprising mixed lipids and peptides were also investigated to determine structure-function relationships between lipids and membrane-resident, hydrophobic surfactant protein. Lung surfactant extract and purified subfraction monolayers were prepared to determine the effects of individual surfactant components on

interfacial lung surfactant structure. Lung surfactant monolayer microstructure is sensitive to the presence of proteins and cholesterol-based lipids. These results suggest that protein and cholesterol-based lipid contents in lung surfactant affect the lateral organization of the major lipid components in lung surfactant, 1,2-dipalmitoylphosphatidylcholine and 1-palmitoyl,2-myristoylphosphatidylcholine.

CHAPTER ONE

INTRODUCTION

1.1 Control of Protein Assembly and Interfacial Response

Principles for tailoring molecular recognition architecture to promote specific intermolecular interactions, host-guest complexation, and organized multimolecular structures are recognized as valuable tools to build sophisticated new materials. Molecular recognition and self-assembly is the basis for the formation of supramolecular species. While solution-phase supramolecular chemistries comprise a significant portion of supramolecular research, it appears that most investigations concerning molecular recognition and molecular self-assembly are focused on interfaces. Moreover, molecular recognition at interfaces leading to biomolecular self-organization is receiving great attention.

By controlling surface chemistry through selective molecular self-organization, tailoring of specific interfacial protein docking events leading to self-assembly of heterogeneous, highly organized protein structures is possible (Table 1.1). The technological ramifications of controlled biomolecular docking and organization become apparent when considering biotechnologies such as sensors [1], alternative energy sources, bioreactors, increased protein biostability, and molecular electronic devices [2]. Many of these biotech applications require the use of immobilized enzymes [3], membrane-based structures [1], and combinations of these architectures for device function. Therefore, a thorough understanding of the forces involved in biomolecular self-organization via natural or engineered receptors is crucial to the development of complex, highly organized biomolecular arrays.

A futuristic application based on highly organized protein assemblies is exemplified by the "biochip" [4], a three-dimensional (3-D) analog of the current solid-state, integrated electronic device. The biochip is foreseen to consist of a 3-D array of highly organized electron transporting proteins. McAlear and Wehrung [4] forecast biochips

1

being 10,000 times more powerful than current two-dimensional (2-D) integrated circuits because of the biochip's extra (third) dimension. Clearly, if such a device is ever to be constructed, a heterogeneous array of electron transporting proteins will have to be positioned on a nanometer scale in specific spatial orientations in volumes probably exceeding a (micrometer)^3. With precise control over intermolecular interactions (natural *and* engineered), self-assembly may be a viable route to the organization of structures such as the biochip. Currently, however, fabrication technologies and heterogeneous self-assembling motifs for proteins on 3-D scales are unavailable. To simplify this situation, and more importantly, to build a foundation for future molecular self-organization techniques by controlling interfacial chemistries, biomolecular self-assembly in systems of lower dimensionality (2-D) have been actively investigated [5-10]. Optimization of protein docking to 2-D architectures may provide the methods upon which a foundation for future 3-D heterogeneous synthetic molecular architectures can be built.

So-called 2-D molecular systems are exemplified by membrane-forming structures. Membrane architectures are self-organizing and provide a physical and chemical basis for additional self-assembling events occurring at the membrane-solvent interface. By controlling the physical and chemical nature of self-assembling membranes, subsequent biomolecular docking interactions at the membrane interface can be tailored [5,6]. Several proteins have been successfully docked and immobilized on membrane surfaces, showing that 2-D protein organization and crystallization (often with different crystal structures compared to previously determined 3-D structures) is possible. Until 1992, close to thirty proteins were successfully crystallized in two dimensions (see ref. 11 for a review). Proteins that have been successfully crystallized in 2-D using monolayer-coated and pure liquid interfaces are listed in Table 1.1.

From Table 1.1, an interesting point is worth noting. Large, water-soluble proteins such as ferritin have been crystallized at Hg-air interfaces without a specific interfacial protein receptor. In these cases, the high interfacial tension of the Hg-air interface is believed to play an important role in 2-D crystallization (through capillary forces acting on the protein during film formation). However, in these cases protein crystallization only seems to work with large, globular proteins. Non-globular, highly asymmetric proteins have not been successfully crystallized using the Hg-air interface. Employing lipid monolayers resolves this problem. It appears that rationally designed monolayer interfaces are the best route for 2-D protein self-assembly.

Table 1.1 Examples of Two-Dimensionally Crystallized, Water-Soluble Proteins at the Air-Water Interface

Protein	Interfacial Ligand Receptor	Reference
Annexin IV	DMPE^a	[12]
Annexin VI	DMPE^a	[13]
α-toxin	Platelet membrane	[14]
Cholera Toxin^b	GM1^c	[15]
Catalase	PBLH^d	[16]
DNA Gyrase B-subunit	Novobiocin	[17]
F1-ATPase	Hg^e	[18]
Ferritin	Hg^e,PBLH^d	[18,19]
Flagellar L-P ring	Hg^e	[20]
IgG/IgE (anti-DNP)	DNP-PE^f	[21,22]
IgG (anti-fluorescein)	FITC-PE^g	[23]
RNA Polymerase II (Yeast)	Stearylamine	[24]
RNA Polymerase II (mutant)	Stearylamine	[25]
Ribonucleotide Reductase^h	dATP^i	[26]
Streptavidin	Biotin^j	[27]
Tetanus toxin	GT1^k	[28]

^{a}Dimyristoylphosphatidylcholine monolayer. ^{b}B subunit of cholera toxin. ^{c}Ganglioside GM1 monolayer receptor. ^{d}Protein crystallized on poly(1-benzyl-L-histidine) monolayers. ^{e}Protein crystallized at the Hg-air interface. ^{f}N-dinitrophenylphosphatidylcholine monolayer receptor. ^{g}Fluorescein-conjugated phosphatidylethanolamine. ^{h}B1 subunit from *E.Coli.* ^{i}dATP-aminocaproyl-phosphatidylethanolamine monolayer ligand. ^{j}Biotinylated phosphatidylethanolamine monolayer receptor. ^{k}Ganglioside GT1 monolayer receptor.

As a means to molecular self-organization, Langmuir-Blodgett film fabrication techniques and molecular self-assembly provide the means of controlling interfacial chemistries and docking processes occurring at the membrane interface.

1.2 Interfacial Molecular Recognition and Self-Organization

1.2.1 Langmuir-Blodgett Film Fabrication from Spread Monolayers at the Gas-Liquid Interface

Monolayers of amphiphilic molecules at the air-liquid interface are the structural building blocks for Langmuir-Blodgett (L-B) film fabrication. A lipid monolayer at the air-liquid interface is schematically depicted in Fig. 1.1.

As shown in Fig. 1.1, the floating film consists of amphiphilic lipid molecules organized at the air-liquid interface where hydrophobic "tails" exposed to the air phase and water-soluble "headgroups" anchored to the aqueous "subphase" characterize the monomolecular assembly [29]. Hundreds of biological and synthetic surfactants have been investigated in terms of their tendencies to form monolayers [30] and L-B films [7,10].
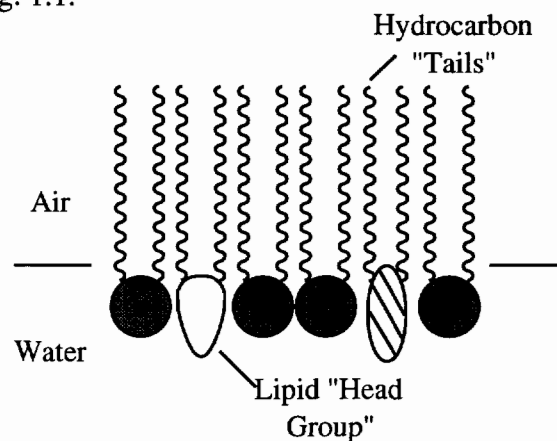
Fig. 1.1 Multi-component lipid monolayer at the gas-liquid interface.

Using protein receptor-doped lipid monolayers at the air-liquid interface, molecular recognition events leading to protein docking can be studied in both mono- and multi-layered systems. Phospholipase [31,32], protein kinase C [33], cholera toxin [33], streptavidin [34], and antibody-lipid [35,36] interactions are examples of protein-lipid systems that have been studied using model monolayer membranes at the air-liquid interface (see also Table 1.1).

Since lipid monolayer headgroups and ligand receptors are exposed to an aqueous environment, effects of ionic strength, pH, and subphase solute content on monolayer membrane physical properties and biomolecular docking events are accessible experimental parameters. Lipid packing densities in monolayers comprise an important physical

property that is also subject to facile control. This is especially important in instances where membrane-soluble protein regions penetrate the lipid membrane matrix.

1.2.1.1 Monolayer physical state determination

Knowledge of monolayer physical states is critical for a complete understanding of processes occurring at the aqueous-membrane interface. Prior to the application of direct monolayer imaging techniques, monolayer phase behavior was inferred from the monolayer compression isotherm. Compression isotherms are plots of monolayer lateral surface pressure versus film density at constant temperature. Similar to 3-D systems, discontinuities in compression isotherms are often indicative of phase changes.

Monolayers can exhibit solid, liquid, and gas analogous phases (Fig. 1.2). Isotherms that display high compression moduli are considered liquid-like, and regions of low compressibility are considered condensed. Regions of monolayer compression isotherms that display nearly horizontal slopes indicate the coexistence of two monolayer phases, suggesting a first-order lipid phase transition [37-39]. Comparison of monolayer phase behavior to that of lipid bilayer membranes has been frequently reported. Although a direct comparison is difficult to assess, it is generally believed that monolayers under a surface pressure in the range of 30-40 mN m^{-1} closely resemble the packing environment of lipid bilayers [38].

Fig. 1.2 Generalized compression isotherm for a monolayer at the gas-liquid interface depicting condensed (C), liquid (L), gaseous (G), and coexisting (C-S and L-G) monolayer states.

1.2.1.2 Characterization of monolayers spread on liquid interfaces

Though much information on monolayer physical states can be inferred from compression isotherms, more direct methods are available to determine phase behavior. Epifluorescence microscopy has been adapted to air-water interfaces [37,40,41], allowing

the direct visualization of the monolayer membrane physical states on the micrometer scale. Many monolayer physical states, as inferred from the isotherms, have been directly detected and confirmed using fluorescence microscopy. Fluorescence microscopy can also be used to study protein docking to monolayer membranes by employing multiple, spectrally distinct fluorescent labels [42-44].

In the 1930's, Langmuir and Blodgett [45] found that spread monolayers of surface-active materials at the gas-liquid interface could be transferred intact to solid substrates. Monolayers of proteins [46], lipids [7,10,29,45], polymers [7,10,29,45] and combinations of these classes of compounds have been successfully transferred as organized films from the air-liquid interface to a multitude of solid supports.
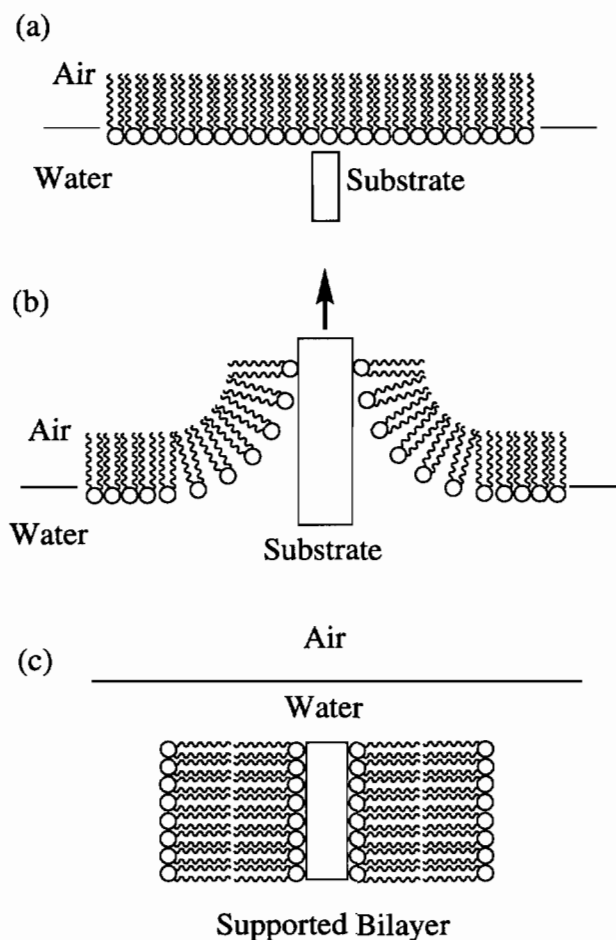
Fig. 1.3 Langmuir-Blodgett film formation. (a) Monolayer at the air-water interface with hydrophilic substrate in subphase. (b) First film deposition. (c) Second deposition, resulting in a supported bilayer.

Common hydrophilic solid supports include mica sheets, glass and quartz slides. These substrates are easily hydrophobized through silanization and have been used as frequently as their hydrophilic counterparts. Lipids are often used for L-B film preparation since most lipids form stable monolayers at the air-liquid interface.

L-B film deposition is schematically depicted in Fig. 1.3. Starting in the aqueous subphase (Fig. 1.3a), a hydrophilic solid substrate is slowly withdrawn (Fig. 1.3b) towards the air phase, resulting in the deposition of a monolayer from the interface, and rendering the substrate hydrophobic. Dipping the monolayer-coated, hydrophobic substrate back into the subphase leads to transfer of another monolayer and the formation of a supported bilayer (Fig. 1.3c). In L-B film formation, hydrophobic substrates are commonly used and, in this instance, the first monolayer deposition occurs when the substrate is lowered from air, through the monolayer, and into the aqueous monolayer subphase.

With the L-B technique, it is possible to construct multi-layered assemblies of complex architectures. Multilayered assemblies consisting of different individual monolayers (e.g., first layer fatty acid, next layer phospholipid) or monolayers doped with photoactive receptors and immobilized enzymes (for biosensing) in the outermost L-B layer have been prepared (reviewed in refs. 7 and 10). The use of supported bilayers as biomembrane models has been extensively investigated for the study of lateral and rotational diffusion of lipids and antibody binding [35,36] confined to the outer supported bilayer leaflet.

Molecular order in L-B films extends over two dimensions. In the direction normal to the solid support interface, layer thicknesses are controlled to the sub-nanometer level. Molecular order within each layer, however, is less controllable. Intralayer physical defects (pinholes) and intralayer domains of different molecular orientational order (disclinations) are often observed.

1.2.2 Molecular Self-Assembly

An alternative route for forming ultrathin films and other highly organized membrane-based molecular architectures used for tailoring protein docking and organization is molecular self-assembly (SA) [5,6,10,47]. SA refers to the spontaneous organization of isotropically dispersed monomeric species to form a supramolecular aggregate. Self-assembled systems relevant to biomolecular organization include micelles,

vesicles, lamellar lipid architectures, and self-assembled monolayers. SA also refers to the specific recognition and binding of chemical species [6,47] to produce well-defined (physical) oligomeric species. The hydrophobic effect, van der Waals forces, hydrogen bonding, electrostatic effects, and covalent bonding (in the case of some SAMs) orchestrate the formation and morphology of self-assembled architectures [30,31,44,48,49]. It is immediately apparent that more diverse architectural morphologies are available through SA as compared to L-B films. Self-assembled structures offer a more diverse set of molecular "scaffolds" for promoting protein binding to their interfaces.
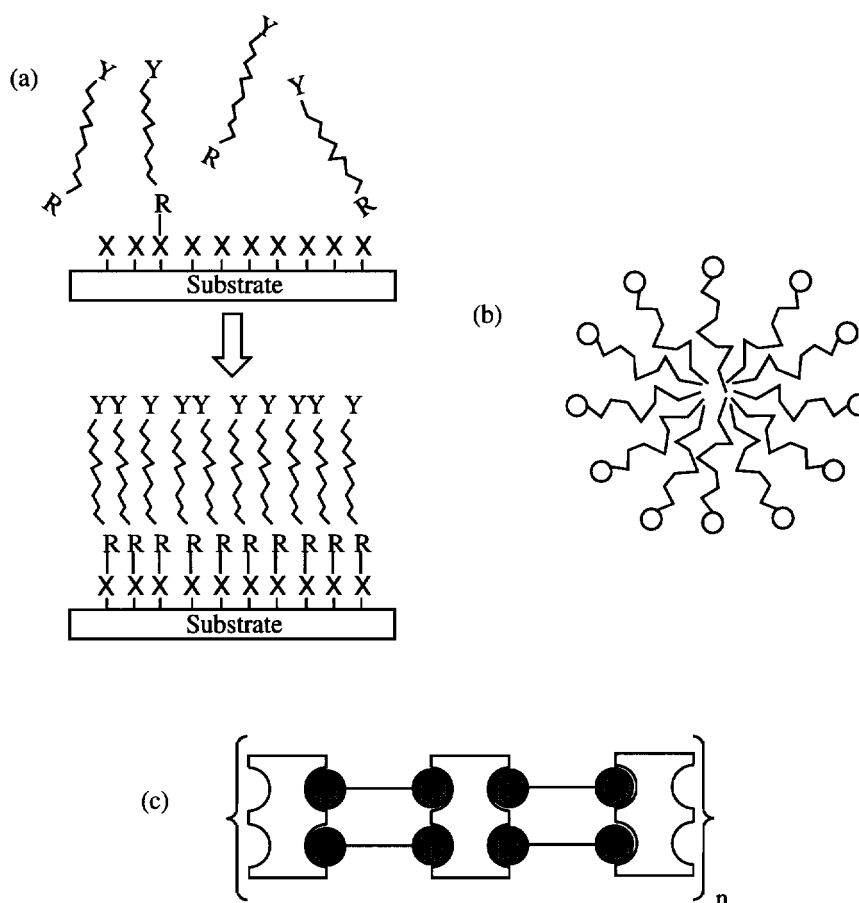
Fig. 1.4 Examples of self-assembled molecular structures. (a) SAMs, (b) micelles, and (c) schematic of biotin-mediated (shaded circles), cross-linked streptavidin.

Self-assembling membranes are conveniently described thermodynamically (see ref. 49), with the most useful criteria for self-assembly given by the critical micelle

concentration (cmc). Although micelles are certainly not the only self-assembled architectures available, the cmc denotes the concentration at which onset of aggregate formation occurs from isotropically dispersed monomers.

Israelachvili demonstrated [49] that the geometric shape of a surfactant species serves as a useful indicator of what types of self-assembled structures are accessible upon reaching the cmc. This is based primarily on geometric packing constraints of the self-assembling surfactants. Cone-shaped surfactants, for example, usually form micelles (Fig. 1.4b) while cylindrically-shaped surfactants are anticipated to form planar bilayers. Surfactants of intermediate shapes form cylindrical micelles, vesicles, and inverted phases. Transitions between these phases can occur through changes in temperature, ionic strength, pH, and water content.

Self-assembled monolayers (SAMs) (Fig. 1.4a) are another important class of self-assembled architectures that may find great utility in designing specific protein-surface interactions, leading to organized protein assemblies. SAMs are formed spontaneously through physical or chemical adsorption events at solid-liquid interfaces [10]. Some of the most commonly studied SAMs are thiol-derivitized organics that chemisorb to gold surfaces. As depicted in Fig. 1.4, bifunctional SAM-forming species can be used for further surface derivitization (i.e., protein receptor coupling to surfaces or other surface derivitization that promotes physical protein adsorption). Covalent immobilization of proteins to SAMs has been reported [50,51].

1.3   Comparison of L-B and SA Techniques

Tailoring the parameters governing protein docking at interfaces of SA or L-B structures offers many physical environments in which to bind and organize enzymes. Depending on what types of self-organizing structures are desired, each method has its advantages. Differences in L-B and SA systems are mainly due to protein accessibility to surface-bound receptors.

Lateral diffusion in L-B films is usually low ($<10^{-7}$ cm^2/sec), since the films are prepared in a condensed state. A drawback with the L-B technique is that, while monolayer diffusion can be precisely controlled, fluid-phase monolayer transfer to solid supports is normally difficult. This situation can be partially overcome by using monolayer diluents that enhance overall monolayer stability, including subphase soluble species that increase inter- and intralayer attractions, or by using modified L-B film techniques [52-55].

This does have some advantage when it comes to L-B film stability. L-B-based biosensing devices need to be robust for adequate device stability. Many L-B preparations are stable in ambient conditions for weeks. Vesicle preparation with lipids that do not easily form L-B structures is normally not a problem, with lipid and receptor diffusion being adjustable through variations in, for example, temperature, cholesterol (or other lipid diluent) content or through the use of polymerizable lipids. In cases where receptor diffusion, or receptor accessibility, prohibits effective protein docking, the use of receptors with water soluble "spacers" has been often used to increase receptor accessibility [56].

Physical protein characteristics, namely their inherent hydrophobicity or hydrophilicity, are also important. Hydrophobic protein incorporation into L-B films is difficult to achieve when protein dimensions exceed the thickness of individual monolayers. With SA structures, incorporation of hydrophobic proteins is also a problem in that protein reconstitution is a major technical difficulty. Since SA structures often consist of bilayer arrangements, asymmetric protein orientation upon reconstitution is another difficulty to overcome. In these cases, a single protein orientation is desired.

Hydrophilic protein interactions with L-B films and SA structures are more easily controlled. Since most proteins will adsorb to a surface and often lose their activity due to denaturation [57,58] and possess some degree of hydrophobic character, L-B films can be prepared to inhibit protein insertion. SA architectures are less easily designed to prohibit non-specific protein insertion.

The L-B method has the advantage in that precise control of the number and thickness of deposited layers is possible. Ultrathin film thickness can be controlled to the sub-nanometer level. Moreover, each layer within the multi-layered assembly can be of a different chemical composition. In terms of experimental variables (from the presence of dust to ambient humidity), great care must be taken during film fabrication. Impurities resulting from any stage in the L-B process can have deleterious effects on multi-layer structure and function. A disadvantage of L-B films preparation is that not all surfactants are amenable to mono- or multi-layer film fabrication.

1.4 Current State of the Art

As a display of the control of protein assembly possible with membrane systems, Ringsdorf and coworkers used protein receptor-doped vesicles, monolayers, and SAMs to model multiple protein binding events [59]. Employing membrane systems as building

blocks, streptavidin was self-assembled to the membrane surface using membrane-bound desthiobiotin receptors. Triple layers of streptavidin-Con A-streptavidin and streptavidin-Fab fragment-human chorionic gonadotropin protein assemblies were produced. The triple layers were assembled using biotin analog receptors that strongly bind streptavidin ($K_a \sim 10^{13}$ M^{-1}). Addition of underivitized biotin led to multilayer dissasembly, showing the process was reversible as long as biotin dervatives were used to assemble the matrix [biotin ($K_a \sim 10^{15}$ M^{-1}) binds streptavidin more strongly than desthiobiotin]. This study demonstrated the extent of interfacial protein self-organization possible using molecular recognition and self-assembled membrane systems. Given streptavidin's binding site topography (four biotin binding sites, two on each side of the protein) and the fact that streptavidin undergoes interfacial 2-D crystallization at biotin-doped membrane interfaces [6,34], this protein has been extensively used in molecular recognition studies pertaining to protein self-assembly in membrane model systems.

From the example above, the similarity of model L-B and SA membranes to natural biomembranes is apparent. Mimicking a biological cascade, multiple protein binding events at an artificial membrane interface is possible. The ability to mimic membrane-associated processes increases our understanding of the interactions necessary for interfacial biomolecular docking and may provide new synthetic routes for docking motifs applicable to biotechnologies. Since many water-soluble proteins are designed to interact specifically with membranes to elicit a biochemical response, it is only natural to investigate these proteins for they exhibit well-defined interactions with membranes. Understanding the biological membrane docking process may lead to the development of synthetic surfaces that display similar binding characteristics.

1.5 Protein-Monolayer Membrane Interactions: Tailoring Protein Docking and Self-Assembly

A protein-lipid system that responds to changes in interfacial chemistry resulting in the mediation of protein docking and self-assembly is phospholipase-mediated phospholipid hydrolysis. Calcium-dependent, secreted phospholipase A_2 (PLA_2) is a small enzyme ($M_r \approx 14,000$ for cobra venom source) that catalyzes the hydrolysis of the sn-2 acyl ester bond of L-α-sn-3-glycero phospholipids [31] (Fig. 1.5). Hydrolytic PLA_2 activity towards organized lipid structures (e.g., micelles, monolayers) is well known, exhibiting activity several orders of magnitude higher than isotropically dispersed monomer

lipid substrate [60], showing that PLA$_2$ activity is a sensitive indicator of lipid physical environment.
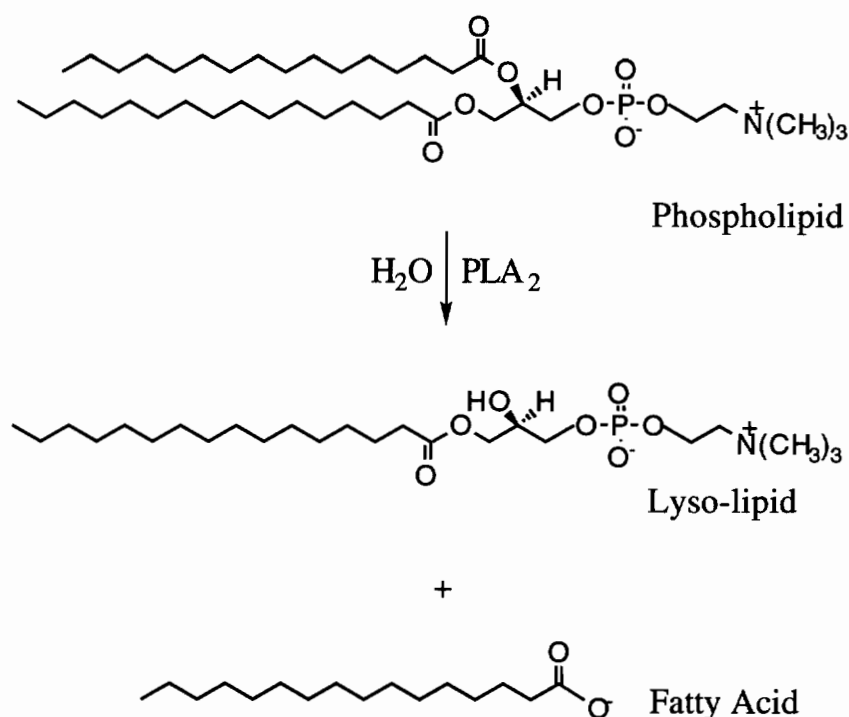
Fig. 1.5 PLA$_2$-catalyzed phospholipid hydrolysis.

PLA$_2$-mediated lipid hydrolysis in vesicles displays a unique property in that, following a slow period of initial activity, enzymatic hydrolysis goes through a burst phase where activity can increase several orders of magnitude [61]. Supporting an earlier suggestion [62] based on the fact that PLA$_2$ exhibited an increase in activity near the bilayer main transition temperature, Jain and coworkers discovered in the early 1980's that, during PLA$_2$-catalyzed lipid hydrolysis, a distinct change in bilayer membrane properties occurred after a critical extent of lipid hydrolysis [63,64]. This bilayer physical change resulted in a rapid increase in PLA$_2$ activity ("burst"), following the so-called "lag period". Several investigations have since probed this phenomenon. Using the water-soluble cationic NK-529 carbocyanine dye, Jain showed that, with ternary mixed lipid vesicles, quenching of dye fluorescence occurred during the lag phase [64]. Maximal NK-529 fluorescence quenching occured at the onset of the burst phase. Fluorescence quenching was believed to be due to dye aggregation at membrane regions consisting of laterally segregated fatty acid

reaction products. Previously, the onset of PLA$_2$'s burst in activity was also suggested by Apitz-Castro [65] to be correlated with a change in bilayer physical properties. These results were interpreted as anionic fatty acid reaction product aggregation within the outer bilayer leaflet. Biltonen and coworkers also showed evidence supporting this observation [66]. Biltonen used ternary mixed lipid vesicles of various compositions representing different extents of PLA$_2$ hydrolysis. With ternary mixed lipid vesicles of PC, lyso-lipid, and pyrene-labeled fatty acid (1-pyrenyldecanoic acid), pyrene excimer formation was studied as a function of reaction product composition. It was found that excimer formation consistently occurred when vesicles contained approximately 20% reaction products, corresponding to the end of the lag period and initiation of the enzymatic burst period. Clearly, PLA$_2$ hydrolysis of lipid vesicles is sensitive to physical membrane properties. The beginning of the burst phase indicates enhanced protein-vesicle binding which could be in response to the lateral phase separation of lipid hydrolysis reaction products (fatty acids). However, lateral phase separation of fatty acids cannot occur exclusively. Otherwise, PLA$_2$ would not have access to lipid substrates. Instead, regions of the membrane that are enriched in fatty acids, but still contain phospholipids, may more closely represent the physical state of the membrane at the beginning of the burst phase.

Enhanced pancreatic PLA$_2$ binding to negatively charged interfaces (either reaction products or negatively charged lipid substrates) is also well known [61], indicating that electrostatic as well as non-covalent molecular recognition events (substrate binding and substrate physical state) play an important role during enzymatic hydrolytic activity towards lipid assemblies.

PLA$_2$ hydrolysis of lipid monolayers also results in drastic membrane phase changes and altered protein-membrane interactions. Using fluorescence microscopy, Grainger and coworkers [42-44] found that, during lipid hydrolysis, PLA$_2$ spontaneously formed 2-D domains at the air-buffer interface. It was proposed that PLA$_2$ docking to the hydrolyzed membrane interface was in response to the presence of phase-separated fatty acid reaction products. Similarly observed in vesicle systems, this directly showed that PLA$_2$ interactions with substrate lipid and reaction products in monolayers are different. PLA$_2$ domain formation occurred during (but not after) hydrolysis, indicating that enzyme self-assembly was induced only after a critical amount of water-insoluble hydrolytic products were built up in the monolayer membrane. Extending this work, Reichert and coworkers examined ternary mixed model monolayers consisting of lipid substrate, lyso-lipid and fatty acid that represented PLA$_2$-hydrolyzed monolayers at various extents [67].

Reichert found that PLA$_2$ domain formation could be mimicked, and in some cases prohibited, using these ternary mixed monolayer systems [67].

In general, protein self-assembly at interfaces occurs in several steps starting with enzyme diffusion to the interface followed by binding, lateral organization, and possible crystallization. PLA$_2$-lipid monolayer systems exhibit these characteristics; a highly organized interface in which components can readily move or re-organize by lateral diffusion and an interfacially active protein that recognizes interfacial membrane chemistry. Understanding PLA$_2$'s interactions in monolayer systems will not only aid in elucidating the domain formation mechanism, but will also add to our current understanding of 2-D protein self-assembly.

1.6 Protein Control of Lipid Organization

PLA$_2$ self-assembly at lipid interfaces is in response to lipid lateral organization. The converse is also important: protein influence on lipid organization. With respect to protein effects on lipid organization (in addition to PLA$_2$ systems), pulmonary surfactant mixtures are also relevant model systems. Pulmonary surfactant is a complex mixture of phospholipids, water-soluble and hydrophobic surfactant proteins, as well as cholesterol-based lipids. Pulmonary surfactant functions to reduce the surface tension within the alveolar air-spaces to allow for proper lung inflation and deflation. Infants born prematurely lack pulmonary surfactant making breathing a serious problem. Hydrophobic protein is believed to facilitate adsorption of pulmonary surfactant at the buffer-air interface in the lungs. This suggests that the protein plays an important role in membrane structural organization. Investigation of monolayer membrane structure in the presence or absence of proteins and other pulmonary surfactant constituents may allow a more complete understanding of the function of the membrane-resident surfactant proteins.

The goal of this research is to probe and understand water-soluble and hydrophobic protein-monolayer membrane interactions and the requirements for protein self-assembly and lipid organization. PLA$_2$ spontaneously forms 2-D assemblies at interfaces, where initial enzyme binding is sensitive to lipid physical state and the docking process, and subsequent non-covalent interactions with reaction products can be tailored through carefully designed lipid substrates. Elucidation of the mechanism of PLA$_2$ domain formation is the chief objective of this research. This includes determining (1) the effect of lipid substrate on PLA$_2$ self-assembly, (2) how reaction products resulting from PLA$_2$ lipid

hydrolysis affect enzyme domain formation, (3) lipid and aqueous solute determinants of hydrolyzed monolayer phase behavior and their effect on enzyme domain formation, and (4) the ability to mimic enzyme domain formation using protein analogs. Hydrophobic protein effects on lipid lateral organization are also investigated using pulmonary surfactant mixtures as model systems. With pulmonary surfactant monolayers, the objective is to determine how the effects of proteins and neutral lipids on monolayer interfacial organization.

CHAPTER TWO

MATERIALS AND METHODS

This chapter outlines general methods and materials used in this research. When needed, more specific descriptions of experimental protocols appear in the respective chapters in which the data are discussed.

2.1 Materials

2.1.1 Proteins

Naja Naja Naja and bovine pancreatic PLA_2 (EC 3.1.1.4) were purchased from Sigma and used as received. Bee venom PLA_2 was obtained from Boehringer Mannheim. *N. naja naja* PLA_2 was also kindly purified and supplied by Prof. Michael Gelb, University of Washington. Results obtained with PLA_2 from Sigma or Prof. Gelb were identical. Bovine serum albumin (BSA, Sigma, <0.005% fatty acid content, globulin free) was used as received.

2.1.2 Chemical Reagents

NaCl (Chempure, >99.9%), $CaCl_2$ (Chempure, >99.9%), tris(hydroxymethyl)-aminomethane (Tris, Sigma, >99.9%), N-(2-hydroxyethyl)piperazine-N'-(2-ethane-sulfonic acid) (Hepes, U.S. Biochemical Corp., 100.9%), chloroform (Fisher, HPLC grade, 1% ethanol stabilized) and fluorescein isothiocyanate (Isomer 5, Sigma, FITC) were used as received. Water was Millipore treated, yielding resistivities greater than 18 MΩ cm^{-1}.

2.1.3 Lipids

Lipids were obtained mainly from Avanti Polar Lipids (Alabaster, AL), with the following exceptions: D-α-DPPC (Sigma), headgroup-labeled, rhodamine phosphatidyl-ethanolamine (Molecular Probes, Eugene, OR), palmitic acid (Fluka AG, *p.a* grade), 1,2-dipalmitoyl-sn-glycero-3-phosphomethanol (Prof. M.K. Jain, University of Delaware), 1-

caproyl-2-palmitoyl-sn-glycero-3-phosphatidylcholine and 1-palmitoyl-2-caproyl-sn-glycero-3-phosphatidylcholine (Prof. Mary Roberts, Boston College).

2.2 Experimental Methods

2.2.1 Lipid Monolayer Compression Isotherms

Surface pressure, π, is defined as the difference in surface tension of a pure liquid (γ_w) and the same liquid covered with a surface-active, generally insoluble monolayer (γ_m).

$$\pi = \gamma_w - \gamma_m \qquad (2.1)$$

For pure water at 20°C, γ_w is 72.9 mN m^{-1}. For water surfaces covered by very dilute, submonolayer surface films (>500 Å^2 molecule^{-1}), γ_m is essentially 72.9 mN m^{-1}, yielding a surface pressure of 0 mN m^{-1}. As the density of the interfacial film increases, γ_m decreases and π increases. For monolayers at the air-water interface, π typically ranges from 0 to 70 mN m^{-1}. High surface pressures reflect the reduction of γ_m to near 0 mN m^{-1}.

Several methods, direct and indirect, are available to measure surface pressure. When a paper or wettable metal plate is placed at the air-liquid interface, the vertical force on the plate changes as the surface tension changes (Fig. 2.1).

a) Edge-on view   b) Side-on view
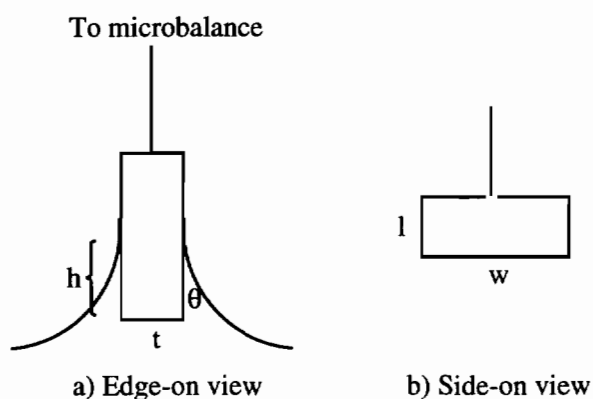
Fig. 2.1 Wilhelmy plate measurement of interfacial tension (see ref. 29).

Surface pressure measured in this manner is referred to as the Wilhelmy plate technique [29]. The vertical force on the Wilhelmy plate is given by [29]:

$$F = \rho_p glwt + 2\gamma(t + w)\cos\theta - \rho_l gtwh \qquad (2.2)$$

where F is the force on the Wilhelmy plate (mN), g is acceleration due to gravity, l, w, and t are the plate length, width, and thickness, respectively, h is the depth of plate immersion, θ is the contact angle between water and the plate, γ is the surface pressure, and ρ_p and ρ_l are densities of the plate and liquid, respectively. The first two terms in eq. 2.1 are due to gravitational and surface tension effects, while the last term is due to buoyancy of the Wilhelmy plate.

Usually, the Wilhelmy plate is completely wetted by the liquid subphase (θ close to zero), and t is small compared to w. Also, if a change in force rather than a change in h is measured, the expression for F (eq. 2.2) reduces to:

$$\Delta F = -2\pi w \qquad (2.3)$$

Thus, π is readily determined by measuring the vertical displacement of the Wilhelmy plate with an electronic microbalance or other suitable linear displacement transducer. Surface pressure is calibrated using a palmitic acid standard or a hanging weight. Upon compression, palmitic acid monolayers undergo a second-order phase transition from a liquid condensed to a solid phase at exactly 22.4 mN m^{-1} on pure water subphases at 20°C [68]. This transition point provides a reliable reference point for calibrating the Wilhelmy plate pressure detection system. Measurement of amphiphile surface pressure as a function of interfacial film density (given in area/molecule) yields the common monolayer compression isotherm (π-A curve).

2.2.2 Experimental Setup

Two monolayer film balances were used in these investigations. A commercial apparatus (KSV Instruments, Helsinki, Finland), milled out of a solid block of Teflon (712.44 cm^2 surface area, 1.1 l total subphase volume) is schematically depicted in Fig. 2.2. Control of monolayer film density is accomplished by sweeping the interface with a microstepped DC motor-driven hydrophilic barrier. Surface pressure is determined with a sand-blasted platinum or filter paper Wilhelmy plate suspended from an electronic

microbalance (Fig. 2.2). The Wilhelmy plate is kept in a null position by an electronic negative feedback loop. The restoring force on the plate is then converted to surface pressure using a computer-stored calibration constant.

π-A curves measured with the KSV film balance were obtained by spreading 80 µl of chloroform-dissolved lipid at the air-liquid interface. This amount of lipid solution was based on a submonolayer (gas phase analog) surface concentration to begin monolayer compression. Monolayer compression began 10 minutes after monolayers were spread to allow for solvent evaporation at room temperature (5 minute waiting period at temperatures above 30°C).
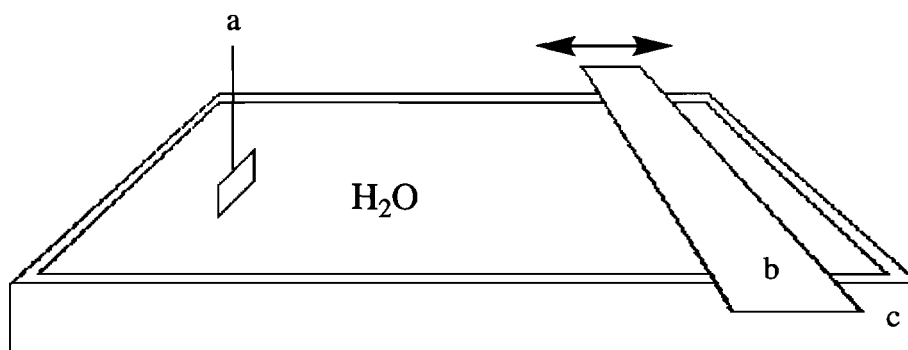
Fig. 2.2 Schematic of a monolayer film balance. Surface pressure is measured with a sandblasted platinum Wilhelmy plate (a) that is coupled to an electrobalance. A hydrophilic barrier (b) sweeps a monolayer-covered interface contained in a Teflon trough (c).

Monolayer π-A curves were also measured on a computer controlled, thermostated, home-built, Teflon monolayer film balance (surface area = 825.6 cm^2, subphase volume ~ 1.8 l). Surface pressure was determined via the Wilhelmy plate method using a linear position transducer (Trans-Tek, model 0200-0000). An A/D converter (MLPI, Vernier Software, Portland, OR) converted analog transducer displacement (mV) to a digital signal for digital recording. Surface pressure was calculated from digital input using a computer subroutine, based on surface pressure calibrations from palmitic acid monolayers on pure aqueous subphases at 20°C or by hanging weights of known mass on the transducer cantilever. In contrast to the KSV, a stepper motor-driven hydrophobic Teflon barrier was used.

Monolayer compression rates on the home-built apparatus were generally 12 Å^2 molecule^{-1} minute^{-1}. Compression rates on the KSV film balance were typically 2-3 Å^2 molecule^{-1} minute^{-1}. Specific rates of monolayer compression are given with the presented data.

2.2.3 Fluorescence Microscopy at the Air-Water Interface

Fluorescence microscopy at the air-water interface was carried out on a thermostated, home-built mini-trough (surface area = 9.6 cm^2, 5.5 ml subphase volume) mounted on the stage of a Zeiss ACM epifluorescence microscope (Fig. 2.3).
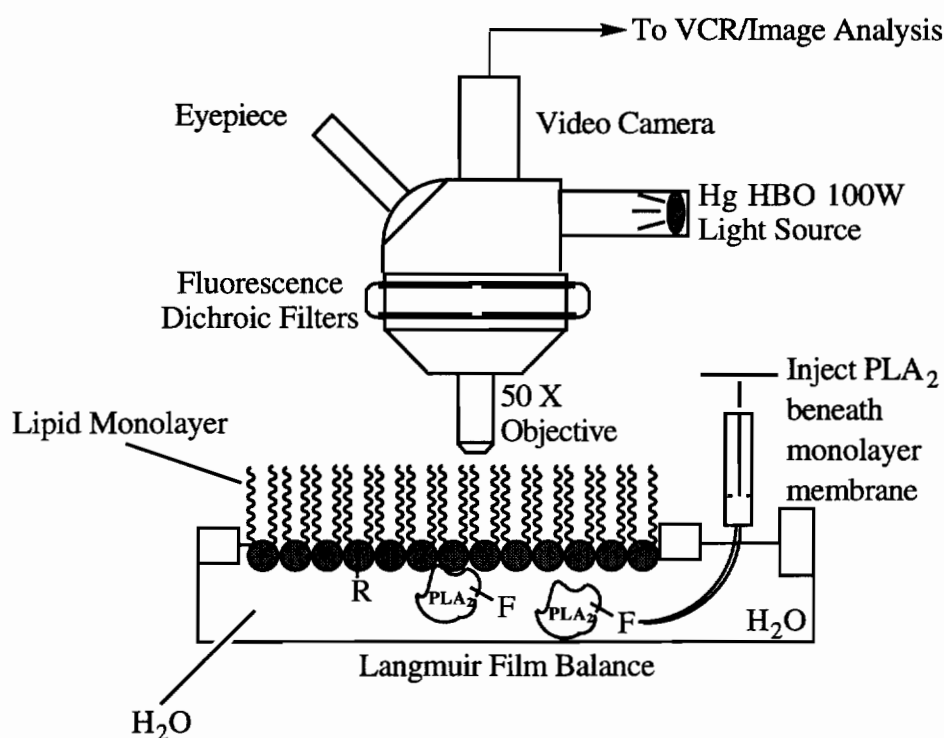
Fig. 2.3 Epifluorescence microscopy of monolayers at the air-liquid interface.

The epifluorescence microscope was outfitted with optical filters to selectively excite and detect fluorescence emission of rhodamine (Zeiss sulforhodamine filter 487714) and fluorescein (Zeiss fluorescein filter 487709). Surface pressure was measured using a cantilever coupled to a linear displacement transducer (Trans-Tek 0200-0000). A paper Wilhelmy plate hung directly from the cantilever into the trough subphase. Surface

pressure was calculated and calibrated by hanging weights of known mass on the pressure cantilever and using eq. 2.3, reading values accurate to ± 0.3 mN m⁻¹, or by adjusting an electronic circuit to read 22.4 mN m⁻¹ coincident with a palmitic acid monolayer second order phase transition. Monolayer compression rates were usually 2 Å² molecule⁻¹ minute⁻¹.

Fluorescence microscopy experiments were also conducted on another home-built Teflon trough (surface area = 130 cm², 130 ml subphase volume). The trough was surrounded with a Plexiglas cover, and a C-shaped Teflon mask [69] with a 1.5-cm inner diameter was placed in the subphase to facilitate monolayer imaging by reducing surface flow. As proof that the mask's presence did not create monolayer artifacts, the physical states of the lipid films, both inside and outside the mask, were frequently compared and found to be identical.
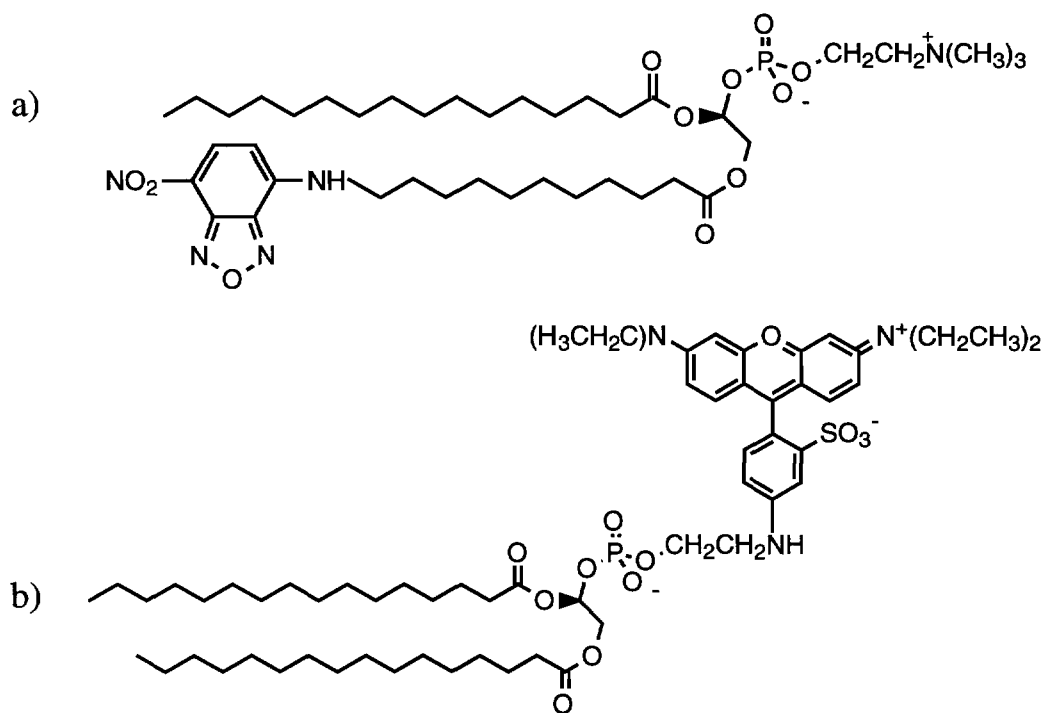
Fig. 2.4 Structures of C12-NBD-DPPC and rhodamine-dipalmitoylphosphatidyl-choline (Rhod-PE) monolayer fluorescent probes. (a) C12-NBD-DPPC: λ^{ex}_{max} = 466 nm, λ^{em}_{max} = 531 nm, ε= 19×10³ M⁻¹ cm⁻¹ (MeOH). (b) Rhod-PE: λ^{ex}_{max} = 563 nm, λ^{em}_{max} = 585 nm, ε= 73×10³ M⁻¹ cm⁻¹ (MeOH).

All fluorescence images were captured and intensified using a Hammamatsu C2400-08 low-light-level SIT camera interfaced to a high-resolution video monitor (Sony PVM-122) and a 4-head video cassette recorder (Sony). Fluorescence images were stored directly on video tape for future image analysis. Monolayer imaging was carried out by doping the mixed monolayers with 1 mol% or less of lipid dye probe (C12-NBD-DPPC or Rhod-DPPE) (Fig. 2.4b) [37,41]. Image contrast in fluorescence microscopy is based on the preferential solubility of lipid probe into fluid monolayer phases [37,41]. Our previous data [42] has shown that C12-NBD-DPPC (Fig. 2.4a) and Rhod-DPPE (Fig. 2.4b) fluorescent lipid show only fluid-expanded behavior, consistent with preferential partitioning into fluid monolayer phases [37,41]. Lipid and dye fluorescence probes were excited using a 100 W OSRAM HBO W/2 Hg lamp (Opti-Quip 1200-1500, Power Supply).
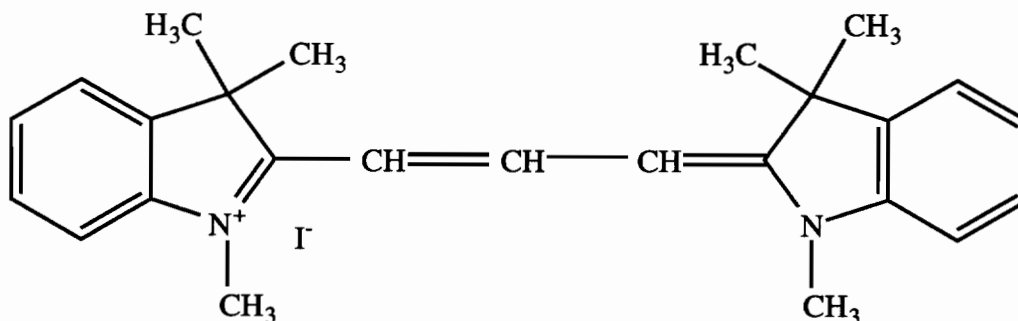
Fig. 2.5 Water soluble, cationic H-379. λ^{ex}_{max} = 539 nm, λ^{em}_{max} = 564 nm, $\varepsilon = 142 \times 10^3$ M^{-1} cm^{-1} (MeOH).

Protein or water-soluble dye (Fig. 2.5) introduction to the monolayer subphase was achieved by snaking a microsyringe Teflon tip from behind the monolayer barrier and into the monolayer covered subphase (see Fig. 2.3). In this manner, protein or dye injection occurred directly in the C-shaped monolayer mask or was carefully dispersed throughout the monolayer subphase to achieve as homogeneous as possible subphase distribution of soluble protein (or dye).

2.2.3.1 Microscopy image analysis

Image analysis of stored fluorescence microscopy video images was conducted using NIH-Image (v1.55, software available in the public domain of zippy.nihm.nih.gov).

Recorded microscopy images were transferred from VCR tape to a Macintosh Quadra 650 using a Scion LG-3 frame grabber (Scion Corp., Hackensack, NJ). Often, VCR image storage was bypassed, with images stored directly to a computer hard disk (TIFF graphics format) during each experiment in real time.

2.2.3.2 Quantitative monolayer texture analysis

Frequently, fluorescence image quality was enhanced using smoothing, reduced noise, and sharpening image analysis tools. Images were then thresholded and converted from gray scale to binary format. Domain areas (black pixels) were then counted. Then, fluid monolayer regions were summed (white pixels). Total field of view was calculated as the sum of black and white pixels. Percent solid monolayer domain areas were calculated by dividing the total domain area (A_s) by the total field of view (fluid area, A_f, and domain area, A_d):

$$A_s = \frac{A_d}{A_f + A_d} \qquad (2.4)$$

Histograms and other image-derived calculations were performed directly with NIH-Image. Monolayer domains that were not completely in the image field of view were not considered in domain area histogram analysis. The total field of view was corrected in this procedure by subtracting the area of these partially obscured domains.

2.2.4 Surface Potential and Surface Hydrolysis Measurements

Monolayer surface potential (ΔV) was measured with an ^{241}Am electrode (Nuclear Radiation Development, Grand Island, NY) positioned approximately 1-2 mm above the subphase. A platinum reference electrode was immersed in the subphase behind the compression barrier. Molecular area and surface potential were simultaneously monitored as a function of hydrolysis time at constant surface pressure using a personal computer. Lipid monolayers were spread and then compressed at 2 $\mathring{A}^2$ molecule^{-1} minute^{-1} to a surface pressure of 15 mN m^{-1}. PLA$_2$ (20 μg) was subsequently injected at the mouth of a milled circular Teflon mask under agitation in order to allow a uniform distribution of the enzyme [42]. This mask was located beneath the indicating surface potential electrode. The size and design of this mask were chosen to eliminate flow of the subphase outside the mask and used under conditions described by Verger for a zero-order trough [70].

2.2.5 General Experimental Considerations

A microsyringe (Kloehn Microsyringe Inc.) was used to spread lipid monolayers at the air-liquid interface by rastering 1-3 µl drops over the entire trough surface. Concentrations of amphiphile spreading solutions were typically 1 mg ml^{-1}, and were prepared according to:

$$\frac{A_t}{N_o V_s A_i} = \frac{m_t}{V_t} \qquad (2.5)$$

where A_t is the effective surface area of the trough, V_t is the volume of the stock spreading solution (typically 5.00 ml), N_o is Avogadro's number, V_s is the spreading solution volume (typically 80 µl), m_t is the lipid mass in the stock solution, and   is the desired area per molecule given the spreading solution volume (150 or 100 Å^2 molecule^{-1} for double or single chain lipids, respectively). Reproducibility of compression isotherms is ascertained if three isotherms from the same stock solution differ in molecular area and surface pressure of less than $\pm$ 2 Å^2 molecule^{-1} and $\pm$ 0.3 mN m^{-1}, respectively.

Prior to running isotherms, the trough was cleaned by soaking in a 5% (vol) solution of Contrad 70 (CMS) and heated at 45°C for several hours before being cooled down to room temperature. The surface-active cleaning solution is removed by filling and aspirating the trough with copious amounts (> 20 l) of Millipore Nano-pure water (18.3 MΩ cm^{-1} resistivity). The miniature troughs used for fluorescence microscopy were cleaned as stated above or by soaking overnight in concentrated H$_2$SO$_4$/No-Chromix™ cleaning solution. After several water rinsings, the sides of the trough and the hydrophilic barrier were wiped down with HPLC grade chloroform (1% ethanol stabilized) and the trough filled with Millipore water (or other subphase). When a platinum Wilhelmy plate was used, the plate was dipped in 200 proof ethanol (Quantum, U.S.P.) and flamed red hot with a Bunsen burner. This cleaning/flaming procedure was repeated three times before placing the plate on the electrobalance. When filter paper plates are used, they are replaced on a continuous basis (~ every 5 experiments, or when making measurements with different lipids). All glassware was cleaned by soaking in H$_2$SO$_4$/No-Chromix™ cleaning solution for a minimum of 24 hours. Occasionally, glassware was also cleaned by ultrasonicating for one hour with Micro or Contrad cleaning solution (CMS).

2.2.6 Protein Assay

PLA$_2$ concentrations were determined using a commercially available colorimetric assay kit (Pierce). The colorimetric determination is based on a bicinchinic acid (BCA, 4,4'-dicarboxy-2,2'-biquinoline) assay. In alkaline protein solutions, Cu(II) is reduced to Cu(I) [71]. Cu(I) binds specifically to BCA and is followed colorimetrically at λ_{max} = 562 nm and is directly proportional to protein concentration [72].

2.2.7 Fluorescein-Protein Conjugation

Fluorescein conjugation to PLA$_2$ was conducted according to a general method of Smith and Nargessi [73]. This reaction is based on the covalent attachment of FITC to PLA$_2$ surface-accessible amino acid side-chain amine functional groups. PLA$_2$ and FITC were separately dissolved in 0.0850 g Na$_2$CO$_3$ / 0.1721 g NaHCO$_3$ (pH 9) buffer. PLA$_2$ and FITC were then mixed in a 1:1 molar ratio and refrigerated for 3-5 hours before being chromatographed. Unreacted fluorescein was separated from FITC-conjugated PLA$_2$ using a Sephedex G-25M dextran column (Pharmacia). FITC-PLA$_2$ was recovered in the void volume using Millipore-treated water as the eluting solvent. The purified enzyme conjugate was then lyophilized. Lyophilized FITC-PLA$_2$ (cotton-like appearance) was recovered and several dilute solutions ($\sim$ 20 µg/ml) were prepared and stored at -20°C. Protein concentrations were determined as mentioned above. Fluorescein concentrations were determined by measuring FITC-PLA$_2$ sample absorbance at 490 nm (ε = 76×10^3 M^{-1} cm^{-1}). Taking the ratio of protein to fluorescein concentration gave the average number of FITC bound to PLA$_2$ (M$_r$ $N.$ $naja$ $naja$ PLA$_2$ = 14 kD, eq. 2.6):

$$\frac{A_{490}}{\varepsilon} \cdot \frac{M_r}{mg\ protein\ /\ ml} = \frac{moles\ FITC}{moles\ PLA_2} \qquad (2.6)$$

Protein labeling was statistical. Typical values in this study ranged from 0.5-0.75 FITC per PLA$_2$.

2.2.8 PLA$_2$ Adsorption to Polymer Monolayer Films at the Air-Water Interface

2.2.8.1 SiO$_2$ hydrophobization

Silicon oxide wafers were cut into 1 cm^2 pieces with a diamond scribe. After sonication for 25 minutes in detergent, the wafers were cleaned with Millipore water. The

sonicated wafers were then exposed to UV light for 15 minutes to destroy any surface active compounds not removed by sonication. Following UV treatment, the wafers were placed in a cone-shaped glass vial containing 10-15 μl of hexamethyldisilazane (HMDS, Nakarai Chemicals, Ltd.) with care taken to prevent the wafer from coming in contact with HMDS liquid. The vial was then capped and placed in an oven at 60°C for one hour. After heating for one hour, the vials were placed in a Petri dish containing cold water to condense HMDS vapors. Freshly hydrophobized wafers were used when possible.

2.2.8.2 Preparation of polymer monolayers

Poly(benzyl-L-histidine) (PBLH) monolayers at the air-water interface were created by spreading 3 μl of dichloroacetic acid-dissolved PBLH (0.6 mg/ml) on a custom-built trough of 7.0 cm^2 surface area and 1.5 ml subphase volume. The monolayer subphase was phosphate or Tris buffered with varying pH and ionic strength (NaCl and $CaCl_2$). The trough was filled with protein-containing subphase and the PBLH monolayer was spread to a surface pressure of approximately 15 mN m^{-1}. Protein-monolayer transfer to the SiO_2 support was conducted using the Langmuir-Schaefer technique [46]. After an incubation period of several hours at constant temperature, HMDS-treated SiO_2 wafers were carefully dropped onto the monolayer from a distance of 2-3 mm above the monolayer-air interface. Wafer removal was accomplished by grasping one edge of the substrate with Teflon-coated forceps and withdrawing the wafer at an angle to the monolayer surface to retard bubble formation on the surface. The wafer surface was then fixed for two minutes using phosphotungstic acid stain.

Scanning electron microscopy (SEM) of the protein-coated wafer surface was conducted on a Hitachi SEM with an electron-accelerating voltage of 30 kV.

Variations in experimental protocol were attempted: namely, injection of protein beneath monolayers as opposed to protein being present in the buffer before monolayer spreading, varying incubation times, ionic strengths, protein concentrations, subphase pH's and staining solutions. Specific details are in the text. SEM imaging of two-dimensional protein crystals was conducted at The Institute of Physical and Chemical Research (RIKEN) in Wako, Japan.

2.2.9 Quartz Crystal Microbalance Measurements of PLA$_2$ Binding to Phospholipid Multilayers

A quartz crystal microbalance (QCM) was used to investigate PLA$_2$ binding to model lipid multilayers. An AT-cut quartz crystal with gold electrodes on each side (16 mm^2 area) resonating at a frequency of 5 MHz was vacuum mounted in a home-built device (Fig. 2.4). A freshly cleaned quartz crystal (chloroform followed by ethanol) was mounted onto the holder and a stable oscillating frequency was obtained. The quartz crystal surface was then rendered hydrophobic by carefully pipetting an isopropanol-dissolved poly(siloxane) solution onto the crystal and then dried with a hair dryer. The crystal holder was then wiped down with chloroform (except the quartz surface) to remove excess siloxane polymer. The entire assembly was then mounted onto a vertical dipping arm of a double-barrier KSV-5000 Langmuir-Blodgett dipping trough.

When the frequency of the hydrophobized quartz crystal in air had stabilized, the
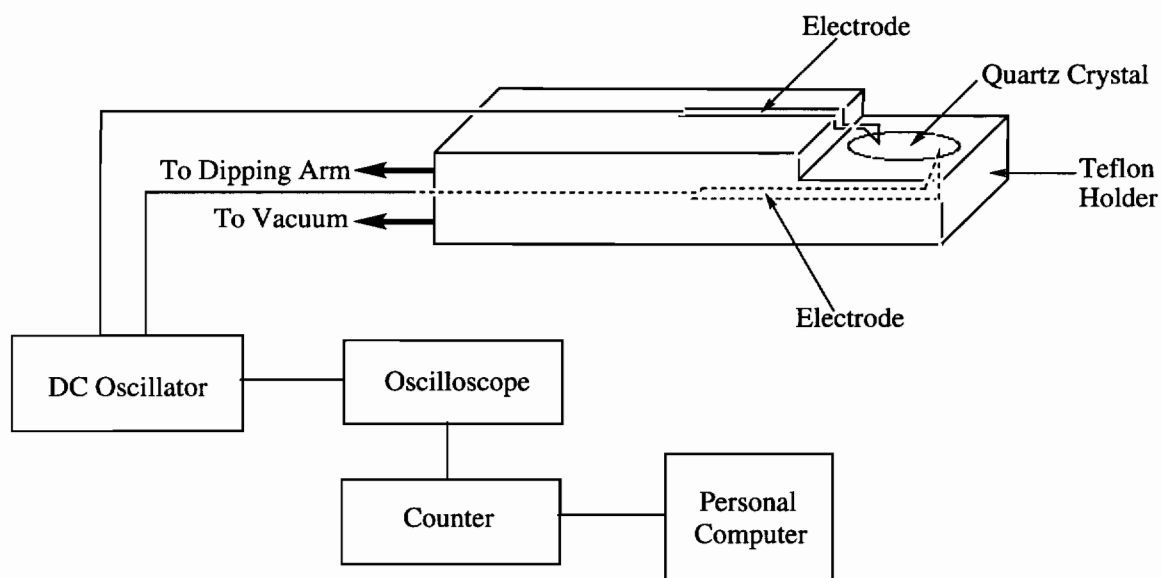
Fig. 2.6 Quartz crystal microbalance experimental setup.

entire assembly was lowered into the trough subphase. When the resonance frequency in water had stabilized, the assembly was withdrawn from the subphase until the frequency in air again had stabilized. This procedure was repeated several times. When frequencies in air and water deviated less than 5 Hz from cycle to cycle, a monolayer of phospholipid was spread and compressed to the desired surface pressure.

After the compressed monolayer had stabilized (change in monolayer molecular area versus time close to zero), Langmuir-Blodgett film deposition was carried out until the desired number of monolayers had been transferred. Transfer ratios were unobtainable because monolayer transfer also occurred on the Teflon QCM holder. Monolayers of dimyristoylphosphatidylmethanol and ditetradecylphosphatidylmethanol were used in this study. Following L-B film deposition, the monolayer-coated QCM was transferred under water into an electrically insulated housing and placed in a Teflon cell (3 ml volume) under magnetic stirring where protein injection occurred. Measurement of QCM frequency versus time was possible using a home-built computer program interfaced with a 60 MHz digital oscilloscope (Hame C) and frequency counter (Iwatsu SC-7201 Universal). Data were stored directly to computer disk for analysis. QCM measurements were conducted in Mainz, Germany.

Fig. 2.7 displays symbols for lipids and fluorescent lipid probes (cf. Chapter 5).
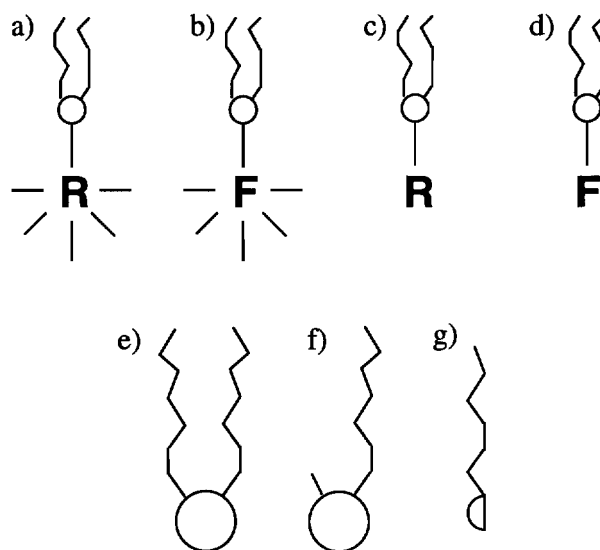
Fig. 2.7 Lipid schematics: (a) excited rhodamine-labeled phospholipid, (b) excited fluorescein-labeled phospholipid, (c) ground state rhodamine-labeled phospholipid, (d) ground state fluorescein-labeled phospholipid, (e) DPPC, (f) lyso-lipid, and (g) fatty acid.

CHAPTER THREE

TERNARY AND BINARY MIXED MONOLAYERS OF DPPC, C16LYSO AND PALMITIC ACID AS MODELS FOR PLA$_2$-HYDROLYZED DPPC MONOLAYERS

3.1   Rationale

PLA$_2$-catalyzed hydrolysis of single component phospholipid monolayers at the air-water interface results in a significant transformation of the chemical and physical properties of the interface. A single-component phospholipid monolayer is transformed into a ternary mixed lipid system during hydrolysis, and then into a binary mixed system upon completion of enzymatic degradation [31]. Prior to PLA$_2$-catalyzed hydrolysis, the membrane system is composed of pure phospholipid substrate. At time t, in addition to thr remaining substrate, fatty acids and lyso-lipids are present in equimolar ratios. Total lipid hydrolysis by PLA$_2$ results in the formation of an equimolar binary mixture consisting of lyso-lipid and fatty acid.

Using fluorescence microscopy, Grainger and coworkers [42,43] found that following PLA$_2$ hydrolysis of DPPC monolayers at the air-buffer interface, PLA$_2$ formed large, two-dimensional aggregates at the interface. It was hypothesized that PLA$_2$ formed these domains in response to lateral phase separation of palmitic acid reaction products. Since hydrolysis conditions are basic (Tris buffered pH 8.9 subphase with 100 mM NaCl and 5 mM CaCl$_2$), fatty acid reaction products exist as anions (apparent fatty acid interfacial pK$_a$ ≈ 5.5). Electrostatic interactions between Ca^{2+} ions in the monolayer subphase and negatively charged fatty acid are possible. Divalent metal-induced lipid chelation, resulting in monolayer lateral phase separation, is well known [74]. Phase separation of fatty acids, driven by calcium chelation, could therefore act as a template for PLA$_2$ interfacial self-assembly.

A region of PLA$_2$'s solvent accessible surface, referred to as the "interfacial recognition surface" (IRS) [75], is hypothesized to interact directly with the membrane interface during binding. Based on X-ray data, Verheij and coworkers have suggested that the IRS, which surrounds the active site, most likely consists of Arg6, Lys10, His17,

Asn23, Asn24, Lys56, Asn67, Lys116, Asn117, Lys121, and Lys122. Ten other uncharged residues are also believed to be part of the IRS [75]. Clearly, many of the residues in the IRS are positively charged. Electrostatic interactions between PLA$_2$'s IRS and negatively charged fatty acid monolayer regions are hypothesized to play an important role in driving PLA$_2$ domain formation at the hydrolyzed lipid monolayer-buffer interface.

To learn more about the interfacial phase behavior of ternary mixed membrane compositions reflecting various extents of PLA$_2$-induced lipid monolayer hydrolysis as well as binary C16Lyso:palmitic acid mixed monolayers, isotherms and fluorescence microscopy of these mixtures were investigated.

The purpose of this portion of the investigation is to determine the physical properties of a partially hydrolyzed monolayer and a completely hydrolyzed film using ternary and binary mixed phospholipid monolayers, *in the absence of* PLA$_2$, as models of PLA$_2$ DPPC monolayers at the air-water interface. Since enzymatic lipid degradation produced charged reaction products (fatty acids), the electrostatic characteristics of ternary and binary mixed monolayers were probed using a water-soluble, cationic dye (Fig. 2.5).

3.2   Experimental

Mixed monolayers containing various amounts of DPPC, C16Lyso, and palmitic acid, corresponding to phospholipid monolayer compositions at different extents of PLA$_2$ hydrolysis, were constructed. Ternary mixed systems investigated included DPPC:C16Lyso:palmitic acid (0.2:1:1, 1:1:1, 2:1:1, 3:1:1, 5:1:1, and 10:1:1; mol:mol:mol). Ternary mixed monolayers always contained C16Lyso and palmitic acid in a molar ratio of 1:1 because PLA$_2$-catalyzed hydrolysis of phospholipids yields the same stoichiometry.

For ternary and binary mixed monolayers, three subphase systems were used in isotherm and fluorescence microscopy experiments: (1) pure water (Barnstead Nano-pure, 18.3 MΩ cm^{-1} resistivity); (2) 10 mM Tris, 115 mM NaCl, 10μM EDTA, pH 8.9, and (3) 10 mM Tris, 100 mM NaCl, 5 mM CaCl$_2$, pH 8.9.

Chloroform was used as the solvent for all lipid stock solutions except those containing C16Lyso, where CHCl$_3$:MeOH (9:1; v/v) was used. DPPC:C16Lyso:palmitic acid solutions (mol %) were made by mixing pure stock solutions of each component in known proportions with chloroform dilution to proper lipid concentration.

Isothermal compressions of the ternary mixed monolayers were measured by spreading 80 μl of approximately 1 mg/ml solutions (see section 2.2) followed by a ten minute waiting period to allow for solvent evaporation. Mean molecular areas were calculated as weighted averages of the individual components. Film compression rates were 12 $Å^2$ molecule^{-1} minute^{-1}. Isotherms were carried out in triplicate at 20°C and were reproducible .

In fluorescence microscopy experiments, monolayers were created by spreading 20 μl of the lipid solution (~ 0.1 mg/ml) on a home-built trough (see section 2.3). 1 mol% of C12-NBD-DPPC fluorescent lipid monolayer probe was used.

The film was compressed to a desired surface pressure, the barrier stopped, and the monolayer image recorded at various locations in the film. A Teflon, C-shaped mask was placed in the monolayer subphase to facilitate monolayer imaging [69].

To probe the electrical nature of phase-separated monolayer regions, the cationic water soluble dye H-379 (80 μl, 2.06 μM, Millipore water solution), was injected into the subphase from behind the trough's movable barrier and into the mask. Using appropriate cut-off filters of the microscope, either C12-NBD-DPPC or H-379 can be selectively excited and its emission detected by imaging microscopy. Monolayer compression rates were 3 $Å^2$ molecule^{-1} minute^{-1}.

3.3   Results

3.3.1 Pure DPPC, C16Lyso, and Palmitic Acid Monolayers

In order to understand the physical characteristics of ternary mixed monolayers containing DPPC, C16Lyso, and palmitic acid, the interfacial properties of the constituent compounds were first investigated.

Fig. 3.1 shows isotherms of pure DPPC, C16Lyso, and palmitic acid on pure water subphases. Pure palmitic acid monolayers show an onset of surface pressure at low molecular areas (27 $Å^2$ molecule^{-1}). Palmitic acid monolayers are observed to undergo a second-order, liquid-solid phase transition at 22.4 mN m^{-1} [68] under these conditions. Monolayer collapse pressure is near 49 mN m^{-1} with a limiting molecular area of 19 $Å^2$ molecule^{-1} [68]. Pure C16Lyso monolayers, on the other hand, show onsets of surface pressure at very large molecular areas (>125 $Å^2$ molecule^{-1}), collapse at fairly low surface pressures (32 mN m^{-1}), and a limiting molecular area of 37 $Å^2$ molecule^{-1} [30].

C16Lyso monolayers do not undergo any observable phase transitions under these

conditions, maintaining a liquid expanded state with low compressibility. DPPC monolayers show onsets of surface pressures at intermediate values (94 $Å^2$ molecule^{-1}), and undergo a first-order phase transition [39] at 4 mN m^{-1} under these conditions. This
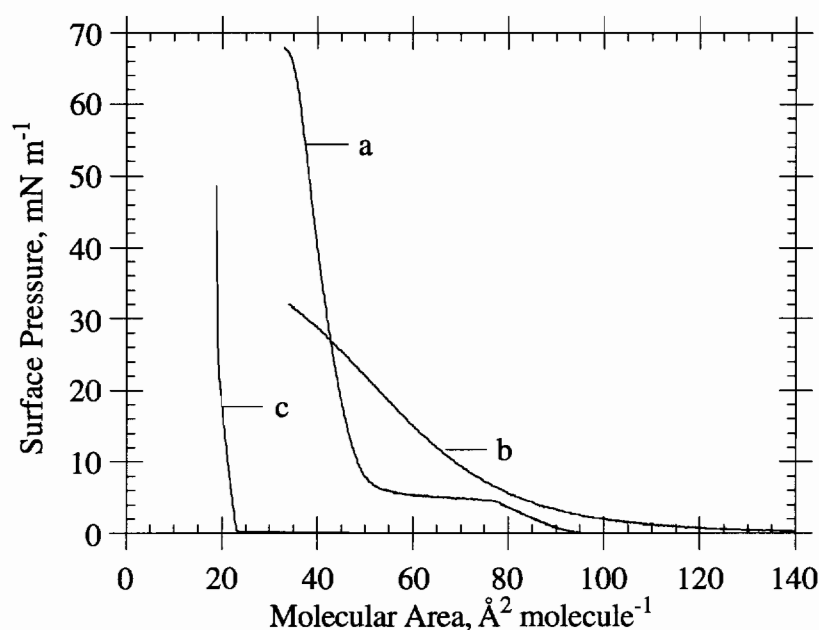
Fig. 3.1 Isotherms of (a) DPPC, (b) C16Lyso, and (c) palmitic acid on pure water at 20°C. Compression rate is 12 $Å^2$ molecule^{-1} minute^{-1}.

horizontal portion of the isotherm has a slope near zero, indicating, in this region of the isotherm, a coexistence of fluid and solid phases. Though the nature of the phase transition is still hotly debated, fluorescence and Brewster angle microscopy have unequivocally confirmed that, in the plateau region of the isotherm, a coexistence of liquid and solid phases exists [37,41]. Monolayers of DPPC collapse at high pressures (65 mN m^{-1}) and limiting molecular areas of 36 $Å^2$ molecule^{-1} [40]. As Fig. 3.1 shows, these three constituents of a hydrolyzed DPPC monolayer feature drastically different phase behavior as pure monolayers at the air-liquid interface.

3.3.2 C16Lyso:Palmitic Acid Binary Mixed Monolayers

Since all the investigated ternary mixed monolayers contain C16Lyso and palmitic acid in a constant equimolar ratio with different amounts of DPPC, isotherms of these

binary mixtures were measured. Fig. 3.2 shows π-A compression curves for the C16Lyso:palmitic acid binary mixture (1:1) on two different subphases. On water subphases (pH 6.4), the binary system exhibits fluid expanded behavior (Fig. 3.2a). Molecular area at surface pressure onset is near 50 $Å^2$ molecule^{-1} with film collapse at a pressure of 52 mN m^{-1}. On pH 8.9 buffered subphases containing Ca^{2+} and 100 mM NaCl (Fig. 3.2b), the monolayers still display fluid behavior. The collapse pressure for these binary mixed monolayers, however, is lower than the same monolayer on water (35 versus 43 mN m^{-1}). Moreover, the onset of surface pressure occurs at much higher mean molecular areas (75 versus 50 $Å^2$ molecule^{-1}). Thus, the presence of Ca^{2+} in the subphase expands the binary mixed monolayers with respect to the films on pure water subphases. Though such binary film expansion in the presence of divalent cations is counter-intuitive, a similar phenomenon has been observed in phosphatidylserine-containing mixed monolayers with Ca^{2+} in the subphase [74].
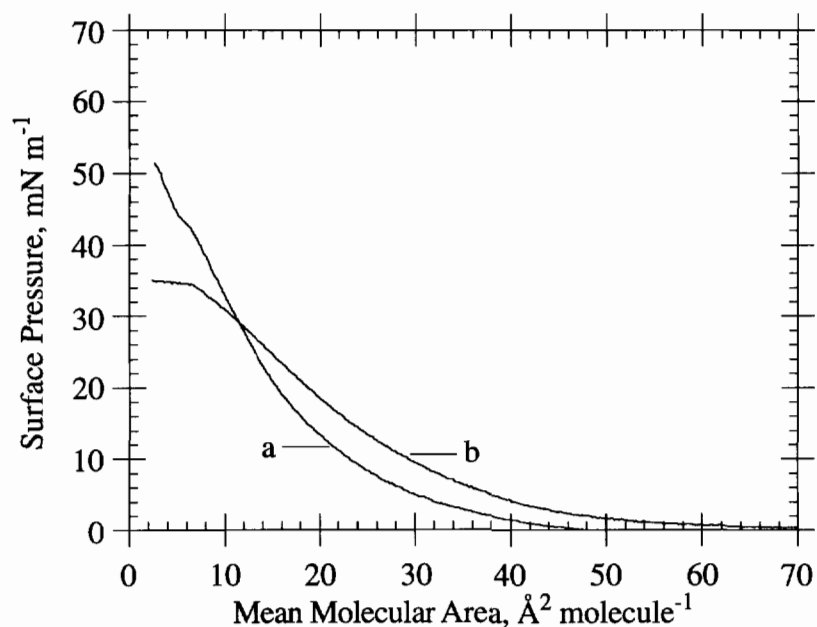
Fig. 3.2 Isotherms of C16Lyso:palmitic acid monolayers (1:1) on (a) pure water and (b) 100 mM NaCl, 10 mM Tris, 5 mM $CaCl_2$, pH 8.9. Compression rate same as in Fig. 3.1.

3.3.3 Ternary Mixed Monolayers

3.3.3.1 DPPC:C16Lyso:palmitic acid (0.2:1:1)

Fig. 3.3 compares isotherms of DPPC:C16-Lyso:palmitic acid (0.2:1:1) ternary mixed monolayers on several different subphases. The 0.2:1:1 system represents a
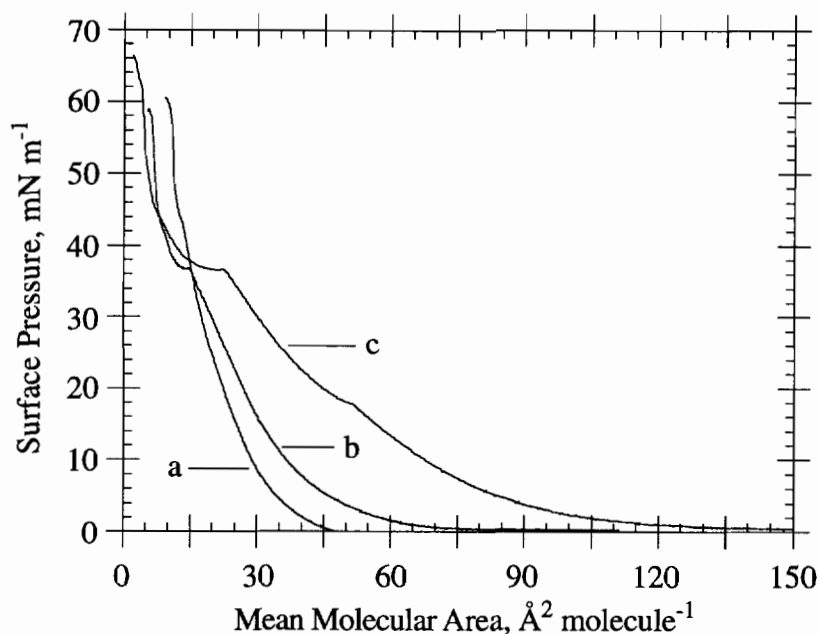
Fig. 3.3 Isotherms of DPPC:C16Lyso:palmitic acid, 0.2:1:1 on (a) water, (b) 100 mM NaCl, 5 mM CaCl$_2$, 10 mM Tris, pH 8.9, and (c) 115 mM NaCl, 10 μM EDTA, pH 8.9. Compression rate same as in Fig. 3.1.

monolayer that has been 90.9% hydrolyzed. Two important features should be noted. First, addition of Ca^{2+} (Fig. 3.3b) to the subphase (pH 8.9) has a drastic effect on monolayer packing. At pH 8.9, take-off areas are decreased by nearly 75 Å^2 molecule^{-1} as compared to films free of Ca^{2+} (Fig. 3.3c). Secondly, a kink in the isotherm is observed at 17.5 mN m^{-1} (52 Å^2 molecule^{-1}, Fig. 3.3b), which is attributed to remnants of a diffuse DPPC phase transition. This lipid mixture on water does not show any bends in the isotherm at low pressures, and monolayer phase behavior is expected to be liquid-like. The kinks observed on all the curves at pressures near 40 mN m^{-1} most likely represent palmitic

acid and/or C16Lyso being squeezed out of the monolayer, as these constituents are not themselves compressible beyond this surface pressure (Fig. 3.1b,c, and Fig. 3.2).

3.3.3.2 DPPC:C16Lyso:palmitic acid (1:1:1)

Fig. 3.4 shows the isotherms for 1:1:1 ternary mixed DPPC:C16Lyso:palmitic acid monolayers. Similarly observed in the 0.2:1:1 mixture, a marked condensation of the film
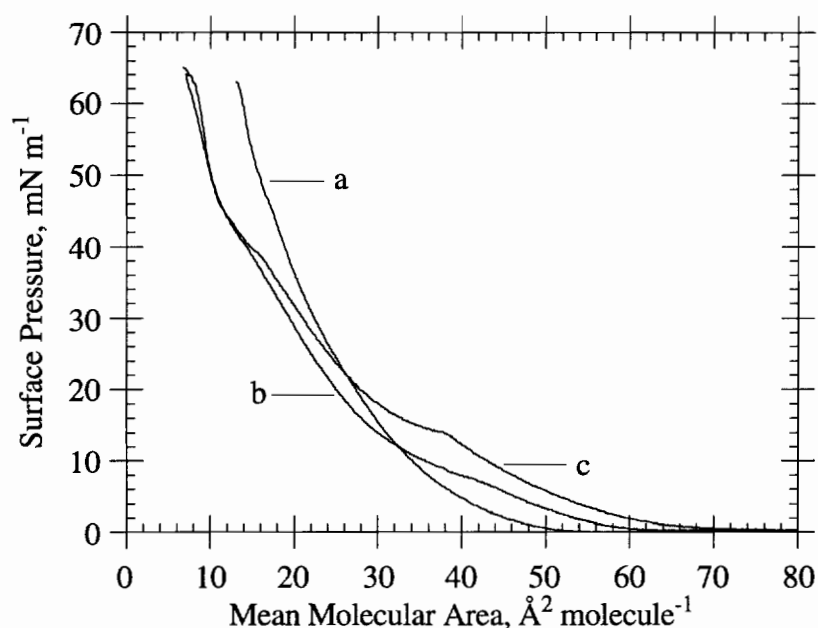
Fig. 3.4 Isotherms of DPPC:C16Lyso:palmitic acid, 1:1:1. Same conditions as in Fig. 3.3.

in the presence of Ca^{2+} is evident (compare Fig. 3.4b,c). At pH 8.9, surface pressure onset is shifted from 80 to 60 $Å^2$ molecule^{-1}. The kink in the isotherm observed in the 0.2:1:1 ternary mixture (Fig. 3.3c) is also observed in the 1:1:1 Ca^{2+}-free system, but at a lower surface pressure of 14.5 mN m^{-1} and increased molecular area of 42 $Å^2$ molecule^{-1} (Fig. 3.4c). At pH 8.9, the presence of Ca^{2+} in the subphase shifts this kink to both lower surface pressures and molecular areas (7 mN m^{-1} and 46 $Å^2$ molecule^{-1}, respectively). As in the 0.2:1:1 system, kinks in the isotherms are observed at high surface pressures and most likely represent loss of material from the monolayer to the bulk subphase.

3.3.3.3 DPPC:C16Lyso:palmitic acid (2:1:1)

Depicted in Fig. 3.5, the 2:1:1 system exhibits the same trends as observed in the 0.2:1:1 and 1:1:1 ternary mixed systems: namely, Ca^{2+} condensation of the mixed film as well as a shift in the presumed diffuse DPPC phase transition to lower pressures (5 mN m^{-1}) and higher molecular areas (62 Å^2 molecule^{-1}). Unlike the 0.2:1:1 and 1:1:1 systems, however, the 2:1:1 mixture does not display the kink at high surface pressure. Similar to the previous ternary mixed systems, the 2:1:1 monolayer collapses at lower mean molecular areas when on salt-containing buffered subphases, indicating electrostatic interactions between ionized monolayer components and the subphase help condense the film at high surface pressure.
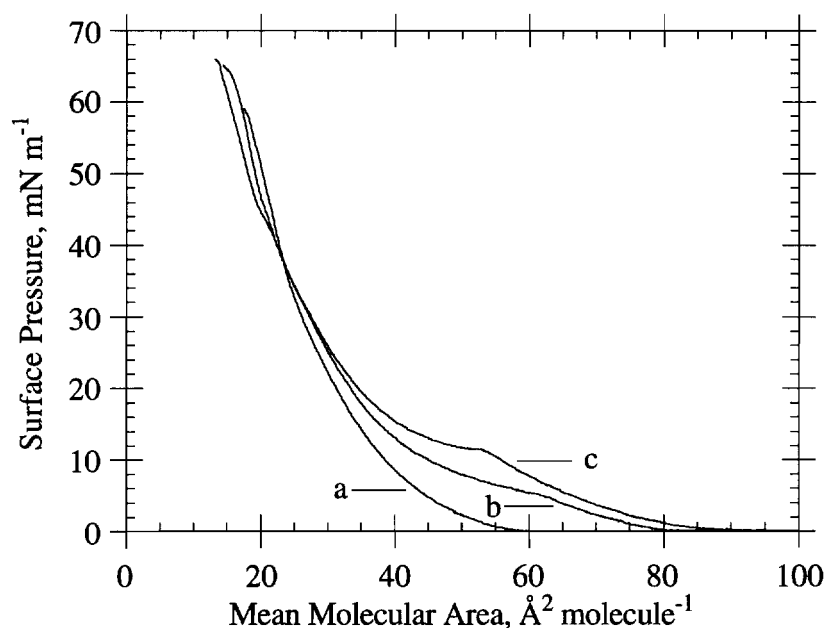
Fig. 3.5 Isotherms of DPPC:C16Lyso:palmitic acid, 2:1:1. Same conditions as in Fig. 3.3.

3.3.3.4 DPPC:C16Lyso:palmitic acid (3:1:1)

Isotherms of the 3:1:1 ternary mixed monolayers (Fig. 3.6) display slightly different behavior than the observed trends in the 0.2:1:1, 1:1:1, and 2:1:1 systems. Predicted phase behavior of the monolayer on water still suggests a fluid monolayer.

However, the 3:1:1 mixture on Ca^{2+}-free subphases lacks the kink that is readily observable in the 0.2:1:1, 1:1:1, and 2:1:1 mixtures. Although not absent, the observed
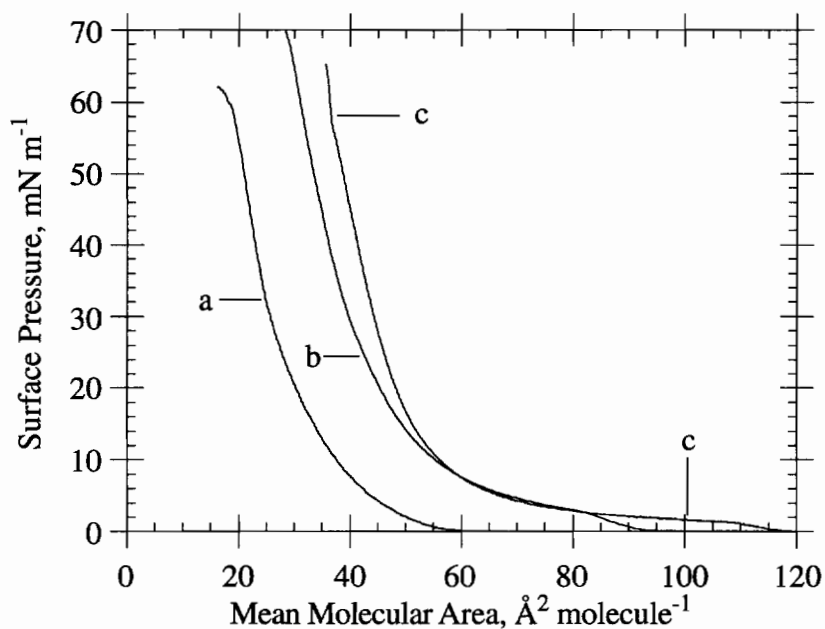
Fig. 3.6 Isotherms of DPPC:C16Lyso:palmitic acid, 3:1:1. Same conditions as in Fig. 3.3.

bend in the isotherm measured on a buffered Ca^{2+} subphase is barely seen. Additionally, molecular areas at collapse differ significantly when comparing isotherms on buffer (Fig. 3.6b,c) and on water (Fig. 3.6a).

3.3.3.5 DPPC:C16Lyso:palmitic acid (5:1:1 and 10:1:1)

Representing a DPPC monolayer that is 28.6% hydrolyzed, 5:1:1 ternary mixed monolayer isotherms are shown in Fig. 3.7. The curve on water (Fig. 3.7a) shows a slight bend in the isotherm at 8 mN m^{-1}. Within the series of ternary mixed monolayers presented so far, this represents the first sign of a monolayer phase transition on pure water subphases. The curves from the other ternary mixtures on water do not show any evidence of a monolayer phase change. The curves on Ca^{2+}-containing and Ca^{2+}-free subphases also show evidence of a monolayer phase change at approximately 9 and 6 mN m^{-1}, respectively. Except for minor differences in the pressure at which this kink occurs and the mean molecular areas at surface pressure onset, the isotherms on calcium-free and calcium-

containing subphases are almost identical. The pressure at which these kinks occur is consistent with that of a diffuse DPPC transition. The trends in the isotherms that are apparent in the 0.2:1:1, 1:1:1, and 3:1:1 ternary mixtures are reestablished in the 5:1:1 system (Fig. 3.7) . The kink present in the monolayer on Ca^{2+}-containing subphases is slightly higher than on Ca^{2+}-free subphases.
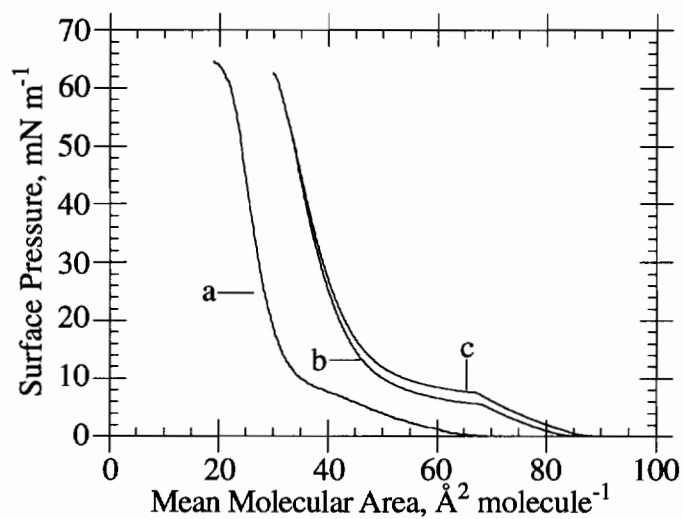
Fig. 3.7 Isotherms of DPPC:C16Lyso:palmitic acid, 5:1:1. Same conditions as in Fig. 3.3.
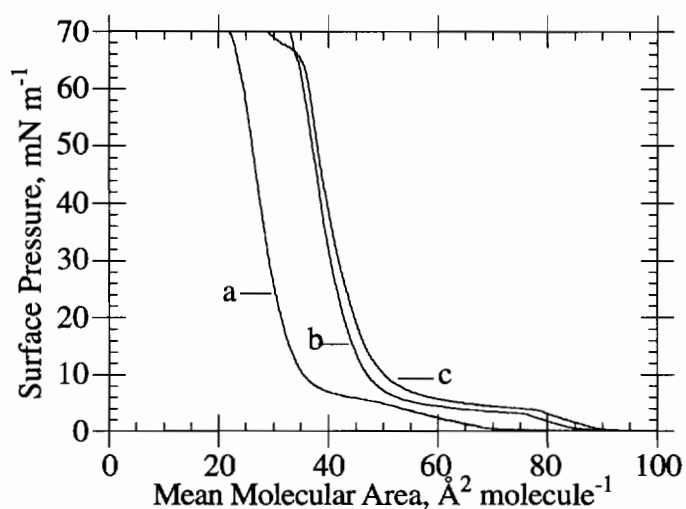
Fig. 3.8 Isotherms of DPPC:C16Lyso:palmitic acid, 10:1:1. Same conditions as in Fig. 3.3.

Finally, representing a 16.6% hydrolyzed DPPC monolayer, isothermal compression data from the 10:1:1 system is shown in Fig. 3.8. More so than in the other mixtures, the Ca^{2+}-free and Ca^{2+}-containing subphase curves are nearly identical. The kink in the 5:1:1 curve on water is more readily observable in the 10:1:1 system on water.

3.3.4 Fluorescence Microscopy Of Binary and Ternary Mixed Monolayers

To gain more information on the microstructures of these binary and ternary mixed monolayers, fluorescence microscopy was used to directly image the physical states of these films during compression. Two fluorescent probes (C12-NBD-DPPC and the carbocyanine cationic dye, H-379, structures in Figs. 2.4a and 2.5) were employed to visually distinguish monolayer microphases in both binary and ternary monolayer systems based on physical state and charge, respectively. These two dyes are spectrally distinct (in physically monomeric forms) so that selective excitation and emission can distinguish dye locations at, or near, the monolayer interface.

Fig. 3.9 shows typical phase-separated domains imaged with a NBD filter in the
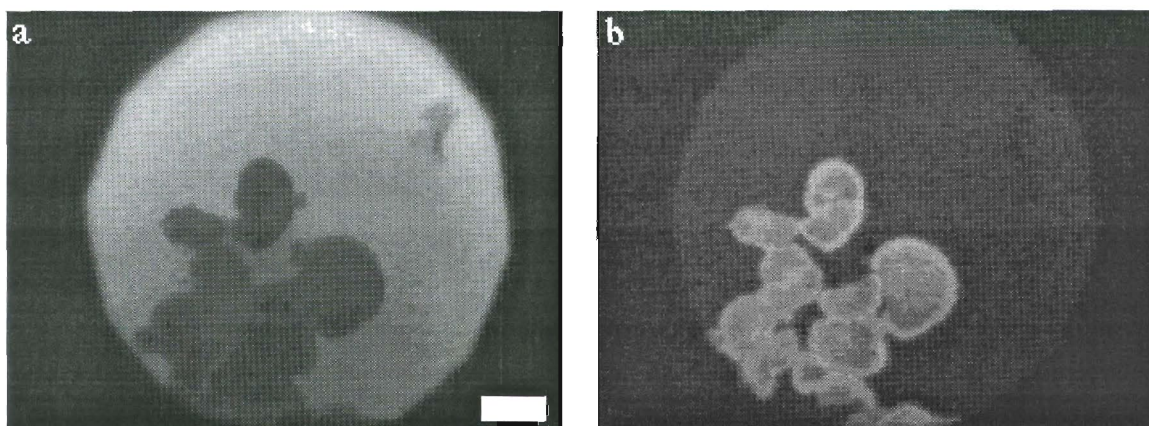
Fig. 3.9 Fluorescence micrographs of 0.2:1:1 ternary mixed DPPC:C16Lyso:palmitic acid monolayers on 100 mM NaCl, 5 mM $CaCl_2$, 10 mM Tris, pH 8.9. Images in (a) and (b) were viewed through fluorescein and rhodamine filters specific for C12-NBD-DPPC and H-379, respectively, at 12 mN m^{-1}. Scale bar is 25 μm.

0.2:1:1 system. The domain appears gray (Fig. 3.9a) on the outside and darker on the inside as viewed through the NBD filter due to selective NBD-C12-DPPC probe partitioning in the fluid lipid matrix. However, the NBD-probe is not completely confined

to the fluid matrix. If this were the case, the phase-separated domains would appear black, not gray, as viewed through the NBD filter (Fig. 3.9a). Thus, depletion of the NBD probe in the exterior regions of the phase-separated domains shown in Fig. 3.9a is not complete. However, probe depletion appears to be complete in the domain interiors. The domain morphology shown in Fig. 3.9 closely resembles the domain shapes observed in PLA$_2$-mediated hydrolyzed lipid monolayers [42,43].

When injected beneath ternary monolayers, water-soluble cationic dye (H-379) binds quickly to phase-separated gray domains depicted in Fig. 3.9a. Dye binding events and monolayer states may be imaged by switching back and forth between the NBD and H-379 specific filters. This result is shown in Fig. 3.9b (excited and observed through the H-379 specific filter), proving that these large gray domains in 0.2:1:1 mixtures contain negatively charged components, namely palmitic acid, under these conditions. This electrostatic interfacial binding process between cationic dye and anionic monolayer domain is very stable but can be blocked under certain conditions when anionic species are protonated (detailed below).

As shown in Fig. 3.10, larger phase-separated anionic domain morphologies exhibited fine inner microstructure in the 0.2:1:1 mixtures. The inner domain heterogeneities often exist as striations, extending non-linearly from domain centers
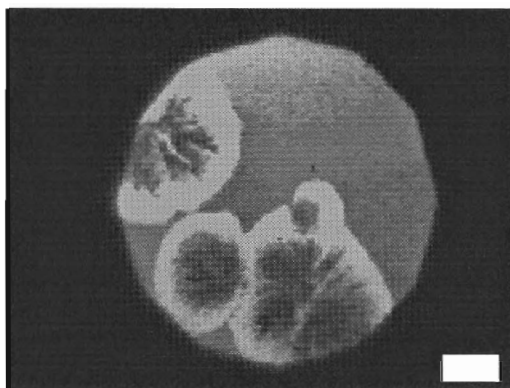
Fig. 3.10 Phase-separated anionic microstructures in 0.2:1:1 ternary mixed lipid monolayers on 100 mM NaCl, 5 mM CaCl$_2$, 10 mM Tris, pH 8.9, subphase. Imaged with rhodamine (H-379) filter. Surface pressure is 15 mN m^{-1}. Scale bar in (a) is 25 μm.

outward. These structures may also be present in the domains depicted in Fig. 3.9, but are laterally unresolvable with the microscope. Exclusively, large phase-separated anionic

domains in the 0.2:1:1 system display this inner microstructure. These domains form spontaneously by monolayer compression to low, lateral surface pressures and are stable up to pressures of at least 20 mN m^{-1}. Phase-separated regions exhibit a morphology similar to domains generated in monolayers using enzyme hydrolysis. When excited through the NBD-selective filter, domains shown in Fig. 3.10 do not appear gray as in Fig. 3.9a because of the presence of adsorbed H-379. Due to the broad excitation band of H-379, the dye may adsorb sufficient light to be excited with the NBD-specific long-pass emission filter. Another possible explanation is that the dye forms aggregates under phase-separated anionic domains. Merocyanine aggregate adsorption bands are blue-shifted relative to monomer dye; thus, dye adsorption and emission could be possible with the fluorescein filter set on the microscope. Without spectroscopic data, this possibility remains unknown. When phase-separated domains in Fig. 3.10 are imaged without H-379 in the subphase, they appear gray (as in Fig. 3.9a) surrounded by a matrix of brighter surrounding fluid lipids.

Fluorescence micrographs of binary mixed monolayers of 1:1 binary mixed C16Lyso:palmitic acid are shown in Fig. 3.11. Fig. 3.11a shows phase-separated lipid domains on pH 8.9 buffered subphases at a surface pressure of 12 mN m^{-1}, as observed
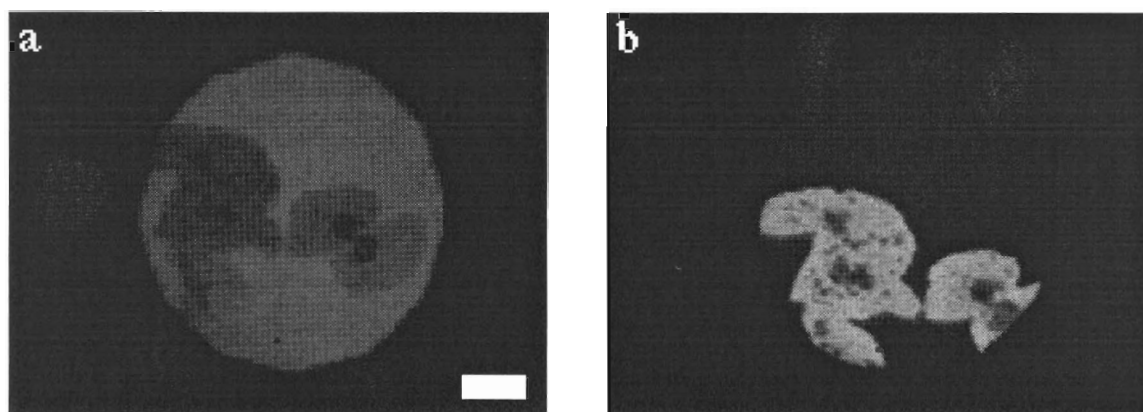
Fig. 3.11 Phase-separated microstructures observed in 1:1 binary mixed C16Lyso:palmitic acid monolayers on 100 mM NaCl, 5 mM CaCl$_2$, 10 mM Tris, pH 8.9, subphase. Surface pressure is 15 mN m^{-1}. Images in (a) and (b) were viewed through NBD- and H-379-specific filters, respectively. Scale bar in (a) is 25 μm.

through a NBD-specific fluorescence filter. As evident in the 0.2:1:1 mixed lipid system, there is also a microstructure gradient in these phase-separated domains. Small black areas are apparent in the interior of these domains while the rest of the domain is gray (Fig. 3.11a).

To probe the charge of these domains, the water soluble cationic dye H-379 was injected into the monolayer subphase. Shown in Fig. 3.11b is the binding of H-379 to these microstructures as viewed through the H-379 specific filter. Thus, these domains contain negatively charged monolayer components (palmitic acid). *Phase separation of anionic domains in binary and ternary mixed systems was not observed at pH 4, or in the*
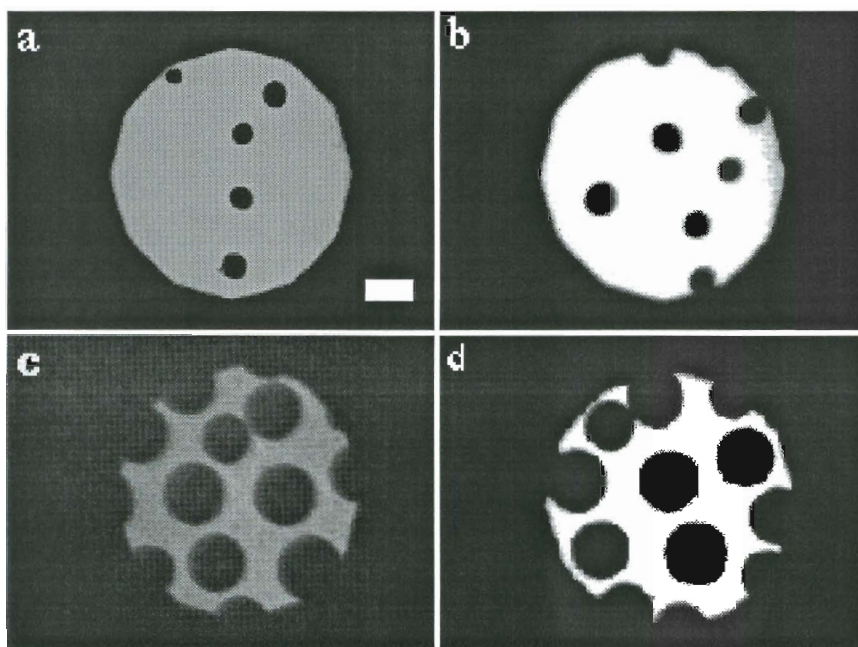
Fig. 3.12 Fluorescence micrographs of C16Lyso:palmitic acid (1:1) monolayers on 100 mM NaCl, 5 mM CaCl$_2$, 10 mM oxalate, pH 4. Surface pressures are (a) 12 mN m^{-1} (as viewed through H-379 filter), (b) 18 mN m^{-1} (H-379 filter), (c) 26 mN m^{-1} (fluorescein filter), and (d) 26 mN m^{-1} (H-379 filter). Scale bar in (a) is 25 μm.

absence of Ca^{2+} *ions.* However, binary mixed monolayers at low pH are microstructured. To further characterize the C16Lyso:palmitic acid binary monolayer systems, their phase behavior was investigated on pH 4, Ca^{2+}-free subphases. At low pH, fatty acid headgroups are unionized, preventing intermolecular chelating by divalent calcium cations.

Examples of binary mixed monolayer textures at pH 4 are shown in Fig. 3.12. In Fig. 3.12a, the monolayer was imaged at 12 mN m^{-1}, just after the onset of domain formation. Fig. 3.12b shows monolayer structure at 18 mN m^{-1}. In Fig. 3.12c, the monolayer was imaged using a fluorescein-specific fluorescence filter (for C12-NBD-DPPC). Imaging the same monolayer field of view with a rhodamine fluorescence filter (specific for the water-soluble cationic H-379, bottom right panel), shows that dye is bound (or near) to the fluid portions of the monolayer but not to the condensed domains. Since the dye is always positively charged (Fig. 2.5), this indicates that the solid domains in the binary mixed monolayers are uncharged. Since C16Lyso is not known to pack into solid structures at the air-water interface, these domains most probably comprise phase-separated, unionized palmitic acid. Quantitative image analysis suggests that whichever component in the 1:1 binary mixture is phase-separated, it has done so completely (49% of the film area is condensed).

In the 1:1:1 ternary mixed lipid system, phase separation of palmitic acid and crystallization of DPPC were observed to be competing kinetic events. Phase separation of fatty acid-enriched regions often occurred with DPPC nucleation and crystal growth. Letting the monolayer stand for long time periods (hours) resulted in the disappearance of DPPC domains, but not the fatty acid regions. The phase-separated fatty acid regions (as evidenced by dye binding) never disappeared.

Fig. 3.13 displays the NBD-excited image of the phase-separated 1:1:1 ternary system, containing bound H-379 dye on the Ca^{2+}-containing buffered alkaline subphase at a surface pressure of 12 mN m^{-1}.
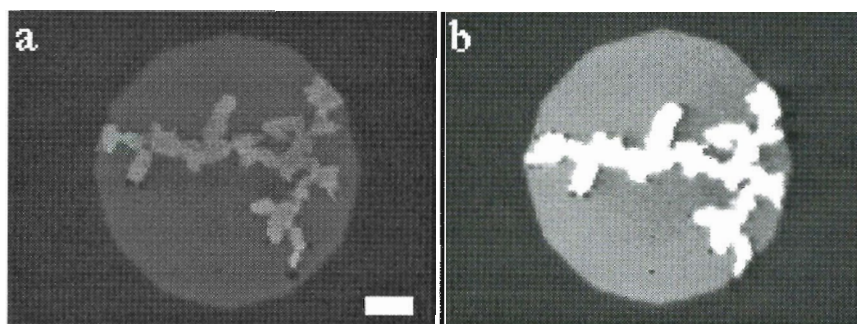
Fig. 3.13 Phase-separated anionic structures in 1:1:1 DPPC:C16Lyso:palmitic acid mixed monolayers. (a) and (b) were imaged with NBD- and H-379-specific filters, respectively. Subphase same as Fig. 3.11. Scale bar is 25 μm.

Phase-separated gray/whitish domains (Fig. 3.13a) surrounded by a fluid lipid matrix are observed as in the 0.2:1:1 case (Figs. 3.9 and 3.10). After injection, the cationic H-379 dye quickly binds to these domains, enhancing their visualization when excited (Fig. 3.13b) through the H-379 filter. Thus, both 0.2:1:1 and 1:1:1 ternary mixed monolayers yield phase-separated anionic domains upon compression that are accessible to H-379 binding. The domains observed in the 1:1:1 system are smaller than those visualized in the 0.2:1:1 system. As the content of DPPC increases in the ternary mixed monolayers, the size of phase-separated anionic domains decreases.

Similar to the domains depicted in Fig. 3.10, images from the 1:1:1 monolayer system show phase-separated domains that appear bright in both fluorescein and rhodamine filter. As shown in Fig. 3.9a, prior to dye injection, phase-separated regions are gray. Again, the adsorption band of H-379 appears to be blue-shifted, allowing its detection through a fluorescein filter. Phase separation also occurred in the 2:1:1 DPPC:C16Lyso:palmitic acid monolayer system on a buffered subphase containing Ca^{2+} at pH 8.9. As in the 1:1:1 system, DPPC was also observed to crystallize during monolayer compression. In the 2:1:1 system, DPPC domains were rarely seen to dissipate. Dissolution rates increase as the DPPC mole fraction in these ternary mixed systems increases. Also notable is the fact that, as DPPC content increases in the ternary lipid systems, phase separation of anionic microstructures decreases. Within the lateral detection limits of fluorescence microscopy (~ 1-5 µm) phase separation of anionic microstructures was not observed to occur in 3:1:1 mixed monolayers.

In the 5:1:1 and 10:1:1 ternary mixed systems, phase separation of anionic domains was not observed with the fluorescence microscope under the same conditions used for visualization of domains in the 0.2:1:1, 1:1:1, and 2:1:1 systems. Though phase-separated anionic microstructures may also exist in ternary mixed systems containing more than 71% DPPC (corresponding to the 5:1:1 mixture), given the resolution of the fluorescence microscope, we are unable to detect them.

Phase separation of anionic fatty acid-containing domains was not observed on either Ca^{2+}-free or acidic subphases (pH 4), regardless of monolayer composition. Neither gray domains under the NBD filter nor bright domains under the H-379 filter are evident under these conditions. Our results are in agreement with the results of Reichert and coworkers [67] in terms of experimental conditions required for anionic domains to phase separate in ternary mixed monolayers. However, their results [67] showed that phase separation of anionic domains was not observed in binary mixed monolayers of 1:1

C16LYSO:palmitic acid. This is contrary to our finding that phase separation of anionic domains is readily observable in this binary mixed system (Fig. 3.11).

3.4 Discussion

A primary motivation to investigate possible phase anomalies occurring in these ternary mixed monolayers has been our observations [42,43], as well as those of our coworkers [67], that PLA_2 hydrolysis of pure phospholipid monolayers first creates a heterogeneous monolayer membrane and subsequently induces PLA_2 aggregation into large, stable, two-dimensional enzyme domains on these interfaces. Our investigations intend to elucidate a mechanism for PLA_2 response to ternary mixed monolayers and the influence of microstructured biomembrane interfaces. We had previously invoked a model where PLA_2 interacted electrostatically, but did not bind, with anionic fatty acid domains [42], plausibly via basic amino acid residues near its binding region. Our adsorption hypothesis was consistent with earlier reports of PLA_2 hydrolysis of lipid vesicles where H-379 dye adsorption and subsequent fluorescence quenching occurs simultaneously with large increases in PLA_2 activity [64]. These phenomena were explained in terms of a lateral phase separation of hydrolytic products within the outer vesicle bilayer leaflet after a critical extent of hydrolysis. More recently, calorimetric data on hydrolyzed vesicles [66,76] appears to confirm this hypothesis that PLA_2 hydrolytic products phase separate in the bilayer at some critical composition, producing complex phase behavior, interfacial microheterogeneity, and an altered membrane that influences subsequent PLA_2 action.

In this present study, the cationic dye H-379 was used as a suitably charged analog of PLA_2 to test this electrostatic adsorption and phase separation hypothesis. Recent results with ternary mixed monolayers now indicate that PLA_2 interacts directly with phase-separated, fatty acid-containing microstructures [42]. Using a diacetylenic carboxylic acid which is immiscible with DPPC in monolayers, Reichert et al. [67] recently showed that PLA_2 would not bind phase-separated carboxylic acid. This result suggests that, along with negative domain charges, lecithin headgroups may also be needed for PLA_2 recognition and binding to phase-separated regions. As reported by Reichert and coworkers [67], however, phase-separated poly(diacetylenic) fatty acid domains appear to exhibit different packing behavior than fatty acid-containing domains visualized in compressed ternary and binary mixed monolayers. Domains observed in this work are gray, suggesting a domain structure that is not closest packed. Reichert's domains [67]

appear black, suggesting a more compact domain structure and higher charge density. It may be that lateral constraints on fatty acid packing, as evidenced in Reichert's work [67], are sufficient to prohibit PLA_2 binding.

In both binary and ternary mixed lipid monolayer systems investigated here, the presence of Ca^{2+} in the subphase has dramatic effects on the ternary mixed monolayer isotherms and fluorescence microscopic observations. This has critical significance to enzyme-induced phase separation because the enzyme requires Ca^{2+} as a hydrolytic cofactor ($K_m = 1$ mM, [77]). As the content of DPPC increases on Ca^{2+}-free alkaline subphases, the isotherm kink seen in Figs. 3.3-3.8 shifts from 16 mN m^{-1} (0.2:1:1 system) to 12 mN m^{-1} (2:1:1 system). This is consistent with the effects of decreasing the relative amounts of perturbing diluents (C16Lyso and palmitic acid) on the DPPC phase transition. As DPPC mole fractions increase in the mixed systems, the phase transitions approach that of a pure DPPC monolayer at these conditions (4 mN m^{-1}) [39].

On Ca^{2+}-containing subphases, this isotherm kink is not observed in the 0.2:1:1 mixture, but is apparent in the 1:1:1 case, and distinct in the 2:1:1 system. This change in behavior compared to Ca^{2+}-free subphases is likely related to the interaction of fatty acid carboxylate anions with Ca^{2+} ions. By referring to the fluid binary C16Lyso:palmitic acid isotherms in Fig. 3.2, it is evident that the 0.2:1:1 monolayers contain large amounts of fluid-expanded "impurities" (C16Lyso) that apparently erase the DPPC phase transition from isothermal detection. *Nevertheless, the fluid-condensed phase transition is readily observable under the microscope in the 0.2:1:1 system (as the appearance of black, condensed DPPC domains).* The condensed DPPC domains quickly disappear, however, when compression ceases and the monolayer relaxes at constant surface pressure (on the order of minutes), indicating that this phase transition is a non-equilibrium result of the monolayer compression. As the monolayer content of DPPC increases, the effects of DPPC phase transition are less prominent (condensed DPPC domains take hours to disappear in systems containing greater than 50 mol% DPPC). This result indicates that microphase separation and full first-order phase transitions may occur under non-equilibrium conditions even though they are not detectable in surface pressure-area isotherms.

Finally, kinks observed at high surface pressure (> 30 mN m^{-1}) are consistent with C16Lyso and/or palmitic acid leaving the monolayer for the bulk subphase, or forming a multilayered film. Smaller molecular areas beyond the collapse points do not reflect true film molecular areas since expelled C16Lyso or palmitic acid no longer contribute to mean

molecular area. Pure DPPC monolayers show collapse at molecular areas of approximately 45 Å molecule^{-1} close to surface pressures of 70 mN m^{-1} 9 (Fig. 3.1a) [39]. We conclude that, while DPPC remains in the film to substantial surface pressures (>65 mN m^{-1}), the other monolayer components are ejected, certainly above a lateral pressure of 34 mN m^{-1} for C16Lyso and 45 mN m^{-1} for palmitic acid.

With respect to the pure isotherm of DPPC and C16Lyso, the first-order DPPC fluid-condensed phase transition remains evident in the ternary mixed monolayer systems under the experimental conditions. The prominence of this transition in the mixtures, however, is strongly correlated to film compression rates. Slower rates (3 Å^2 molecule^{-1} minute^{-1}) still yield kinks in the mixed isotherms; however, they are not as sharp as the kinks observed using compression rates of 12 Å^2 molecule^{-1} minute^{-1}. This behavior is consistent with the rate dependence of DPPC SC phase coexistence in fluorescence observations at the air-buffer interface. Thus, the DPPC SC phase coexistence can be suppressed using slow compression rates. The molecular areas of the ternary mixed systems, as expected, resemble those of the PC constituents; palmitic acid has a very small contribution to monolayer mean molecular area except at high molar contents.

Comparing the binary mixed monolayer isotherm (Fig. 3.2) with the isotherms of pure palmitic acid and C16Lyso (Fig. 3.1b,c), we observed that the phase transition of palmitic acid is also absent in these binary mixed systems. Due to palmitic acid's relatively small headgroup area, the mean molecular areas of the binary films are closer to those of pure C16Lyso than palmitic acid. As previously noted for the ternary mixed systems, caution must be used in interpreting the isotherms at low molecular areas where C6Lyso or palmitic acid do not contribute to molecular area due to possible collapse mechanisms. C16Lyso is unlikely to remain in the monolayer at lateral pressures greater than 34 mN m^{-1} (Figss 3.1c and 3.2) unless significant cooperative interactions with palmitic acid exist to condense the monolayer molecular areas and increase collapse pressures.

Regardless of subphase pH, when Ca^{2+} is absent, lateral phase separation of anionic domains is not observed with fluorescence microscopy. Since 100 mM NaCl is used in two subphase systems, it appears that charge screening is not strong enough to prevent phase separation by divalent cations. Unfortunately, isothermal compressions provide ambiguous information on phase separation behavior. The observed kinks in the isotherms at pressures below 16 mN m^{-1} are consistent with DPPC transitions and not fatty acid phase separation, since fatty acid domains phase separate at lower pressures (fluorescence microscopy). In the 0.2:1:1 monolayer system, lateral phase separation is

observed to occur at low surface pressures, well below those for the kinks (< 5 mN m^{-1}), and remains to surface pressures of at least 20 mN m^{-1}. The same holds true for the 1:1:1 and 2:1:1 systems. The isotherm exhibits no inflections in the high molecular areas (low pressure) that are consistent with fluorescent microscopic detection of monolayer phase separation. However, comparison between isotherms on Ca^{2+}-containing and Ca^{2+}-free subphases indicates major monolayer packing differences which are attributed to the presence and absence of monolayer microstructure, respectively.

We have noticed that the kinks observed in isotherms of these mixed lipid systems are sensitive to film compression rates. One interesting aspect of this problem is the kinetic dependence of ternary miscibility and its possible significance to the formation of enzyme domains in hydrolyzed monolayers. Using very slow compression rates (<1 Å^2 molecule^{-1} minute^{-1}) on the microscope film balance, DPPC fluid-condensed phase transitions (crystallization) can be avoided under these conditions in mixed monolayers, yet phase separation of fatty acid-containing domains is observed. Faster compression rates (>3 Å^2 molecule^{-1} minute^{-1}) lead to transient formation of condensed DPPC domains which disappear at constant surface pressure as the monolayer relaxes. DPPC solid domain dissolution is coupled with the appearance of phase-separated fatty acid domains. With an increasing mole fraction of DPPC, solid DPPC domain-dissolution time is increased (from minutes with 0.2:1:1 to hours with 2:1:1). The observed coexistence of transient DPPC solid phases and stable phase-separated palmitic acid-containing domains at constant surface pressure is interpreted as a non-equilibrium condition created by rapid mixed monolayer compression. Relaxation towards equilibrium occurs by kinetically controlled phase separation of fatty acid simultaneously with the disappearance of DPPC condensed phases. Previous reports of PLA$_2$ domain formation indicate that these domains build slowly [42,43] as fatty acid is released from hydrolytic monolayer sites and must laterally diffuse to form surface aggregates. Therefore, both mixed ternary monolayer and enzyme-hydrolyzed monolayers share this element of diffusion control which appears to be important to similarities in their phase behavior.

Although the anionic nature (ionized fatty acid content) of phase-separated areas has been shown directly by cationic dye binding, the molecular composition of phase-separated regions remains unelucidated. Moreover, the anionic domains in the 0.2:1:1 and binary mixed systems show interior structure (Figs. 3.10 and 3.11). The central regions of these domains contain surface-active material which appears black in both fluorescence filters (area devoid of fluorescent probe). The areas spiral out from each domain center, but never

extend completely to the outer domain edges. These arms are not observable in the 1:1:1 or 2:1:1 ternary mixed lipid systems. This may be due to the decreased size of the 1:1:1 and 2:1:1 phase-separated domains (as DPPC content increases, anionic domain size decreases). Thus, these radial arm structures may be present in the other ternary mixed monolayers but are beyond the resolution of the optical instrumentation.

At this time, we are unable to explain this observation but surmise that it may be a result of non-equilibrium processes associated with phase separation induced by monolayer compression. Justification for this argument comes from our previous reports [42,43], and more recent evidence [67] where slow, enzyme-induced monolayer phase separation yields optically homogeneous domain structures lacking these dark, inner microstructures. Although both enzymatically hydrolyzed and compressed mixed monolayers exhibit somewhat similar phase-separated behaviors and domain morphologies, dye adsorption often yields domain heterogeneities under compressed ternary monolayers.

To summarize this chapter's findings, duplication of phase-separated anionic monolayer domains in ternary mixed lipid systems that resemble the shape and size of two-dimensional PLA_2 domains obtained in monolayer hydrolysis experiments [42,43] is possible. Our results with the ternary mixtures are in agreement with the results of Reichert and coworkers [67], but we have been able to visualize phase separation in binary mixed C16Lyso:palmitic acid systems in which they reported a homogeneously mixed monolayer [67,78].

The cationic dye probe H-379 has proven to be a simple, yet effective model for clarifying the PLA_2 adsorption hypothesis. Moreover, we are able to delineate monolayer phase anomalies as a function of surface pressure, resulting directly from ternary mixing incompatibilities. Additionally, Ca^{2+} plays a major role in condensing and inducing microstructure in the investigated ternary mixed monolayers. The presence of Ca^{2+} and alkaline subphases are mandatory to visualize lateral phase separation of palmitic acid-containing domains in ternary systems. Regardless of whether or not Ca^{2+} is present, phase separation of negatively charged, palmitic acid-containing domains on acidic subphases is not observed. Phase-separated anionic domains in mixed monolayers are accessible to the cationic PLA_2 model probe H-379 and closely resemble previously observed PLA_2 domains produced by phospholipid hydrolysis [42,43].

These data support a type of monolayer phase behavior where miscibility of components depends on monolayer composition and interfacial charge. Conditions which create net neutral monolayer-resident species (protonated fatty acid, zwitterionic C16Lyso,

and phospholipid) abolish monolayer microstructuring in the presence of Ca^{2+}. Consistent with this behavior is an electrostatic dependence for PLA_2 and H-379 adsorption to negatively charged, phase-separated regions. Duplication of PLA_2 domain formation [42,43] with charged dye (H-379) is compelling evidence for electrostatically driven enzyme interaction with phase-separated regions of hydrolyzed monolayers and possible interfacial mechanistic control of enzymatic activity.

CHAPTER FOUR

PLA$_2$ DOMAIN FORMATION IN HYDROLYZED ASYMMETRIC PHOSPHOLIPID MONOLAYERS AT THE AIR-WATER INTERFACE

4.1 Introduction

Previously, Grainger and coworkers showed that PLA$_2$-hydrolyzed phospholipid monolayers at the air-water interface exhibit two-dimensional enzyme domains in the monolayer plane [42,43]. A scheme describing interfacial PLA$_2$ domain formation has been proposed [42,43] where PLA$_2$ adsorbs electrostatically to phase-separated regions enriched in fatty acid reaction products released by PLA$_2$ in the monolayer membrane.

Using fluorescence microscopy at the air-water interface, we have recently investigated ternary mixed monolayers of phospholipid, lyso-lipid, and fatty acid [79]. In complete absence of enzyme, negatively charged, phase-separated domains resembling PLA$_2$ domains are observed in these ternary mixed monolayers and adsorb water-soluble cationic fluorescent dye. Ternary mixed monolayer phase separation and dye adsorption can be blocked by lowering monolayer subphase pH, indicating that the phase-separated monolayer domains comprise negatively charged fatty acids. Moreover, the presence of Ca^{2+} in alkaline monolayer subphases is essential for fatty acid phase separation [79]. This is most likely related to the ability of Ca^{2+} to chelate multiple ionized fatty acid carboxylate headgroups at the monolayer interface. Further work with binary mixed monolayers of lyso-lipid and fatty acid (no enzyme present) also showed that phase separation of fatty acid regions occurred simply in response to monolayer compression. Thus, compression of binary and ternary mixed monolayers containing lipid, lyso-lipid and fatty acid results in film phase separation, leading to monolayer regions comprising fatty acid [79].

In a separate study by coworkers [67], phase-separated fatty acid regions were purported to also contain lyso-lipid and/or phospholipid since PLA$_2$ did not adsorb to laterally phase-separated, polymerized anionic diacetylenic carboxylic acid domains in a fluid phospholipid monolayer matrix. Control experiments consisting of PLA$_2$ injection beneath pure palmitic acid or pure C16Lyso monolayers at the air-buffer interface did not

result in the formation of regular 2-D enzyme domains similar to those evidenced in DPPC hydrolysis experiments [42,43]. Instead, we now show that PLA2 can electrostatically bind pure palmitic monolayers, forming a homogeneous, dense protein interfacial film having solid-like properties and lacking any resemblance to the enzyme domains. Pure lyso-lipid monolayers bind no detectable PLA2 as determined by fluorescence microscopy.

Clearly, the presence of monolayer-resident fatty acid or lyso-lipid alone is insufficient in inducing PLA2 domain formation that is observed during phospholipid monolayer hydrolysis. This is supported by previous work which showed that (1) enzyme domains form in partially hydrolyzed phospholipid films when substrate is still present [43], and (2) phase-separated regions of regular morphology are only observed in mixed monolayers when phospholipid is present. During lipid hydrolysis, membrane regions enriched in fatty acid and most likely containing small amounts of lyso-lipid and/or substrate are compelled to phase separate. While the presence of lyso-lipid and/or DPPC substrate may be important for PLA2 interfacial binding, phase-separated fatty acid reaction products are crucial for domain formation. The presence of lyso-lipid and/or phospholipid substrate together with fatty acid appears to be essential to promote phase separation into the observed regular microstructure. If phospholipid is present in phase-separated monolayer regions, the stoichiometry of phospholipid to fatty acid is unknown.

We present here our investigations of PLA2 hydrolysis of asymmetric lipid monolayers containing either 1-caproyl,2-palmitoyl- and 1-palmitoyl,2-caproyl-sn-3-phos-phatidylcholine (Fig. 4.1) at the air-water interface. Three different enzyme sources (pancreatic, bee and N. naja naja) were used in this study. Asymmetric lipid hydrolysis at the air-water interface was characterized using film balance techniques, and "cut-off" surface pressures for PLA2 activity were determined. Dual-label fluorescence microscopy was employed to visualize lipid monolayer-enzyme interactions in situ. In addition, measurement of surface potential as a function of monolayer hydrolysis time allowed the electrochemical characterization of these hydrolyzed asymmetric monolayers.

According to the PLA2-fatty acid adsorption hypothesis, enzymatic hydrolysis of asymmetric lipids which contain short chain, water-soluble fatty acids in the sn-2 position should not produce 2-D enzyme domains. Dissolution of fatty acid reaction products into the bulk subphase should prevent lateral monolayer phase separation of fatty acids, thus inhibiting PLA2 domain formation. Conversely, observation of PLA2 domains upon hydrolysis of asymmetric phospholipids containing a long-chain, water-insoluble fatty acid

in the sn-2 position and a water-soluble lyso-lipid would suggest that the presence of the corresponding lyso-lipid species is not necessary for enzyme domain formation.
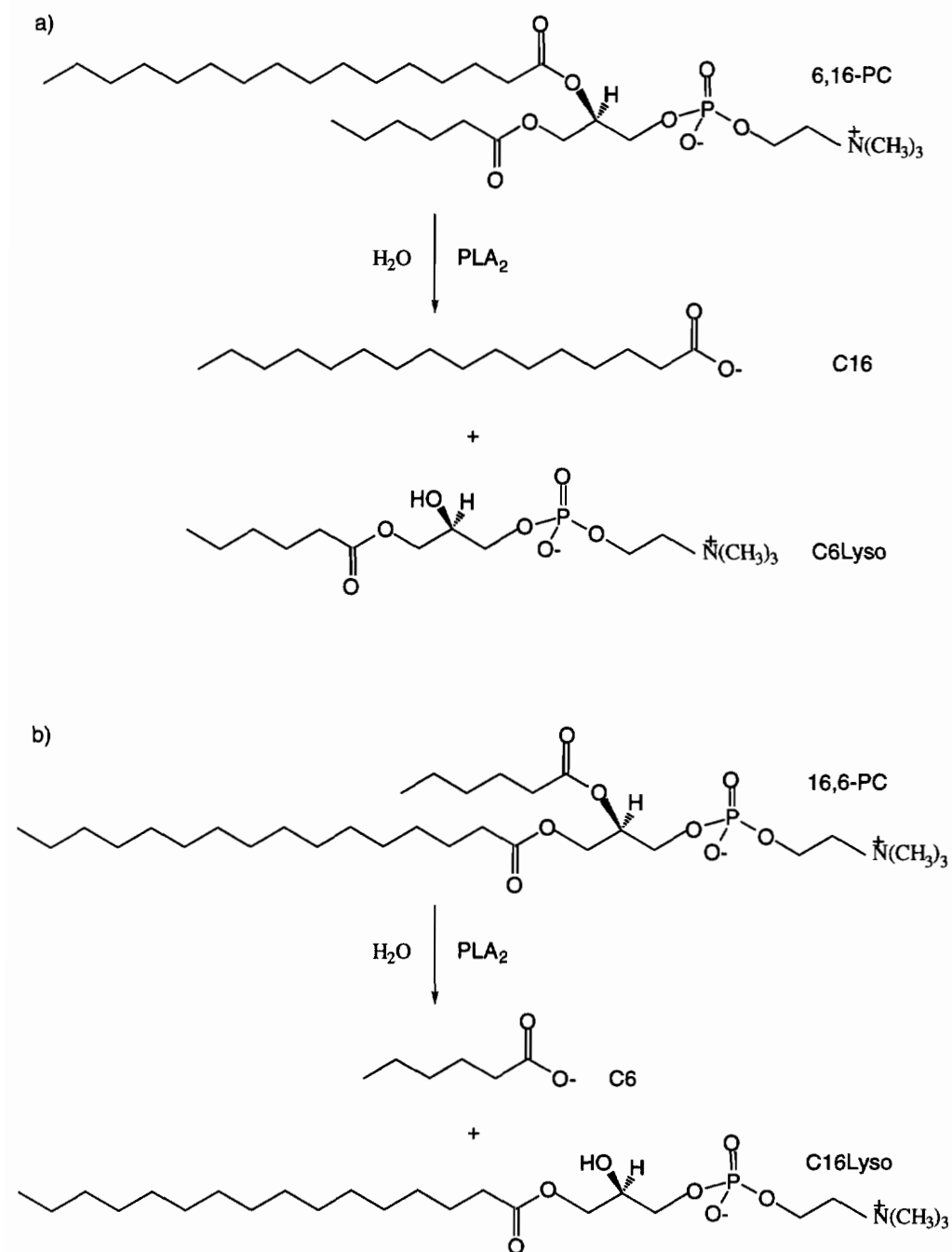
Fig. 4.1 Reaction products of PLA$_2$-catalyzed hydrolysis of (a) 6,16-PC and (b) 16,6-PC.

4.2 Experimental

4.2.1 Materials

Asymmetric phospholipids 1-caproyl-2-palmitoyl-sn-3-phosphatidylcholine and 1-palmitoyl-2-caproyl-sn-3-phosphatidylcholine (Fig. 4.1) were synthesized by the fatty acid imidazole method using the appropriate lyso-lipid (Avanti Polar Lipids, AL) and fatty acid in a ratio of 1:5:6 lyso-lipid:fatty acid:carbonyldiimidazole (Aldrich) as described previously [80,81]. The asymmetric phospholipids were purified by elution through two silicic acid (BioRad) columns with a $CHCl_3$/MeOH gradient. Analysis of the pooled PC fraction by thin layer chromatography revealed a single spot whose R_f was consistent with diacyl-PC. Isomeric purity was judged by two methods: ^{13}C NMR spectroscopy and GC analysis after PLA_2 hydrolysis. The ^{13}C chemical shifts of α-CH_2 carbons are sensitive to chain length (especially if one is relatively short) as well as sn-1 versus sn-2 placement [81,82]. A natural abundance ^{13}C NMR spectrum of 16,6-PC will exhibit more than two resonances for the α-carbon if a significant portion of 6,16-PC is also present; the detection limit by NMR is <10%. Only two α-CH_2 resonances were visible in the ^{13}C NMR spectrum of each asymmetric lipid dissolved in CD_3OD, consistent with contamination by the other isomer of <10%. A more quantitative estimate of this value was provided by GC analysis of the fatty acids generated by PLA_2 hydrolysis of each preparation [82]. GC analysis of fatty acyl methyl esters, prepared using BF_3/methanol catalysis [83] of the two separate synthetic batches of 6,16-PC, yielded 2.0 and 4.4% contamination by caproic acid; for two separate batches of 16,6-PC, the contamination was 3.8 and 6.1% contamination by palmitic acid. Thus, each asymmetric PC is contaminated with the other isomer to, at most, 6%.

4.2.2 Fluorescence Microscopy

Monolayer compression rates were typically 2 $Å^2$ molecule^{-1} minute^{-1}. PLA_2 was injected into the monolayer subphase (approximately 5 μg) from behind the trough barrier at 15 mN m^{-1}. When BSA was used, PLA_2 injection always followed BSA addition (30 minutes after BSA injection). Monolayer subphase BSA concentration was 25 nM. Fluorescence experiments were carried out at 30°C.

4.3 Results

4.3.1 Asymmetric Lipid Isotherms

Surface pressure-area isotherms for 6,16-PC and 16,6-PC on buffered subphases are shown in Fig. 4.2.
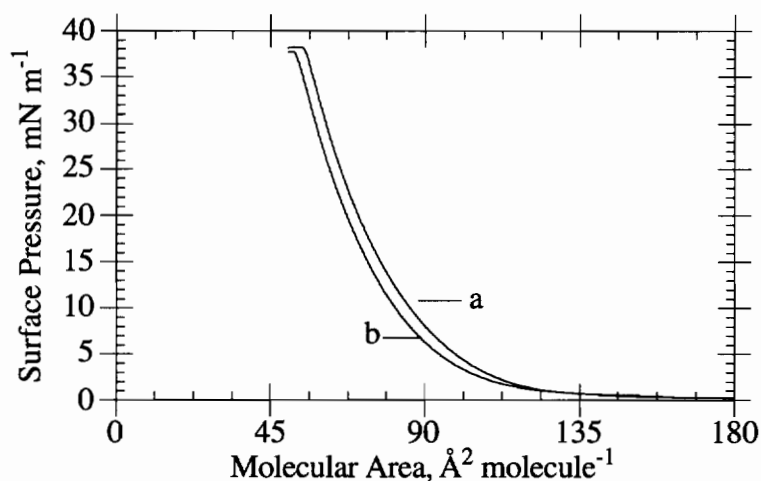
Fig. 4.2 Monolayer compression isotherms for (a) 6,16-PC and (b) 16,6-PC. Compression rate is 1.1 Å^2 molecule^{-1}. Subphase conditions: 100 mM NaCl, 5 mM CaCl$_2$, 10 mM Tris, pH 8.9, T = 20°C.

Monolayer compression isotherms for both lipids are nearly identical and exhibit only liquid-expanded behavior with no apparent phase transitions. Onsets of surface pressure occur at 175 Å^2 molecule^{-1} for both monolayers with collapse at 37 mN m^{-1} and 52 Å^2 molecule^{-1}. Pure 6,16-PC and 16,6-PC monolayers are very stable as Δarea/Δtime is 0.02 Å^2 molecule^{-1} minute^{-1} at a constant surface pressure of 30 mN m^{-1}. 16,6-PC monolayers collapse at low pressures (37 mN m^{-1}) and at a molecular area of 52 Å^2 molecule^{-1}. Comparison of 16,6-PC with DPPC monolayers at the air-water interface shows that the 6 carbon difference in the sn-2 acyl chain length leads to very different monolayer phase behavior. 16,6-PC does not undergo any detectable phase transitions (even at 5°C) as observed by fluorescence microscopy and surface pressure isotherms. Monolayer compression isotherms and fluorescence microscopy of DPPC show a phase transition characterized by a coexistence of solid and fluid monolayer phases [37,39]. 16,6-PC monolayers at 30°C collapse at low pressures (37 mN m^{-1}) and at a molecular area

of 52 Å^2 molecule^{-1}. In contrast, DPPC monolayers are well-known to collapse at high surface pressures (70 mN m^{-1}) at 53 Å^2 molecule^{-1} at the same temperature [39]. Comparing 16,6-PC (or 6,16-PC) molecular areas at monolayer collapse with DPPC collapse areas (above critical temperature, T_c) we find that these collapse areas are similar (52 Å^2 molecule^{-1} for 16,6-PC and 6,16-PC, and 53 Å^2 molecule^{-1} for DPPC at 43°C [39]). Thus, fluid monolayer packing for 16,6-PC and 6,16-PC resembles fluid phase DPPC monolayer packing above T_c. Interestingly, interchanging the palmitic and caproic acid acyl chains in phosphatidylcholine positional isomers has little effect on observed physical monolayer properties.

4.3.2 PLA$_2$-Catalyzed Hydrolysis of Asymmetric Lipid Monolayers

N. naja naja and bee venom PLA$_2$ exhibit hydrolytic activity towards both 6,16-PC and 16,6-PC at all lateral surface pressures up to monolayer collapse, while pancreatic PLA$_2$ exhibits hydrolytic activity only at lower pressures. Decreasing monolayer surface pressures for each lipid step-wise from 30 mN m^{-1}, the upper surface pressure onset of pancreatic PLA$_2$ hydrolytic activity was found to be approximately 18 mN m^{-1} for both 16,6-PC and 6,16-PC [data not shown]. Blocking of pancreatic PLA$_2$ hydrolytic activity at high monolayer surface pressures has been similarly reported using dinanoylphosphatidylcholine substrate monolayers [84]. This previous work showed source-specific cut-offs: cobra and bee venom PLA$_2$ exhibited hydrolytic activity up to monolayer surface pressures of 34.8 and 35.3 mN m^{-1}, respectively, while pancreatic PLA$_2$-catalyzed lipid monolayer hydrolysis occurred only at much lower surface pressures (16.5 mN m^{-1}).

As shown in Figs. 4.3 and 4.4, lipid molecular area and surface potential (ΔV) at constant surface pressure (15 mN m^{-1}) are plotted as functions of hydrolysis time for *N. naja naja* PLA$_2$-catalyzed hydrolysis of 16,6-PC and 6,16-PC monolayers, respectively. Three distinct regions can be seen in these curves. The first segment, AB, corresponds to a stable monolayer molecular area at 15 mN m^{-1} as a function of time for both pure lipid monolayers prior to the introduction of PLA$_2$. PLA$_2$ was injected into the monolayer subphase at point B (see arrow). An immediate decrease in molecular area and surface potential after enzyme injection is apparent and continues until point C is reached. Point C corresponds exactly to the point where extrapolated segments BC and CD cross: the end of monolayer hydrolysis. Segment CD shows the molecular area of the hydrolysis products

remaining at the surface once hydrolysis is complete. This last segment reflects the stability of the remaining hydrolyzed mixed film.

Upon completion of 16,6-PC monolayer hydrolysis (Fig. 4.3, point C'), short-chain caproic acid reaction products (C6) (Fig. 4.1) should be solubilized in the monolayer subphase (C6 solubulity in $H_2O \sim 9.6$ mg/ml, [85]), with monopalmitoyl-PC (C16Lyso) remaining at the air-buffer interface.

Fig. 4.3 Surface potential (—) and molecular area (— — —) versus 16,6-PC monolayer hydrolysis time at constant surface pressure (15 mN m^{-1}). 20 μg cobra PLA$_2$ injected into monolayer subphase at point B. Subphase conditions same as in Fig 4.2.

Molecular area at the end of 16,6-PC hydrolysis should thus correspond to the area of a pure C16Lyso monolayer at this surface pressure (50 Å^2 molecule^{-1}). Fig. 4.3 shows that the molecular area for PLA$_2$-hydrolyzed 16,6-PC monolayers decreases from 74 to 49.5 Å^2 molecule^{-1} (from point B' to C'), almost identical to the area of a pure C16Lyso monolayer under these conditions. Slow decreases in molecular area subsequently observed in segment C'D' from 49.5 to 45 Å^2 molecule^{-1} are due to the intrinsic instability of the residual C16Lyso monolayer. Indeed, pure C16Lyso monolayers compressed to 15

mN m^{-1} show time-dependent molecular areas which slowly decrease with a slope very similar to the slope of segment C'D' [data not shown].

Similarly, in Fig. 4.3 the observed decrease in surface potential from 357 to 248 mV (from point B to C) upon PLA$_2$ hydrolysis is due to the change in the electrochemical properties of the film. The surface potential for pure 16,6-PC monolayers before PLA$_2$ hydrolysis (point B, 357 mV) decreases to a value (point C, 248 mV) close to the surface potential for pure C16Lyso monolayers (220 mV) [data not shown] under the same conditions. In contrast to molecular area data, the slope of segment CD remains nearly zero once PLA$_2$ hydrolysis is complete with only a small observable increase in surface potential (248 to 257 mV) over time. For this experiment, we have estimated that the 6% 6,16-PC impurity can lead to a difference of approximately 10 mV in the final value for the surface potential and approximately 3 Å^2 molecule^{-1} in the final molecular area. It is thus clear that such a small difference does not affect our results.
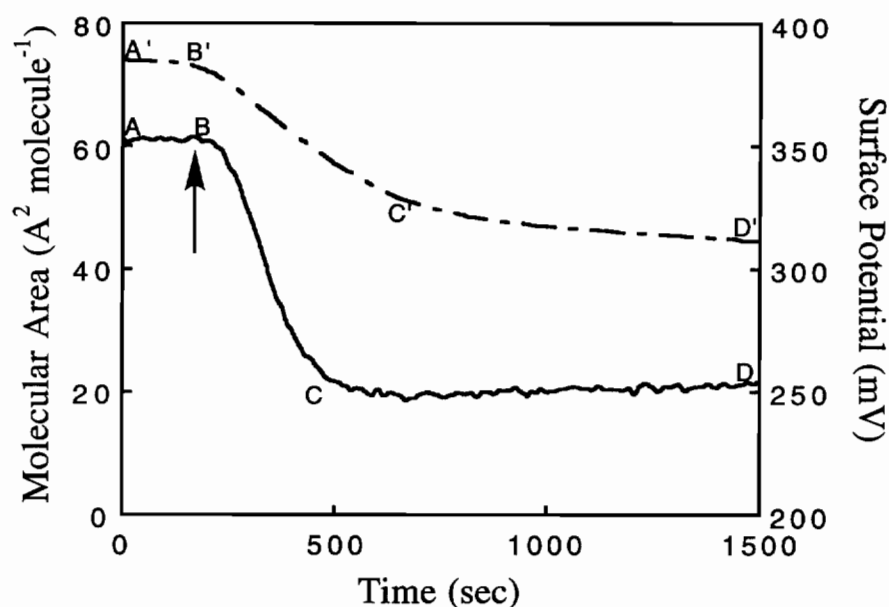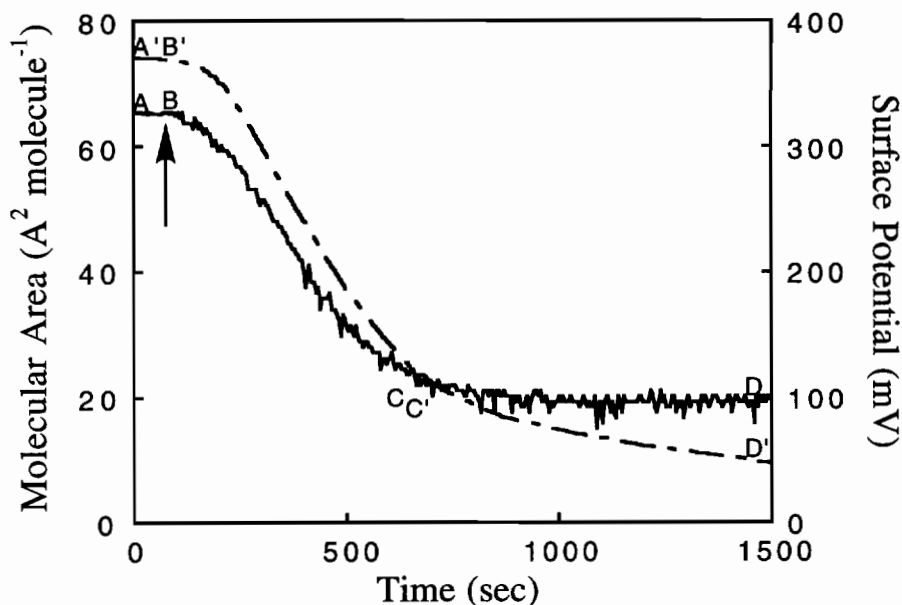

Fig. 4.4 Surface potential (—) and molecular area (— – —) versus 6,16-PC monolayer hydrolysis time at constant surface pressure (15 mN m^{-1}). 20 μg cobra PLA$_2$ injected into monolayer subphase at point B. Subphase conditions same as in Fig. 4.2.

Similar behavior can be seen in Fig. 4.4 for *N. naja naja* PLA$_2$-catalyzed hydrolysis of 6,16-PC monolayers. However, in this case, palmitic acid reaction products remain at the interface and C6Lyso product is solubilized in the monolayer subphase (Fig. 4.1). Dissolution of C6Lyso leads to very large decreases in molecular area (from 74 to 19 Å^2 molecule^{-1}, segment B'C') and in surface potential (from 328 to 100 mV, segment BC). Monolayer molecular area at point C' very closely matches the area for pure palmitic acid monolayers under these conditions (19.4 Å^2 molecule^{-1}) [68,79]. However, the surface potential at point C (100 mV) is much larger than that for pure palmitic acid monolayer under similar conditions (-30 mV) [data not shown]. We have estimated that the 4% 16,6-PC impurity leads to a difference of approximately 5 mV in the final surface potential measurements and 1 Å^2 molecule^{-1} in the final film molecular area. These small differences can also be neglected and do not affect our results. A flat plateau in surface potential is observed when lipid hydrolysis is complete (segment CD), whereas a steady decrease in molecular area is observed from point C' to D'. This decrease in molecular area is due to the intrinsic instability of pure palmitic acid monolayers under these conditions. Pure palmitic acid films compressed to 15 mN m^{-1} show molecular areas which decrease slowly over time. This rate of change in molecular area is similar to that seen in the slope of segment C'D'. Use of bee or pancreatic PLA$_2$ produces surface potential and molecular area kinetics similar to those shown in Figs. 4.3 and 4.4 for the cobra PLA$_2$.

4.3.3 Fluorescence Microscopy of PLA$_2$ Hydrolyzed 6,16-PC and 16,6-PC Monolayers

PLA$_2$ action on 6,16-PC and 16,6-PC monolayers was further characterized using dual-label fluorescence microscopy at the air-water interface. Fig. 4.5 shows fluorescence micrographs of PLA$_2$-hydrolyzed 6,16-PC monolayers after 90 minutes. Image pair 4.5a and b correspond to *N. naja naja* PLA$_2$-hydrolyzed monolayers while c and d, and e and f correspond to bee venom and bovine pancreatic PLA$_2$-hydrolyzed monolayers, respectively. Figs. 4.5a, c, and e are imaged through a rhodamine-specific filter, revealing the location of lipid monolayer (Rhod-DPPE) probe approximately 90 minutes after enzyme injection. Phase-separated gray regions surrounded by brighter fluid phase lipid are evident. These domains appear gray due to selective partitioning and enrichment of the rhodamine-labeled lipid probe into the surrounding fluid monolayer phase [37,41]. Figs.
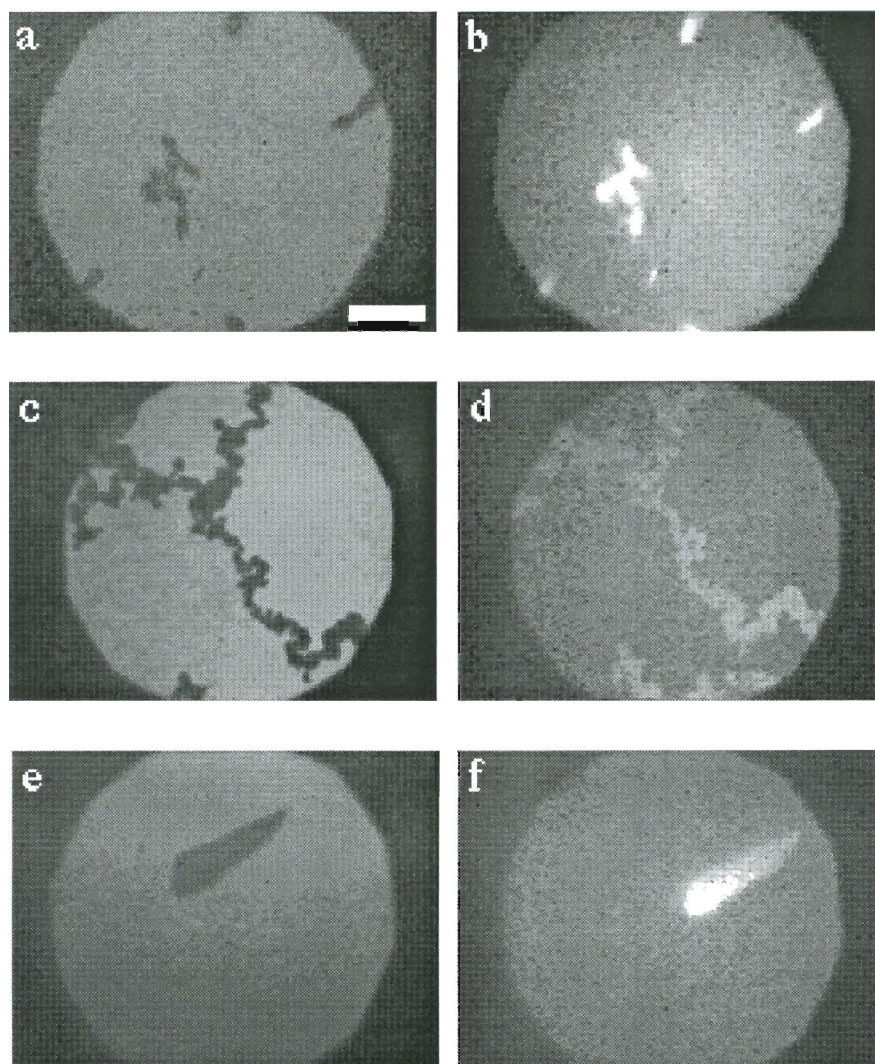
Fig. 4.5 Fluorescence micrographs of PLA$_2$-hydrolyzed 6,16-PC monolayers 90 minutes after enzyme injection. Micrographs in (a), (c), and (e) were imaged through a rhodamine-specific fluorescence filter, whereas (b), (d), and (f) were imaged through a fluorescein-specific fluorescence filter. Phase-separated regions observable in (a), (c) and (e) correspond exactly to the location of FITC-labeled PLA$_2$ fluorescence in (b), (d) and (f). Image pairs (a)-(b), (c)-(d) and (e)-(f) correspond to cobra, bee and pancreatic PLA$_2$-hydrolyzed monolayers, respectively. Monolayer hydrolysis was carried out at constant surface pressure (15 mN m^{-1}). Subphase conditions same as in Fig. 4.2. Scale bar in (a) is 25 μm.

4.5b, d, and f are imaged with a fluorescein-specific filter and show the location of fluorescein-labeled PLA$_2$ [42,43]. The location of FITC-PLA$_2$ consistently corresponds to the phase-separated gray regions shown in micrographs 4.5a, c, and e, supporting adsorption of PLA$_2$ specifically to these areas.

With 6,16-PC monolayers, PLA$_2$ formed interfacial domains prior to the completion of hydrolysis. In contrast, several hours are necessary to observe any PLA$_2$ domain formation upon hydrolysis of fatty acid-soluble 16,6-PC lipid monolayers, and it appears that domain formation does not occur during hydrolysis. PLA$_2$ domains that are observed after long waiting periods are smaller and fewer in number than PLA$_2$ domains observed with fatty acid-insoluble 6,16-PC monolayer hydrolysis (Fig. 4.6). They also lack any appreciable regular morphology. Moreover, addition of fatty acid-binding bovine serum albumin (BSA) to the 16,6-PC monolayer subphase results in total suppression of PLA$_2$ domain formation. Several control experiments were conducted to assess the possibility that lipid impurities in 16,6-PC monolayers might be responsible for the observed PLA$_2$ domain formation. In particular, lipid positional isomers as byproducts of the synthesis and acyl chain migration products could contribute to the presence of 6,16-PC contaminants in otherwise pure 16,6-PC samples. As described in the experimental section, 16,6-PC lipid samples contained between 3.8 and 6.1% 6,16-PC. Given this level of impurity in the 16,6-PC lipid sample, a completely hydrolyzed 16,6-PC monolayer should consist of 94% C16Lyso (from 16,6-PC) and 6% palmitic acid (from the 6,16-PC impurity). The caproic acid and C6Lyso reaction products from 16,6-PC and 6,16-PC, respectively, are solubilized. Therefore, a binary mixed monolayer consisting of 94% C16Lyso and 6% palmitic acid would be expected from this experiment in the worst case. To test this scenario for possible influence on PLA$_2$ domain formation, a monolayer of 94% C16Lyso and 6% palmitic acid was compressed to 15 mN m^{-1} and imaged using fluorescence microscopy. Results showed that at 15 mN m^{-1}, the monolayer remained completely fluid, showing no evidence of palmitic acid phase separation within the microscope's resolution. Moreover, compression of this binary mixed monolayer to 15 mN m^{-1} followed by injection of FITC-labeled PLA$_2$ into the subphase lead to no observable enzyme domain formation even after a 10-hour incubation period. Based on the enzyme domain data presented in Fig. 4.6 and the results of the preceding control experiments, PLA$_2$ domain formation in the 16,6-PC case does not appear to be due to the 6% 6,16-PC impurity found in 16,6-PC lipid samples.

Addition of BSA to 6,16-PC monolayer subphases during PLA_2-catalyzed hydrolysis does not have any effect upon PLA_2 domain formation. Additionally, identical hydrolysis experiments performed with PLA_2 using platelet activating factor (PAF, 1-O-alkyl-2-acetyl-sn-3-phosphatidylcholine), resulting in the formation of water-soluble acetic acid and a long-chain surface active lyso-lipid, were compared with the behavior of 16,6-PC. PLA_2 hydrolysis of PAF monolayers failed to produce PLA_2 aggregates at the air-buffer interface as evidenced by fluorescence microscopy [data not shown]. Significantly, pure monolayers of palmitic acid and lyso-lipid were each exposed to fluorescently labeled PLA_2. Both experiments failed to produce monolayer domains resembling those from other hydrolysis experiments. While lyso-lipid monolayer experiments were identical to PAF results (i.e., no observable enzyme binding), pure palmitic acid monolayers promoted the rapid, homogeneous adsorption of enzyme to the interface, producing condensed, rigid protein films shown in Fig. 4.7.
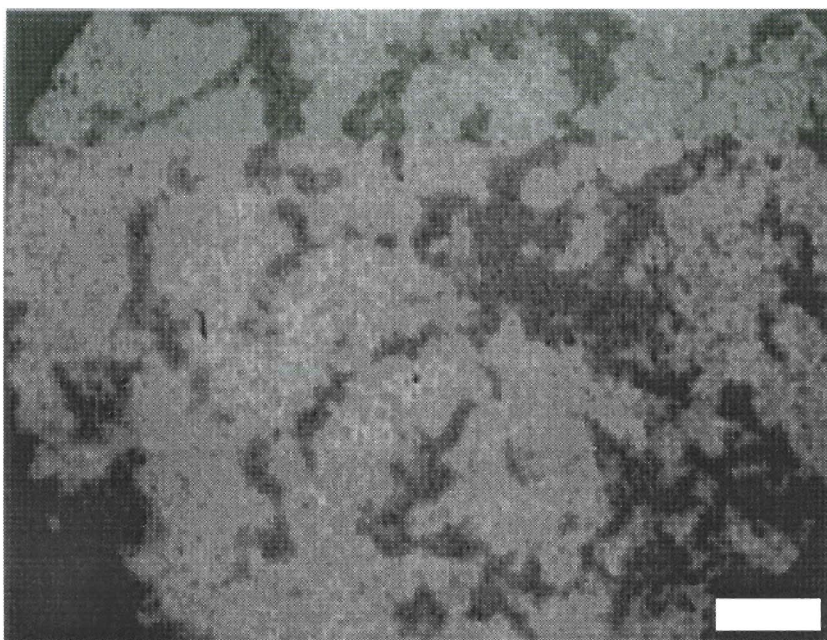
Fig. 4.7 PLA_2 adsorbed to pure palmitic acid monolayers on 100 mM NaCl, 10 mM Tris, 5 mM $CaCl_2$, pH 8.9, subphase at 15 mN m^{-1} (courtesy M. Grandbois). Scale bar is 50 μm.

Except for regions of the monolayer that exhibit fissures, these adsorbed PLA_2 films do not exhibit any monolayer microstructure; protein adsorption to the fatty acid

membrane is uniform and featureless. Moreover, upon monolayer expansion after adsorption at a lateral pressure of 15 mN m^{-1}, the protein-fatty acid composite film becomes more highly fissured [data not shown], indicative of a solid-state film property inconsistent with results from previous enzyme domains in other monolayer systems [42,43,67,79].

4.4   Discussion

We and coworkers have previously proposed that, under suitable conditions, critical amounts of PLA$_2$-produced fatty acids lead to hydrolyzed monolayer lateral phase separation of negatively charged fatty acids [42,43]. Positively charged PLA$_2$ amino acid residues, known from the three-dimensional crystal structures of these enzymes to form surface-exposed cationic patches [86-88], then bind electrostatically to negatively charged fatty acid microstructures. PLA$_2$ hydrolysis studies, using isomeric asymmetric phospholipid monolayers that produce water-soluble fatty acid products in one case and water-soluble lyso-lipid in another (Fig. 4.1), have been used in this work to help elucidate the mechanism of enzyme domain formation.

The central tenet of the enzyme domain formation hypothesis is that PLA$_2$-produced fatty acid reaction products laterally phase separate after hydrolysis, with electrostatically driven enzyme adsorption either concomitant with or subsequent to this monolayer microstructuring [42,43]. Consequently, if fatty acid reaction products are removed from the monolayer interface, PLA$_2$ adsorption would be inhibited. This is accomplished using enzyme-produced water-soluble fatty acid reaction products such as the 16,6-PC substrate (Fig. 4.1b).

Surface potential and molecular area hydrolysis kinetic data for 16,6-PC (Fig. 4.3), support the formation of pure C16Lyso monolayers following PLA$_2$ action. This directly supports rapid solubilization of short-chain caproic acid products into the subphase during hydrolysis. However, fluorescence microscopy does not entirely support this conclusion. Small PLA$_2$ domains are still observed with microscopy after long periods of incubation (Fig. 4.6). If the hypothesis is correct, caproic fatty acids should be associated with these PLA$_2$ domains at the interface. These results could be explained by the well known interactions between PLA$_2$ and solubilized fatty acids [89] which would occur in the bulk subphase, promoting delayed enzyme adsorption to the interface. PLA$_2$ interaction with soluble caproic acid in the subphase by an acylation mechanism or simply ion-pair

formation with basic amino acids [89] would render the enzyme more surface active and promote interfacial domain formation.

Although the precise mechanism remains unelucidated, the involvement of caproic acid in the formation of these small PLA$_2$ domains has been clearly demonstrated by removing surface-bound or water-solubilized fatty acids with the BSA-fatty acid binding protein. In addition to PLA$_2$-fatty acid interactions, the affinity of bovine serum albumin to solubilized fatty acid species is also well documented [90]. PLA$_2$ hydrolysis of 16,6-PC monolayers with BSA in the monolayer subphase yields no observable interfacial enzyme aggregation (even after long incubation periods). Addition of BSA thus completely prevents formation of PLA$_2$ domains. In accord with our adsorption hypothesis [43,67,79], enzyme-produced water-soluble fatty acid apparently leaves the interface, thereby preventing monolayer fatty acid interfacial aggregation, the critical step for PLA$_2$ domain formation.

In PLA$_2$-hydrolyzed 6,16-PC monolayer systems, reaction products are the water-soluble monocaproyl-PC (C6Lyso) and the water-insoluble palmitic acid (Fig. 4.1a). Since palmitic acid remains in the monolayer after hydrolysis, positively charged PLA$_2$ surface residues are able to interact electrostatically with anionic fatty acid carboxylate headgroups resident at the interface, forming 2-D domains as evidenced by fluorescence microscopy (see Fig. 4.5). Results in Fig. 4.4 show that monolayer molecular area reaches that expected for palmitic acid (point C) after hydrolysis, suggesting that it is the only product remaining at the interface. However, the surface potential at the end of the hydrolysis (point C, 100 mV, Fig. 4.4) does not correspond to that for pure palmitic acid at this surface pressure (-30 mV).

For net neutral monolayers like phosphatidylcholine and lysophosphatidylcholine, the surface potential depends mainly on the vertical component of the resultant dipole moment of the molecules present at the interface [29]:

$$\Delta V = 4\pi n \mu_{\perp} \tag{4.1}$$

Thus, net neutral compounds, 16,6-PC, 6,16-PC and lyso-lipid, contribute the following dipole moments to the observed surface potential [91]: the terminal methyl at the end of each fatty acid chain, the carbonyl group (one for each fatty acid), the ester bond between each fatty acid and the glycerol backbone, the dipole between the negative charge on the

phosphate moiety and the positive charge on the choline quaternary nitrogen (see Fig. 4.1), as well as oriented interfacial water molecules.

Once the hydrolysis of 6,16-PC is completed (point C, Fig. 4.4), only the fatty acid hydrolysis product should contribute to the observed surface potential: all lyso-lipid species should be solubilized into the subphase (as evidenced by the observed molecular area). However, a large difference exists between the observed final value of surface potential (100 mV) and that expected (-30 mV) for a film of pure palmitic acid. The only apparent explanation is the contribution of adsorbed PLA_2 to the surface potential data. As observed in Fig. 4.5, PLA_2 forms numerous, large, two-dimensional domains after 6,16-PC hydrolysis. Any charge or dipolar contribution from surface-bound PLA_2 will continuously change the surface potential during the course of formation of these PLA_2 domains.

When considering the size of these domains (see Fig. 4.5) and the number of charges and dipoles present in this enzyme (e.g., pI of *N. naja naja* PLA_2 is 4.95 [92]), this large difference (130 mV) between the surface potential at the end of the hydrolysis and that for pure palmitic acid is not surprising. This result also strongly suggests that bound PLA_2 does not change the molecular area (or surface pressure) of the fatty acid monolayer. PLA_2 in these domains thus does not significantly protrude into the fatty acid monolayer, contrary to what is observed when a phospholipid monolayer is present. In this case, enzyme-substrate recognition and binding occurs and, in order to hydrolyze the phospholipid monolayer, PLA_2 must at least partially penetrate into the substrate monolayer. The result is the frequent observation of small increases (<5 mN m^{-1}) in surface pressure at hydrolytic onset. In the present case, the data suggest that PLA_2 does not protrude into the fatty acid monolayer because it does not change the final molecular area. Nevertheless, the surface potential properties of the film are drastically affected by its presence. It is thus proposed that the interfacial binding of PLA_2 onto final palmitic acid films involves electrostatic interactions. This is supported by results of PLA_2 adsorption to pure palmitic acid films (Fig. 4.7) where homogeneous and uniform PLA_2 adsorption actually solidifies the film by electrostatic interactions.

BSA experiments were also performed with 6,16-PC monolayers to determine if BSA was able to remove or block monolayer resident palmitic acid reaction products. Results of these experiments with *N. naja naja*, bee venom, and pancreatic hydrolyzed monolayers are all nearly identical to those of Fig. 4.5, showing identical locations for phase-separated gray monolayer regions and FITC-labeled PLA_2. Apparently, BSA cannot

bind or remove surface-resident, largely water-insoluble palmitic acid reaction products. This result is consistent with previous investigations showing BSA unable to bind interfacial long-chain fatty acids [93]. Furthermore, BSA is unable to remove this insoluble fatty acid from the interface and is not effective in inhibiting formation of PLA_2 domains.

The goal of our research is to elucidate the mechanism of PLA_2 domain formation in hydrolyzed lipid monolayers. The data presented here show that release of PLA_2-produced water-soluble fatty acid reaction products from 16,6-PC into the subphase inhibits enzyme domain formation, indicating monolayer-bound fatty acids play an essential role in both the monolayer phase separation and the enzyme-binding event.

Our previous work [67,79] demonstrated with DPPC:C16Lyso: palmitic acid (1:5:5; mol:mol:mol) ternary mixed monolayers that lateral phase separation was observed at basic pH in the presence of calcium even in the absence of PLA_2, yielding monolayer lipid domain morphologies that are similar to PLA_2 microstructures yet without enzyme. The DPPC:C16lyso:fatty acid ternary mixed monolayers used in these phase-separation studies represented monolayer compositions present at different extents of enzyme hydrolysis (PLA_2 was absent, yet phase separation still occurred). In addition, we observed binding of cationic water-soluble carbocyanine dyes to the phase-separated domains in DPPC:C16Lyso:fatty acid (1:5:5) ternary mixed monolayer systems [79], showing that phase-separated domains in the monolayer are negatively charged (fatty acid enriched). We also showed that phase separation of negatively charged domains in DPPC:C16Lyso:fatty acid ternary mixed monolayers could be readily blocked by removing Ca^{2+} from the subphase, as evidenced by fluorescence microscopy [79]. Since divalent cations are well known to induce lateral phase separation in negatively charged monolayers at the air-water interface [74], this further supports our contention. Furthermore, reducing the pH of DPPC:C16Lyso:palmitic acid (1:5:5) monolayer subphases (with Ca^{2+} present in subphase) did not inhibit phase separation [79], but we were unable to observe cationic dye binding to these monolayer domains. Thus, electrostatic interactions in heterogeneous ternary mixed monolayers comprising diacylphosphatidylcholines (PLA_2 substrates), lyso-lipid, and fatty acid reaction products are essential determinants of monolayer phase behavior. These previous results and those presented in this paper support the conclusion that PLA_2-produced fatty acids play a crucial role in controlling both subsequent enzyme interfacial response and the formation of enzyme domains.

Compared to results reported by Reichert and coworkers [67], work presented here extends and complements what is known about these monolayer systems. Monolayer phase separation into regular morphologies, and subsequent dye or enzyme binding, only occurs in the presence of both interfacial phosphatidylcholine and fatty acid species. Phase-separated monolayer microstructure, as revealed by fluorescence microscopy [67,79], shows grayish domains, indicating that these regions contain small amounts of fluorescent monolayer probe and are not highly condensed phases. If phase-separated monolayer regions were void of probe, the domains would appear black. Thus, if fluorescent-labeled phospholipid probe is contained in these monolayer microstructures, it is not surprising that some level of PC substrate might also be present. This is consistent with Reichert and coworkers' results that showed PLA_2 was unable to bind to phase-separated, polymerized diacetylenic fatty acid regions surrounded by D-DPPC fluid matrix [67]. Collectively, these observations suggest that, during PLA_2 hydrolysis [42,43] or during ternary mixed monolayer compression [67,79], PC substrate becomes entrapped in phase separating regions of high fatty acid content. This is also consistent with the observation that PLA_2 domain formation occurs in the presence of excess substrate well before monolayer hydrolysis is complete [42,43]. Specific PLA_2-substrate binding, coupled with electrostatic attraction to fatty acid-enriched membrane regions, may be required to form regular phase-separated enzyme domains.

The shapes of PLA_2 domains in hydrolyzed DPPC and 6,16-PC systems are dissimilar. It is, therefore, possible that two different PLA_2 aggregation mechanisms are occurring in hydrolyzed DPPC and 6,16-PC systems. As previously reported, domains from hydrolyzed isomerically pure lipid monolayers are typically bean-shaped. Similar bean-shaped domains are also observed in PLA_2-*free* , phase-separated ternary mixed monolayers containing enantiomerically pure DPPC, C16Lyso, and palmitic acid (0.2:1:1, [79]). The well-characterized property of DPPC enantiomers to induce chiral lipid domains during lipid monolayer phase transitions [37,41,69,94] may also play a role in templating or structuring PLA_2 interfacial aggregation into specific morphologies. This property would also extend to DPPC's chiral hydrolysis product, C16Lyso, resident after PLA_2 hydrolysis even though it lacks an observable phase transition and does not form monolayer domains [79]. Nevertheless, hydrolysis of asymmetric phospholipid substrates (Fig. 4.5) results in PLA_2 domains that are irregularly shaped and often comprise multiple domains clustered together. To obtain the regular bean-shaped PLA_2 domains during hydrolysis, C16Lyso and/or DPPC residual in phase-separated fatty acid enriched regions

may play an important role in monolayer phase separation, enzyme domain formation, and its resulting morphology. In 6,16-PC hydrolyzed monolayers, however, lyso-lipid products are solubilized during hydrolysis; the remaining monolayer is pure fatty acid. In this case, PLA_2 domain formation is still observed but with distinctly different morphology (Fig. 4.5). It is our assertion that, in this case, PLA_2 adsorbs interfacially to fatty acid without the morphology imposed by chiral lipids. This is supported by control experiments showing PLA_2 adsorbs to pure palmitic acid monolayers, lacking any specific microstructure. Therefore, we now alter our original domain formation hypothesis based primarily on fatty acid hydrolysis products to include some level of chiral PC in fatty acid-enriched phase-separated monolayer regions and its influence on resulting domain morphologies. Future work will be directed at elucidating the lipid composition of the phase-separated domains.

In conclusion, asymmetric 6,16-PC and 16,6-PC lipids have been shown to be valuable model compounds to test our hypothesis concerning PLA_2 binding to heterogeneous model monolayer membranes. The capability to selectively produce water-soluble or water-insoluble PLA_2 hydrolysis products in lipid monolayers has allowed us to further describe the role of fatty acids and lyso-lipids on influencing PLA_2 interaction with lipid monolayer membranes. Furthermore, these data have allowed direct correlation of the presence of insoluble, monolayer-localized fatty acids with binding of PLA_2 from the subphase and formation of laterally phase-separated monolayer microstructures of both lipids and enzymes.

CHAPTER FIVE

PLA$_2$ HYDROLYSIS DATA AND IMPLICATIONS TOWARDS AN ENZYME DOMAIN FORMATION MECHANISM

5.1 Summary

The original PLA$_2$ domain formation hypothesis by Grainger and coworkers [42,43] (Fig. 5.1) proposed that, following a critical amount of PLA$_2$-mediated lipid hydrolysis, fatty acid reaction products laterally phase separate, providing PLA$_2$ a negatively charged membrane region in which to adsorb. A specific portion of PLA2's surface is believed to interact with the lipid membrane. PLA2's interfacial recogntion surface consists of several positively charged amino acid residues [75].
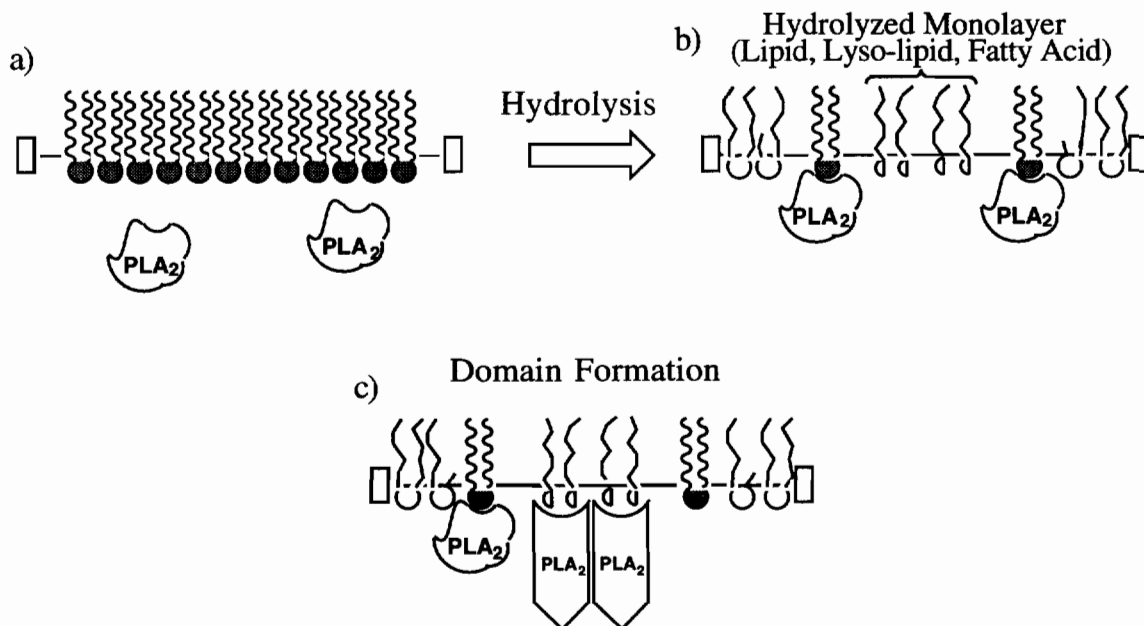
Fig. 5.1 PLA$_2$ domain formation hypothesis (adapted from ref. 43). (a) PLA$_2$-catalyzed lipid hydrolysis, (b) phase-separated fatty acid regions, and (c) PLA$_2$ adsorbtion to phase-separated regions.

It is suggested that this region of the enzyme's solvent accessible surface interacts electrostatically with phase-separated membrane regions containing fatty acid. Effects of substrate, lyso-lipid, fatty acids and monolayer physical state on PLA$_2$ domain formation are important to elucidate in order to determine an enzyme domain formation mechanism.

The domain formation hypothesis proposes that deprotonated fatty acids are immiscible with substrate and lyso-lipid in the presence of divalent cations. PLA$_2$ substrates that contain unsaturated acyl chains in the sn-2 position that yield unsaturated fatty acid reaction products upon hydrolysis were studied. Diacyl-PC's with unsaturated sn-2 acyl chains are not expected to yield interfaces suitable for PLA$_2$ docking and subsequent domain formation because monounsaturated fatty acids are known to exhibit fluid monolayer phases under a wide variety of experimental conditions. These types of fatty acids cannot pack into condensed structures because of hydrocarbon chain unsaturation. As expected, PLA$_2$-mediated hydrolysis of DOPC and POPC monolayers did not lead to enzyme domain formation (see Tables 5.1-5.3 for a summary of PLA$_2$-lipid monolayer systems that were investigated). Moreover, compression of ternary and binary mixed monolayers of DPPC:C16Lyso:palmitoleic acid (0.2:1:1) and palmitoleic acid:C16Lyso were also not observed to exhibit microstructured interfaces. This supports the contention that unsaturated fatty acid components are unable to form condensed domains upon compression or during hydrolysis. The only difference between these experiments and the ternary and binary mixtures presented in Chapter 3 is fatty acid acyl chain unsaturation. Under appropriate experimental conditions, saturated fatty acids in the ternary and binary mixtures studied all lead to monolayer phase separation upon compression (Chapter 3). Fatty acid structural properties, therefore, play an important role in the phase behavior of these mixtures relevant to PLA$_2$ monolayer hydrolysis. As the results of Chapter 4 have shown, the length of fatty acid chains also is important for enzyme self assembly. By decreasing the sn-2 acyl chain length of lipid substrates to six carbons, the solubility of the corresponding caproic acid reaction product is increased to the point where caproic acid is solubilized under reaction conditions (15 mN m^{-1}). Since saturated lipid chains 10-12 carbons in length define the boundary between being water soluble and water insoluble, it is anticipated that PLA$_2$ hydrolysis of most lipids that contain a saturated sn-2 acyl chain of approximately 10-12 carbons in length will lead, upon hydrolysis, to enzyme domain formation.

Table 5.1 Summary of Lipid Monolayer Microstructuring Relevant to PLA$_2$
Domain Formation: Pure Monolayers

Monolayer[a]	Subphase			Interfacial Domains	Reference
	[Ca^{2+}]	[Na$^+$]	pH		
L-α-DPPC	5 mM	0.1 M	8.9	Yes	[42,43]
D-α-DPPC	"			No	[42,43]
L-α-DMPC	"			Yes	[42]
L-α-DPPE	"			Yes	[42]
L-α-DMPM	"			Yes	unpub.
L-α-DOPC	"			No	unpub.
L-α-POPC	"			No	unpub.
L-α-DIAC-PC[b]	"			No	unpub.
PA	"			Yes[c]	unpub.
C16LYSO	"			No	unpub.
6,16-PC	"			Yes	accep. BBA
16,6-PC	"			Yes	accep. BBA

[a]All monolayers contain 1-2% fluorescent labeled lipid probe; lipid abbreviations: DPPC (dipalmitoylphosphatidylcholine), POPC (1-palmitoyl,2-oleoylphosphatidylcholine), DMPC (1,2-dimyristoylphosphatidylcholine), DMPE (1,2-dipalmitoylphosphatidylethanol-amine, DMPA (1,2-dimyristoylphosphatidic acid), palmitic acid (PA), C16Lyso (1-palmitoyl,2-hydroxyphosphatidylcholine), DMPM (1,2-dimyristoylphosphatidylmethanol), DIAC-FA (10,12-(tricosadiynoic) acid), DIAC-PC (di-10,12-tricosadiynoylphosphatidyl-choline), DOPC (1,2-dioleoylphosphatidylcholine), 6,16-PC (1-caproyl,2-palmitoylphos-phatidylcholine), 16,6-PC (1-palmitoyl,2-caproyl-phosphatidylcholine). [b]Pre- or unpoly-merized DIAC-PC. [c]PLA$_2$ adsorbs to PA monolayers on subphases containing Ca^{2+} at pH 8.9, but domains similar to those in hydrolyzed DPPC monolayers are not observed.

Table 5.2 Summary of Lipid Monolayer Microstructuring Relevant to PLA$_2$
Domain Formation: Binary Mixed Monolayers

Monolayer[a]	Subphase			Interfacial Domains	Reference
	[Ca^{2+}]	[Na$^+$]	pH		
L-α-DPPC: Chol.	5 mM	0.1 M	8.9	Yes	unpub.
C16Lyso:PA (1:1)	"			Yes	[67,79]
C16Lyso:PA (1:1)	5 mM	0.1M	4.0	No[b]	[67,79]
DIAC-FA:DPPC (1:1)	5 mM	0.1 M	8.9	No[c]	[67,79]
DPPA:DOPC (1:1)	"			No[d]	unpub.
C16Lyso:palmitoleic acid; (1:1)	"			No	unpub.
D-DPPC:PA; (x:1, x=1, 1.5, 2.3)	"			Yes[e]	[67,79]

[a]Chol. (Cholesterol), DIAC-FA (10,12-tricosadiynoic acid). [b]Monolayer is microstructured, but H-379 adsorption does not occur. [c]Phase-separated DIAC-FA in fluid DPPC matrix. [d]H-379 does not adsorb to phase-separated SC DPPA. [e]Phase-separated PA in fluid D-DPPC matrix.

Table 5.3 Summary of Lipid Monolayer Microstructuring Relevant to PLA_2
Domain Formation: Ternary Mixed Monolayers

Monolayer	Subphase $[Ca^{2+}]$	$[Na^+]$	pH	Interfacial Domains	Reference
L-DPPC:C16Lyso:PA					
x:1:1 (0.2<x<3)	5 mM	0.1 M	8.9	Yes	[67,79]
x:1:1 (x>3)	"			No	[67,79]
L-DPPC:C16Lyso:PA					
x:1:1 (0.2<x<3)	0	0.1 M	8.9	No	[67,79]
x:1:1 (x>3)	"			No	[67,79]
L-DPPC:C16Lyso:PA					
x:1:1 (0.2<x<3)	0	0	6	No	[67,79]
x:1:1 (x>3)	"			No	[67,79]
L-DPPC:C16Lyso:pal-					
mitoleic acid (0.2:1:1)	5 mM	0.1 M	8.9	No	unpub.

Abbreviations same as in Tables 5.1 and 5.2.

These observations clearly implicate fatty acid reaction products in PLA$_2$ self assembly. Laterally phase-separated fatty acids are absolutely necessary to observe PLA$_2$ domain formation. A control experiment aimed to determine PLA$_2$ adsorbtion behavior on pure fatty acid monolayer surfaces was conducted. Pure palmitic acid monolayer compressed to 15 mN m^{-1} on Ca^{2+}-containing pH 8.9 buffered subphases exhibit large lateral viscosity and condensed phase as observed with fluorescence microscopy [unpublished data]. Introducing PLA$_2$ beneath condensed palmitic acid monolayers leads to enzyme adsorbtion. However, PLA$_2$ does not form domains as normally observed during DPPC hydrolysis. In palmitic acid monolayers, PLA$_2$ adsorbs to the entire monolayer surface, not forming any specific domain microstructure. This is in contrast to another case where PLA$_2$ was not observed to adsorb to another fatty acid, DIAC-FA [67]. Monolayers consisting of fluid D-DPPC surrounding condensed DIAC-FA domains were prepared and the fatty acid domains polymerized by irradiating the monolayer with UV light. Water-soluble cationic H-379 adsorbed to the DIAC-FA domains, but PLA$_2$ did not [67]. Why PLA$_2$ does not adsorb to DIAC-FA domains but does adsorb to pure palmitic acid monolayers is not clear. Polymerized DIAC-FA molecules and palmitic acid monolayers most likely exhibit similar interfacial charge densities, so adsorption most likely cannot be explained on electrostatic grounds. However, since DIAC-FA is polymerized, restricted lateral motion within the monolayer plane may have an effect on PLA$_2$ adsorption. Even this does not sufficiently explain this observation because hydrolysis kinetics presented in Chapter 4 support the contention that PLA$_2$ does not penetrate the monolayer membrane when forming domains (PLA$_2$ did not contribute to the monolayer molecular area during lipid hydrolysis, Fig. 4.3). The explanation given by Reichert and coworkers for this behavior is that PC substrate was excluded from DIAC-FA domains during monolayer compression [67]. If PC were needed to induce enzyme binding to the membrane interface, than PLA$_2$ would not be expected to adsorb to palmitic acid monolayers. This situation is clearly not resolved.

The importance of lyso-lipid reaction products on PLA$_2$ domain formation is clearer. Hydrolysis of asymmetric 6,16-PC monolayers led to enzyme domain formation (lyso-lipid is solubilized in the monolayer subphase during hydroysis). If lyso-lipid was crucial for domain formation, enzyme self-assembly would have been reduced or suppressed. As shown in Fig. 4.4, this was not the case. Moreover, control experiments consisting of injecting PLA$_2$ beneath pure C16Lyso monolayers did not lead to enzyme domain formation. Though the composition of phase-separated microstructures presented

in Chapter 3 and in previous studies [42,43] are not known, it is highly unlikely that these domains contain lyso-lipid because lyso-lipid is not known to exhibit any condensed monolayer phases, alone or in mixtures.

Based on these results, phase-separated microstructures in compressed binary and ternary monolayers as well as in hydrolyzed films are most likely comprised of fatty acid reaction products and some PC. This contention is supported by fluorescence microscopy. Phase-separated regions in binary and ternary mixed monolayers (as well as phase-separated regions observed in hydrolysis experiments) appear gray when imaged. Solid, close-packed monolayer regions, as viewed with fluorescence microscopy, appear totally black (as in the case of DIAC-FA), indicating that exteremely low amounts of monolayer probe are present in highly condensed monolayer microstructures. Gray domains, therefore, indicate that monolayer fluorescent probe is partially excluded from fatty acid microstructures. If fluorescent monolayer probe can penetrate phase-separated anionic microstructures in binary and ternary mixed model membranes, it is not unreasonable to suggest that PLA_2 PC substrate can also penetrate these structures. The presence of these components would facilitate specific PLA_2 binding, and not non-specific adsorption. This leads to an improtant facet of PLA_2 domain formation: the chirality of enzyme domains resulting from DPPC hydrolysis and the chirality of domains observed in ternary mixed monolayer model systems.

It is possible that two different PLA_2 aggregation mechanisms are occurring in hydrolyzed DPPC and 6,16-PC systems. PLA_2 domains from hydrolyzed, isomerically pure lipid monolayers are typically bean-shaped [42,43]. Similar bean-shaped domains are also observed in PLA_2-free, phase-separated ternary mixed monolayers containing enantiomerically pure DPPC, C16Lyso, and palmitic acid (0.2:1:1, Fig. 2.10). The well-characterized property of DPPC enantiomers to induce chiral lipid domains during lipid monolayer phase transitions [37,41,69,94] may also play a role in templating or structuring PLA_2 interfacial aggregation into specific morphologies. This property would also extend to DPPC's chiral hydrolysis product, C16Lyso lipid, resident after PLA_2 hydrolysis even though it lacks an observable phase transition and does not itself form monolayer domains [79]. Nevertheless, hydrolysis of asymmetric phospholipid substrates (Fig. 4) results in PLA_2 domains that are irregularly shaped and often comprise multiple domains clustered together. To obtain the regular bean-shaped PLA_2 domains after hydrolysis, residual chiral DPPC in phase-separated fatty acid regions may play an important role in structuring monolayer phase separation, enzyme domain formation, and its resulting morphology. In

6,16-PC hydrolyzed monolayers, however, lyso-lipid products are solubilized during hydrolysis; the remaining monolayer is pure fatty acid. In this case, PLA_2 domain formation is still observed but with distinctly different morphology. It is our assertion in this case that PLA_2 adsorbs interfacially to fatty acid without the morphology imposed by chiral lipids. This is supported by control experiments showing PLA_2 adsorbs to pure palmitic acid monolayers resulting in highly irregular protein domain morphologies. We therefore alter our original enzyme domain formation hypothesis to include chiral PC in phase-separated monolayer regions and its influence on resulting domain morphologies. PLA_2 adsorbs to pure palmitic acid monolayers, but to observe chiral protein domains [43], enzyme substrate is necessary at some point during the enzyme domain formation time course.

Other lipid monolayer systems were investigated to determine the effect of reaction product structure on enzyme domain formation. PLA_2 hydrolysis of DIAC-PC did not lead to enzyme domain formation. This is interesting because the fatty acid product 10,12-tricosadiynoic acid (DIAC-FA) is able to pack into solid structures as evidenced by fluorescence microscopy. However, as predicted by the domain formation hypothesis, some degree of lateral phase separation must occur during hydrolysis (or compression for the model mixed systems). Examining the diacetylenic C23Lyso lipid product, this lipid species is structurally more rigid than an unsaturated lyso-lipid. The location of the acetylenic groups in the middle of the acyl chain is such that maximal structural rigidity results. The explanation for lack of PLA_2 domain formation in DIAC-PC systems is due to reaction product miscibility. It is noted that hydrolysis of DIAC-PC systems leads to very viscous films (evidenced with fluorescence microscopy as monolayer probe is rapidly bleached). Apparently, phase de-mixing in these systems does not occur to the extent that diacetylenic fatty acid species can laterally phase separate. An experiment that would help clarify this purported mixing problem would entail PLA_2-mediated hydrolysis of a lipid containing a saturated acyl chain in the sn-1 position and a diacteylenic (10,12-substituted) acyl chain in the sn-2 position. The lyso-lipid species produced upon hydrolysis is hypothesized to produce a fluid monolayer while the diacetylenic fatty acid would phase separate under appropriate experimental conditions. It is predicted that hydrolysis of such a monolayer would lead to PLA_2 domain formation.

The hypothesis originally proposed by Grainger and coworkers (Fig. 5.1) should, therefore, be revised (Fig. 5.2). Fatty acids alone can bring PLA_2 electrostatically but cannot promote PLA_2 docking into specific domain structures of regular morphology. PC

headgroups confined within monolayer microstructures appear necessary for regular enzyme self-assembly. PC headgroups and/or chirality undoubtedly play an important role in the structure of PLA$_2$ domain morphology. As observed in DPPC hydrolysis experiments, PLA$_2$ forms chiral-type domains during lipid hydrolysis. The enzyme domains possess bean-shaped geometries similar to those of the DPPC substrate. Chiral structure clearly indicates a net orientation of PLA$_2$ at the hydrolyzed interface. Otherwise, irregular domain shapes would be observed (as in the case of hydrolyzed 6,16-PC systems: PC is not present at the interface).
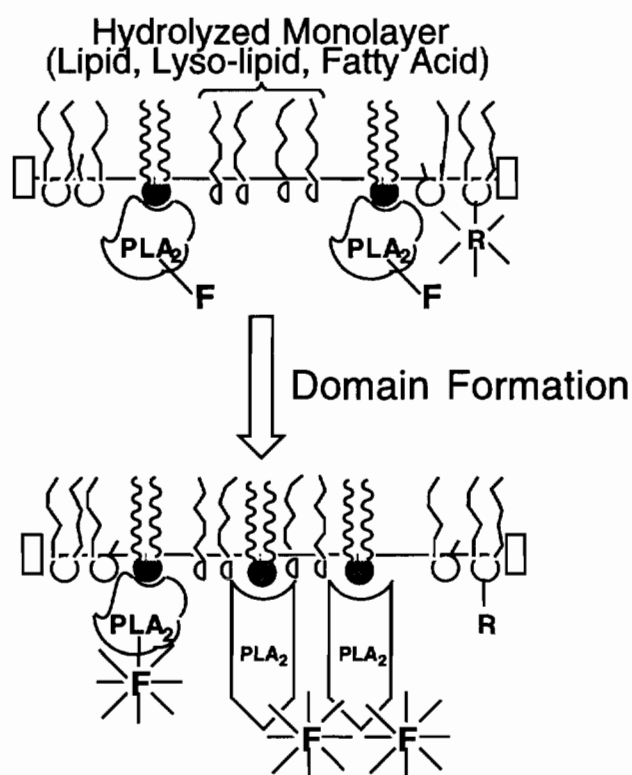
Fig. 5.2 Revised PLA$_2$ domain formation hypothesis.

Recently solved high-resolution PLA$_2$ crystal [86-88] structures show that several cationic amino acid residues (Lys, Arg) located near the enzyme's interfacial recognition site are solvent accessible. It is reasonable to expect that these residues possess the ability to interact with negative charges concentrated within phase-separated fatty acid domains. In fact, PLA$_2$ from porcine pancreas is well known to prefer substrate present in a negatively charged interface [61]. Additional support for electrostatic interactions between

PLA$_2$ and fatty acids is given by surface potential data for PLA$_2$-hydrolyzed 6,16-PC monolayers. The final surface potential obtained after completion of hydrolysis was 100 mV (Fig. 4.4), which does not correspond to that of a pure palmitic acid monolayer under enzyme-free conditions (-30 mV). As shown in Fig. 4.4, PLA$_2$ domain formation occurred during 6,16-PC hydrolysis. Therefore, PLA$_2$'s dipoles and surface charges will also contribute to the surface potential. Though we cannot separate PLA$_2$'s and palmitic acid's contribution to the surface potential, this suggests PLA$_2$ electrostatically interacts with fatty acids since the monolayer surface potential following completion of hydrolysis was not that expected for a pure palmitic acid monolayer. Moreover, since PLA$_2$ was not observed to contribute to the final monolayer molecular area during 6,16-PC hydrolysis, this suggests that PLA$_2$ does not penetrate the monolayer and that PLA$_2$ domains appear to be two-dimensional.

5.2 Future Considerations

Though the data presented here support the PLA$_2$ domain formation mechanism presented in Fig. 5.3, there is much to learn about PLA$_2$ self-assembly in lipid monolayers. Since chirality is evident in phase-separated monolayer domains (Chapter 3) and in enzyme domains [42,43], ternary (or binary) mixed monolayers consisting of achiral phospholipids should be studied. Racemic PC and lyso-lipid mixed with achiral fatty acid would not be expected to yield chiral phase-separated microstructures on subphases containing Ca^{2+} at pH 8.9. If this were found, this would support the contention that phase-separated ternary mixtures contain chiral PC.

With the asymmetric lipid data presented in Chapter 4, it would be interesting to determine the cut-off length required for PLA$_2$ domain formation. Most likely, the saturated sn-2 acyl chain representing the cut-off for enzyme domain formation is about 12 carbons. Additional substrates that deserve attention are PC's that contain saturated sn-1 chains but diacetylenic sn-2 chains. If domain formation occurred in these systems, then the phase-separated, fatty acid-enriched microstructures could be polymerized, possibly facilitating the transfer of the hydrolyzed monolayer to grids for electron or other scanning probe microscopy. As reported by Reichert [95], PLA$_2$-hydrolyzed monolayers that were transferred to electron microscopy grids were observed to exhibit long-range hexagonal order. A more in-depth analysis of PLA$_2$ domain structure on the nanometer scale may provide more information regarding 2-D protein crystal structure. Since PLA$_2$ appears to

be inactivated upon domain formation [42,43] and intermolecular protein-protein interactions are involved (domains resist compression and dissolution at high and low surface pressures, respectively [42,43]), it seems reasonable that a different protein 2-D structure is present as compared to the recently solved 3-D structures [86-88].

Finally, as described in Appendix B, quartz crystal microbalance techniques appear sufficient to study PLA_2 interactions with monolayer membranes. Either using multi-layered L-B assemblies or directly placing the QCM at the monolayer-subphase interface [Y. Okahata, unpublished data], more quantitative information concerning PLA_2-monolayer interactions may be realized.

CHAPTER SIX

STRUCTURED DOMAINS IN INTERFACIAL FILMS
OF PULMONARY SURFACTANT

6.1 Introduction

The interfacial film of pulmonary surfactant which lowers surface tension in the lung is generally thought to have a composition which differs from the complete mix of surfactant originally secreted by type II alveolar pneumocytes. Pulmonary surfactant occupies the surface of the liquid layer which coats the peripheral air spaces of the lungs and reaches extremely high surface pressures when compressed by the decrease in interfacial area during normal exhalation. The biophysical behavior of the surfactant films at high surface pressures suggest that their composition is mostly dipalmitoylphosphatidyl-choline (DPPC). This compound constitutes approximately one third of the complete material, which suggests that membrane compositional refinement may occur during film compression (Fig. 6.1).

Watkins' hypothesis [96] that more fluid components of the film with phase transition temperatures below 37°C collapse from the interface at high pressures, leaving behind a film enriched in DPPC, has received wide-spread acceptance. DPPC is the only constituent of pulmonary surfactant with a gel-to-liquid crystal phase transition temperature
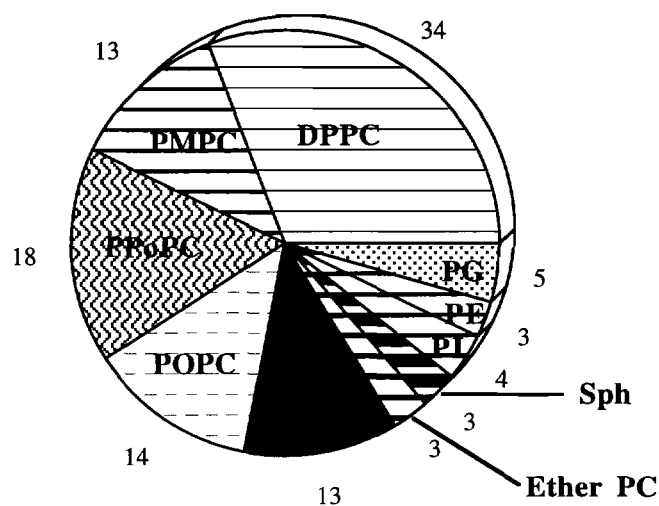

Fig. 6.1 Lipid composition of pulmonary surfactant. Values for lipid constituents are given as weight percentages.

which lies above body temperature. Pure films of DPPC exhibit the relatively ordered fluid-condensed phase at equilibrium spreading pressures and, when compressed on a Wilhelmy balance, can reach the high surface pressures seen in the lung. The complete mix of pulmonary surfactant reaches these high pressures only after prolonged compression through a plateau at approximately 47 mN/m, or after multiple cycles of compression and expansion. The hypothesis of selective collapse requires that the interfacial film of pulmonary surfactant must be heterogeneous, that regions of the film must vary in stability to lateral compression, and that more stable regions must contain a high percentage of DPPC. The studies reported here used epifluorescence and Brewster angle microscopy to determine if regions of different structure could be detected with methods sensitive to interfacial domains on a microscopic scale. Epifluorescence microscopy uses the difference in solubility of fluorescent lipids in ordered and disordered domains to distinguish regions with different structures in interfacial monolayers [37,41,94]. Brewster angle microscopy provides an alternate method of detecting structural heterogeneity without the need to add exogenous probes, although at somewhat lower spatial resolution [37,41,94]. Both methods clearly distinguish between DPPC in the fluid and condensed forms and should be capable of detecting domains of structured lipids in an otherwise fluid film.

We have also investigated the role of minor constituents of surfactant in the formation of structured domains. Although pulmonary surfactant contains 90% phospholipids, it also includes small amounts of protein and neutral lipid. The two hydrophobic surfactant proteins SP-B and SP-C, in particular, are considered essential for biophysical activity. In these studies, we have worked with preparations made from extracts of calf surfactant which lack proteins and/or neutral lipids to determine their role in the formation of interfacial domains.

6.2 Experimental

6.2.1 Lung Surfactant Preparation

Complete extracts of surfactant from calf lungs (calf lung surfactant extract, CLSE) were obtained as described previously [97]. Surfactant was removed from freshly excised calf lungs by repeated lavage with 150 mM NaCl. Centrifugation at 250g for ten minutes, and higher speed centrifugation of the resulting supernatant at 12,500g for 30 minutes pelleted large surfactant aggregates. Following resuspension, the hydrophobic constituents of surfactant were extracted into chloroform [98] to yield CLSE.

Preparations of CLSE constituents were fractionated using a slight modification of protocols published previously [99]. Gel permeation chromatography separated the proteins, phospholipids, and neutral lipids into three separate peaks. By pooling selected fractions, preparations were obtained which contained the purified phospholipids (PPL), the neutral and phospholipids (N&PL), and the surfactant proteins and phospholipids (SP&PL). Although the protein and phospholipid peaks overlapped with the original protocol, a longer column achieved complete separation on a single pass for the materials studied here. Preparations were eluted from the LH-20 matrix (LKB-Pharmacia, NJ) with a solvent of acidified chloroform-methanol (0.1N HCl:CHCl$_3$:CH$_3$OH; 1:9:9, v:v:v) [100,101], followed by extraction of the constituents into chloroform [98]. Samples of SP&PL suffered variable losses of proteins and were supplemented with protein purified separately to obtain the protein/phospholipid ratio found for CLSE [98].

6.2.2 Biochemical Assays

Phospholipid concentrations were determined by measuring the phosphate content [102] of measured aliquots of extracted material. Protein assays used the amido black method of Kaplan and Pedersen [103] with bovine serum albumin as a standard, and cholesterol (free and esterified) was assayed by reduction with ferrous sulfate [104].

6.2.3 Compression Isotherms

Surface pressure-area isotherms (π-A curves) of interfacial monolayers were measured on a commercially available trough (KSV-3000, KSV Instruments, Helsinki, Finland). Monolayers were compressed at a rate of 1.0 Å^2 molecule^{-1} minute^{-1}. Monolayers were created by spreading 80 μl of a 0.95mM phospholipid stock solution in chloroform at the air-liquid interface. Molecular areas were expressed in terms of phospholipid only, with no attempt to correct for the presence of neutral lipid or protein molecules. All monolayer experiments, including epifluorescence and Brewster angle microscopy as well as compression isotherms, used a subphase containing 10 mM Hepes, pH 7.0, 150 mM NaCl, and 1.5 mM CaCl$_2$ (HBS-Hepes buffered saline).

6.2.4 Brewster Angle Microscopy

Brewster angle microscopy (BAM) [105,106] of monolayers was carried out to determine if monolayer microstructures were an artifact of lipid dye probe used in fluorescence microscopy. BAM of monolayers was conducted on a home-built apparatus.

A home-built trough was placed on the stage of an optical setup consisting of a He-Ne laser, optical analyzers, polarizers, and a CCD camera. The trough was computer controlled using a graphical programming interface (Lab View, National Instruments, TX), and monolayer images were stored directly to computer disk using Image software (NIH, Bethesda, MD). BAM was performed at the Univ. of Washington, courtesy of Prof. Viola Vogel.

6.2.4 Image Analysis

Images of fluorescent monolayers were digitized and subjected to computer analysis. Images were initially recorded on VHS video tape, then digitized onto a Macintosh computer (Apple Computer, Inc., Cupertino, CA) using a frame grabber (Model LG-3 frame grabber, Scion Corp., NJ) and analyzed with the program Image. The marked contrast between domains from which the probe was excluded and the fluorescent background allowed direct measurements of the size of all dark domains in any given image. Four experiments were performed for each preparation of surfactant constituents. Each data point represents analysis of a minimium of twelve recorded images from different regions of the monolayer. The fraction of the monolayer present as solid domains was calculated by expressing the sum of all domain areas as a percent of the total area analyzed for each experiment and then averaging the several experiments. Histograms expressing the relative frequency of different domain sizes used the areas of all domains from all experiments. Domains whose perimeter was interrupted by the edge of the microscope aperture were not included in the histograms because their true area was not known.

6.3   Results

Isotherms of CLSE, PPL, SPPL, and N&PL on HBS are depicted in Fig. 6.2. CLSE, PPL, and N&PL show nearly identical interfacial behavior as inferred from compression the isotherm. Compared to CLSE, PPL, and N&PL, SPPL shows more condensed behavior at all pressures up to monolayer collapse.

Epifluorescence microscopy and monolayer compression isotherms of CLSE films clearly show that interfacial films contain domains which differ in solubility for Rhod-DPPE (Fig. 6.3). Although compression of monolayers produces smooth isotherms with
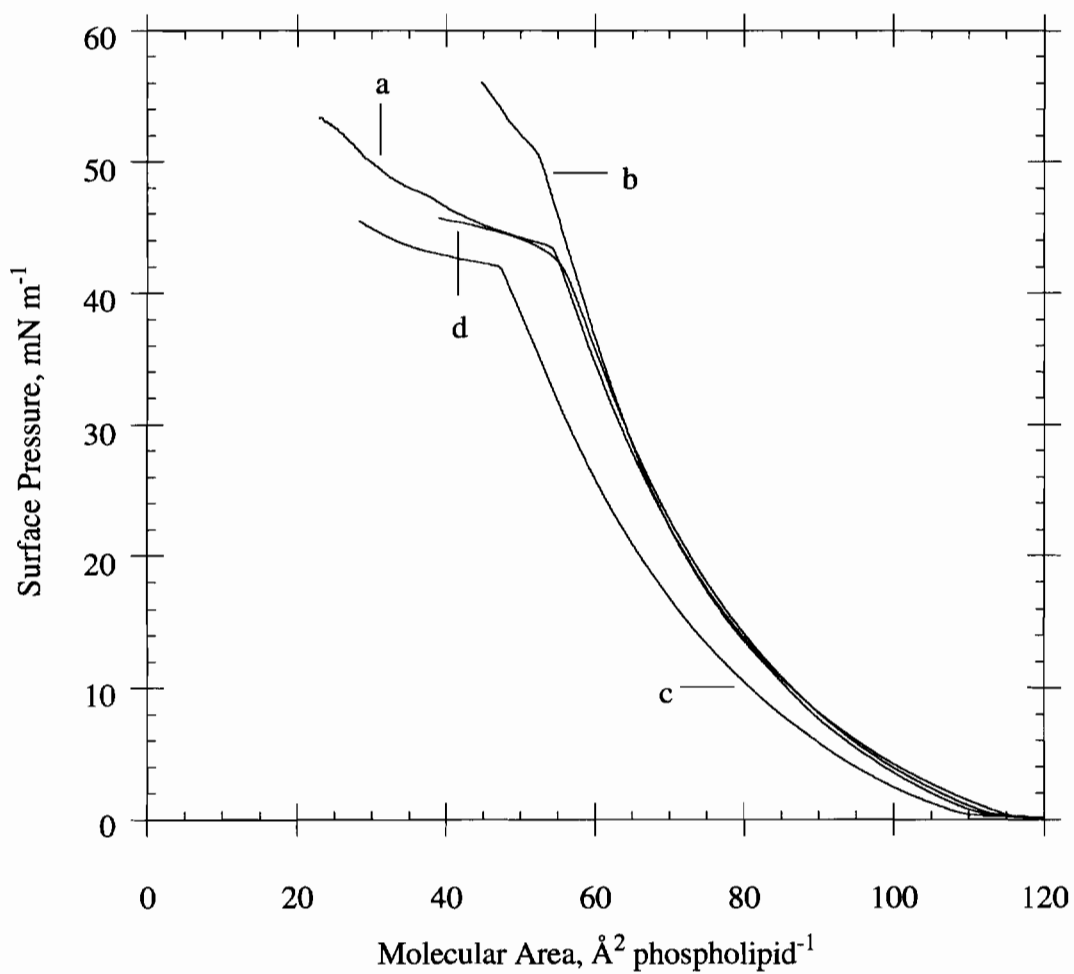
Fig. 6.2 Compression isotherms for (a) CLSE, (b) PPL, (c) SPPL, and (d) N&PL on 10 mM Hepes, 150 mM NaCl, 1.5 mM CaCl2, pH 7.0, at 20°C. Compression rate = 1.0 Å^2 phospholipid^{-1} minute^{-1}.

Fig. 6.3 Fluorescence microscopy of CLSE monolayers and corresponding histograms obtained from image analysis. Top, middle, bottom: 10, 20, and 30 mN m^{-1}, respectively. Subphase: HBS at 20°C.

no apparent discontinuities which would suggest a phase transition, regions of film with low solubility for Rhod-DPPE are apparent at relatively large molecular areas. Films of CLSE produced detectable surface pressure at 114 Å^2 phospholipid^{-1}. Compression speeds as low as 0.1 Å^2 phospholipid^{-1} minute^{-1}, reduction of temperature to 5°C, or the use of water rather than buffered electrolyte as subphase did not result in a significant alteration of the shape of the isotherm. Fluorescence microscopy demonstrated the presence of discrete domains at surface pressures above approximately 5 mN m^{-1} (Fig.

6.3). If domains were present at lower pressures, they were smaller than the lateral resolution of our microscope (a few micrometers).

Minor monolayer constituents did not alter the fundamental observations inferred from the isotherms, but effects on domain microstructure as evidenced with epifluorescence microscopy were observed. These experiments used preparations of surfactant constituents, separated by gel permeation chromatography, from which specific components were excluded. The purified phospholipids (PPL) (Fig. 6.4),contained the
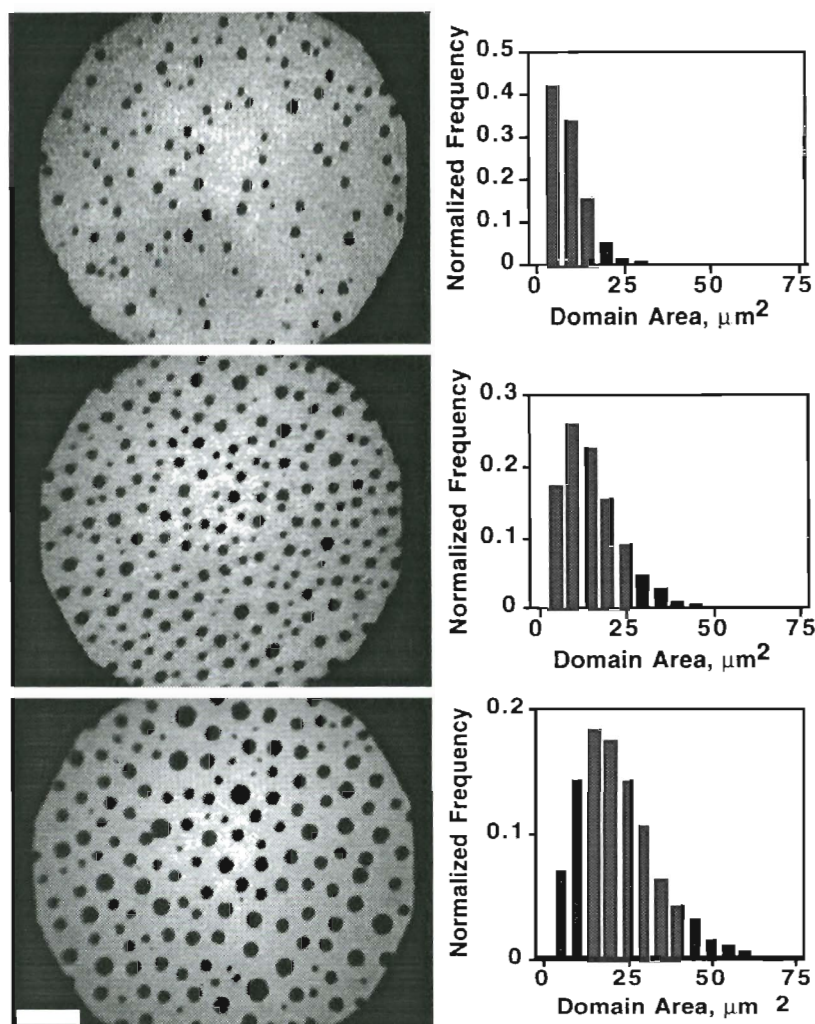

Fig. 6.4 Fluorescence microscopy of PPL monolayers and corresponding histograms obtained from image analysis. Top, middle, bottom: 10, 20, and 30 mN m^{-1}, respectively. Subphase: HBS at 20°C.

complete set of surfactant phospholipids, but no protein or neutral lipids. The preparation of N&PL specifically excluded the surfactant proteins, while the SP&PL preparation omitted the neutral lipids. The isotherms for these preparations differed only in the

Fig. 6.5 Fluorescence microscopy of SPPL monolayers and corresponding histo-grams obtained from image analysis. Top, middle, bottom: 10, 20, and 30 mN m^{-1}, respectively. Subphase: HBS at 20°C.

molecular area at which surface pressure first became apparent, and in the pressure and area of collapse. The pressure of collapse in particular was significantly higher for the phospholipids alone, occurring at 51 mN m^{-1} for PPL. Collapse occurred for SP&PL and

N&PL at 43 and 44 mN m^{-1}, respectively, similar to the values observed for CLSE. Isotherms were otherwise smooth, but fluorescence microscopy again demonstrated
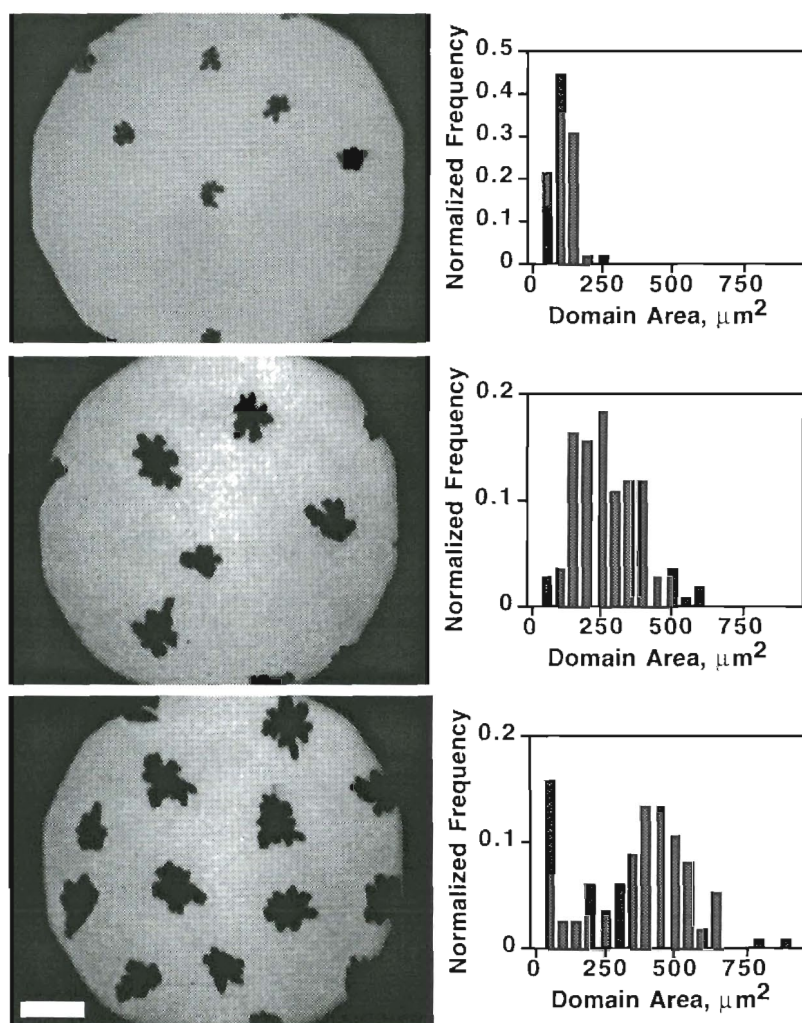

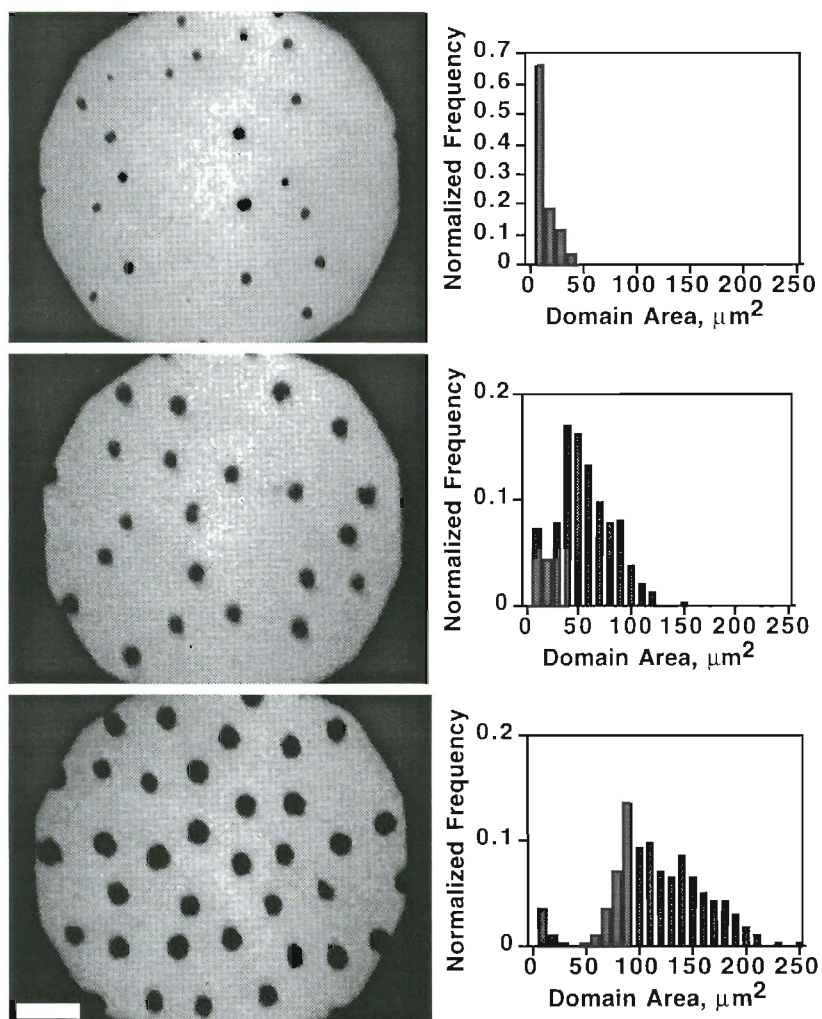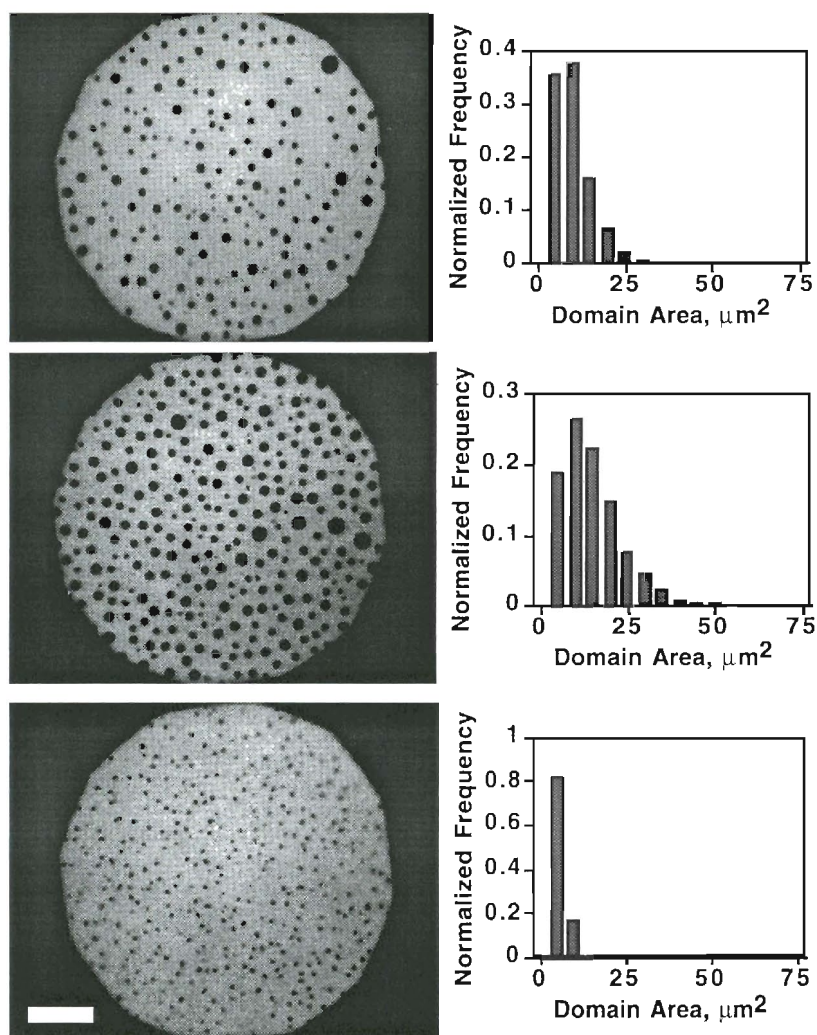Fig. 6.6 Fluorescence microscopy of N&PL monolayers and corresponding histo-grams obtained from image analysis. Top, middle, bottom: 10, 20 and 30 mN m^{-1}, respectively. Subphase: HBS at 20°C.

the presence of domains deficient in Rhod-DPPE. These domains were clearly apparent for N&PL at 5 mN m^{-1} (Fig. 6.6), but required 10 and 6 mN m^{-1} for SP&PL and PPL, respectively (Figs. 6.5 and 6.7).

The fraction of the monolayer occupied by the dark domains showed an initially progressive increase with surface pressure for all preparations (Figs. 6.3-6.7). The additional presence of the neutral lipids in N&PL produced a significant increase in ordered area at most surfaces pressures relative to the phospholipids alone (PPL) (Fig. 6.7). Conversely, the surfactant proteins in SP&PL proved deleterious, and the ordered domains occupied a significantly smaller area than with PPL (Fig. 6.7). When the neutral lipid and protein were both present in CLSE, the beneficial effect of the neutral lipid proved dominant, and the area of dark domains exceeded that for PPL (Fig. 6.7).

At higher pressures, however, N&PL showed a sudden and dramatic decrease in the total area of the dark domains (Figs. 6.6 and 6.7). The fraction of the monolayer occupied by regions deficient in probe fell from a maximum of $26 \pm 4\%$ at 25 mN m^{-1} to $4 \pm 2\%$ at 30 mN m^{-1} (Fig. 6.7). Domains were essentially absent at 35 mN m^{-1}. No obvious loss of fluorescent probe from the interface occurred over this interval. Total dark area showed a much smaller decrease for PPL between 35 and 40 mN m^{-1} (Fig. 6.7). The precipitous decrease in ordered domains specifically did not occur for CLSE, which is the other preparation that, like N&PL, also contains the neutral lipid.
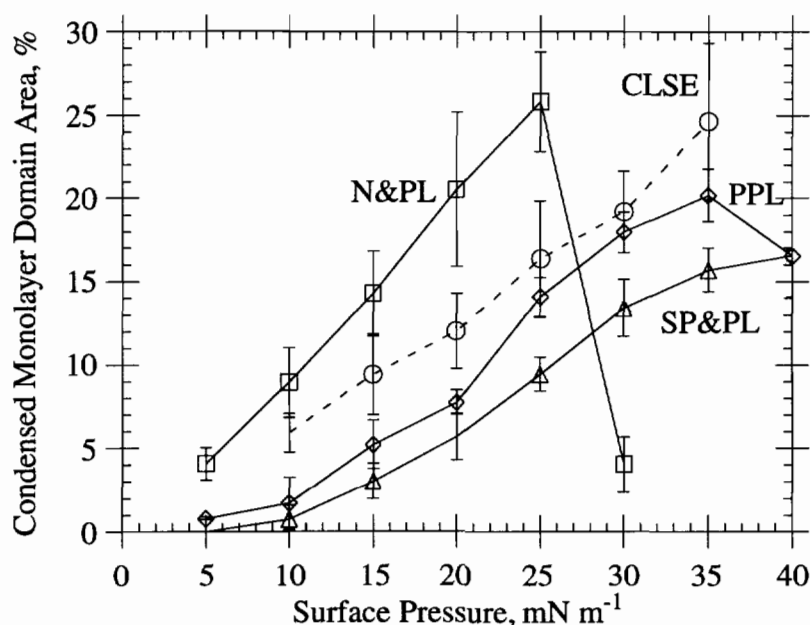

Fig. 6.7 Monolayer condensed phase domain area versus surface pressure for lung surfactant and related subfraction monolayers at the air-buffer (HBS) interface at 20°C.

The manner in which condensed domains increased in size differed for the four preparations of surfactant constituents (Figs. 6.2-6.6). PPL initially formed a small number of relatively large domains which grew in size without much change in number when surface pressure increased (Figs. 6.4 and 6.7). At the highest pressures, a second set of much smaller domains also appeared which were distinct from the original domains in shape as well as size, but the major mode of increased dark area with increased pressure was by enlargement of individual domains rather than by an increase in their number. The additional presence of surfactant protein in SP&PL (Figs. 6.5 and 6.7) had little effect on this general pattern of growth by enlargement of initial domains, although the domains were smaller and more numerous than for PPL. SP&PL also developed small domains at high pressure similar to those seen for PPL. In contrast, the neutral lipid in N&PL significantly changed the variation of domains. The total dark area increased by adding a larger number of domains, the size of which remained relatively constant and small relative to PPL (Fig. 6.4). The dark domains in CLSE increased both in number and slightly in size (Fig. 6.3).

Fig. 6.8 shows a Brewster angle micrograph of a PPL monolayer at 35 mN m^{-1}. At Brewster's angle, the intensity of p-polarized light reflected from the interface is minimized [107]. Optical parameters affecting the condition of minimized reflectance include the thickness and refractive index of the monolayer. Regions of inhomogeneous interfacial film that satisfy conditions of minimized reflectance appear dark, while other monolayer domains that reflect light (not at the Brewster angle) appear bright. As the micrograph in Fig. 6.8 depicts, bright and dark regions of the monolayer show that the
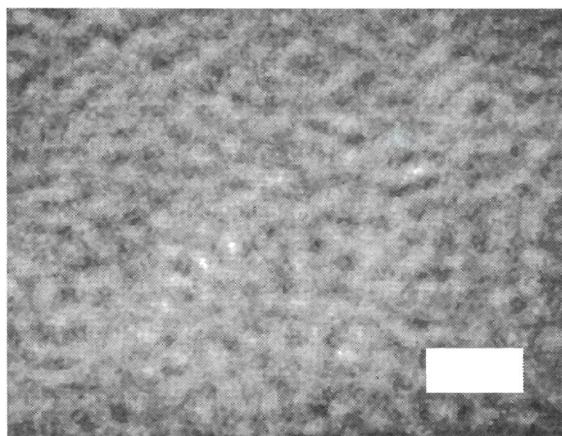

Fig. 6.8 Brewster angle micrograph of PPL at 35 mN m^{-1} HBS at 20°C. Scale bar = 100 μm.

PPL film is heterogeneous. Though the scales of the Brewster angle micrograph and the fluorescence micrographs in Figs. 6.2-6.6 are different, the size of monolayer domains observed with both optical techniques are consistent.

Finally, the shapes of phase-separated microstructures presented in Figs. 6.3-6.6 for CLSE, PPL, SPPL, and N&PL are distinct for each preparation. CLSE and N&PL monolayer domain structures are more compact than those observed for SPPL. Domain shapes for CLSE, N&PL and SPPL are roughly circular, though the size distribution is different (Figs. 6.3-6.6). On the other hand, phase-separated PPL monolayer regions exhibit shapes distinct from the other three preparations. PPL monolayer domains exhibit asymmetric, flower-like appearances.

6.4   Discussion

Pulmonary surfactant is believed to exist at the air-buffer interface in the lungs as a monomolecularly thin film. Pulmonary surfactant films achieve high surface pressure during compression (reducing the interfacial tension of water) as shown in model systems. A large number of lipids comprise pulmonary surfactant, most of which, by themselves, exhibit fluid-like monolayers. Compression of pure fluid-like lipid monolayers to high surface pressures similar to those obtained with a complete mix of pulmonary surfactant suggest that during compression the monolayer composition is "refined." By refinement, fluid-like lipid components in pulmonary surfactant would leave the interface at or above monolayer collapse leaving behind a surfactant film that is enriched with lipids that are able to exist at the interface at high surface pressures. Watkins' refinement mechanism [96] suggests that pulmonary surfactant components that resist leaving the interface during collapse may be present as distinctly ordered membrane phases as opposed to the fluid components that remain in a disordered phase and are eventually removed from the interface. Based on this, we hypothesized that pulmonary surfactant monolayers at the air-water interface may exist as heterogeneously ordered films at the interface, rather than a disordered single-phase film.

In Figs. 6.3-6.6, fluorescence microscopy of CLSE, PPL, SP&PL and N&PL monolayers reveals that lateral monolayer microstructuring results upon monolayer compression. It is not clear if microstructures presented in Figs. 6.3-6.6 result from an interfacial lipid phase transition or a chemical phase separation event. It is clear from

fluorescence microscopy that a heterogeneous film is present at the interface for each of the pulmonary surfactant mixtures investigated since image contrast is based on the preferential solubility of Rhod-DPPE in fluid, disordered lipid monolayer phases [37,41,94]. Therefore, the dark monolayer regions presented in Figs. 6.3-6.6 represent a phase that is more ordered than the surrounding bright regions which are fluid-like.

To determine if Rhod-DPPE probe used in fluorescence microscopy was responsible for pulmonary film microstructuring, BAM was employed to image pulmonary surfactant monolayers in a probe-free environment. At Brewster's angle, the intensity of p-polarized light reflected from the interface is minimized. Optical parameters affecting the condition of minimized reflectance include the thickness and refractive index of the monolayer. Regions of a heterogeneous interfacial film that satisfy conditions of minimized reflectance appear dark, while other monolayer domains that reflect incident light (not satisfying minimized reflectance conditions) appear bright. As shown in Fig. 6.8, dark and bright monolayer regions are present, showing that PPL monolayers are microstructured and that the fluorescent Rhod-DPPE probe used in fluorescence microscopy is not responsible for monolayer domain formation and growth.

Although a direct elucidation of the chemical composition of microstructured pulmonary surfactant monolayer regions is not possible, several observations suggest they comprise DPPC and/or PMPC. DPPC and PMPC are the major lipid components in the surfactant mixtures, present at levels of 33 and 13 wt%, respectively. DPPC and PMPC contain saturated acyl chains and both compounds exhibit critical phase transition temperatures (T_c) above 20°C. T_c for DPPC and PMPC is 43 [39] and 37°C, respectively. Therefore, pure DPPC and pure PMPC monolayers are expected to display ordered phases at 20°C. In ideally mixed lipid systems, the ability for DPPC and PMPC to exhibit an ordered phase would be dependent on the T_c for the mixture, but in non-ideal cases where lipid de-mixing occurs, the T_c for DPPC or PMPC hold and would not be affected by the presence of the other lipid components. Monolayer isotherms presented in Fig. 6.2 do not display evidence for a monolayer phase transition in terms of a discontinuity in the compression isotherm. This may suggest that the ordered domains observed for each pulmonary surfactant mixture arise from lipid de-mixing and not an interfacial lipid phase transition. This situation is unclear, though, and the contention of lipid de-mixing or a lipid phase transition requires additional investigation. The other lipid components in pulmonary surfactant are either unsaturated lipids, or other saturated lipids present in low amounts that possess T_cs below 20°C. The unsaturated lipids or other saturated species present in these

small amounts cannot alone account for the fraction of condensed monolayer displayed in Fig. 6.7. Incorporation of these minor lipid components within condensed monolayer regions observed for each surfactant mixture probably does not occur. This suggests that DPPC and/or PMPC comprise phase-separated structures in pulmonary surfactant monolayers.

Neutral lipid (free and esterified cholesterol) and hydrophobic surfactant protein affect monolayer domain formation in two ways: (1) the total monolayer area existing as condensed phase and (2) the morphologies of the phase-separated structures. Relative to PPL, addition of hydrophobic surfactant protein SP-B and SP-C ($\sim$ 1 wt%) results in a minor decrease in the total monolayer area that exists as condensed phase at high surface pressure (Fig. 6.7, compare PPL and SP&PL). Given the calculated standard deviation for PPL and SP&PL percent solid area at any given pressure, PPL and SP&PL exhibit similar behavior within a few percent. A possible explanation for SP-B and SP-C having little effect on monolayer condensation may be a result of the protein function. In the case where pulmonary surfactant monolayers are created by adsorption from bulk, and not by spreading, surfactant protein facilitates interfacial adsorption [100,108]. In spread monolayers, protein function is not needed since the film is created by spreading and not adsorption from bulk subphase.

The effect of neutral lipid on monolayer domain formation and growth is more apparent. Addition of neutral lipid to PPL results in a much larger increase in total condensed domain area (except at 30 mN m^{-1}, see below). At 25 mN m^{-1}, condensed structures in N&PL monolayers occupy 26% of the total film area, whereas PPL films occupy only about 16% (Fig. 6.7). Neutral lipids facilitate monolayer domain growth, while surfactant protein, to a much smaller extent, inhibits solid domain yield. In Fig. 6.3, N&PL condensed monolayer area shows a precipitous drop from 26% to 4%. PPL shows similar behavior, but to a much smaller extent and at higher surface pressure (Fig. 6.7). The observed drop in condensed monolayer area may be an imaging artifact. Rhod-DPPE is used as a fluorescence probe for fluid monolayer areas and prefers fluid phases at low surface pressures. At high surface pressures, the Rhod-DPPE may become solubilized in condensed monolayer regions. This would lead to a decrease in condensed N&PL domain size based on dye solubility (Figs. 6.6 and 6.7) when, in fact, the domain size may be increasing.

Addition of both neutral lipid and surfactant protein to PPL appears to cancel out the other in terms of altering total monolayer condensed area, since CLSE percent solid area

versus surface pressure is similar to that observed with PPL (Fig. 6.7). However, the morphologies of pulmonary surfactant domains are more sensitive to the presence of neutral lipid and hydrophobic, membrane-resident proteins as evidenced by fluorescence microscopy. Using PPL as a reference, addition of hydrophobic protein reduces the tendency of condensed monolayer domains to exhibit appendages (compare Figs. 6.4 and 6.5). This shows that the hydrophobic proteins interact directly with condensed monolayer domains. The proteins SP-B and SP-C together constitute about 1 wt% of the pulmonary surfactant material. It is remarkable that such a small amount of membrane-resident material can exert a significant effect on monolayer microstructure. SP-B and SP-C also do not significantly affect the monolayer domains' nucleation process since the number of domains in PPL and SP&PL monolayers are quite similar.

In contrast, neutral lipids have a much more noticeable effect on monolayer nucleation and domain growth as seen by comparing N&PL and CLSE with PPL and SP&PL (Figs. 6.3-6.6). Addition of neutral lipid to PPL causes an increase in domain number as well as a decrease in domain size (Fig. 6.6). In the case of CLSE (Fig. 6.3), the neutral lipids appear to dominate any effect by surfactant protein in that domain number increases and domain size decreases, similar to N&PL. Neutral lipids and surfactant protein thus affect the microstructure of pulmonary surfactant in two distinct ways: (1) addition of neutral lipid results in an increase in domain nuclei while their size is diminished with respect to PPL and (2) surfactant protein only appears to significantly affect the morphology of phase-separated microstructures and not the number of nuclei.

In summary, pulmonary surfactant monolayers at the air-buffer interface were investigated in terms of their tendencies to form ordered monolayer membranes. A hypothesis regarding the refinement of pulmonary surfactant monolayers during compression was the basis for this study. It was found that pulmonary surfactant extract and purified extract fractions all exhibited different phase behavior at the air-buffer interface during film compression. Using the purified phospholipid fractions as a reference state, the presence of hydrophobic proteins within the monolayer membrane affected the shapes of phospholipid domains, while lipid nucleation and domain growth was relatively unaffected. Neutral lipids had a larger effect on phase-separated lipid domain nucleation and growth. Addition of neutral lipids to purified pulmonary surfactant phospholipid extracts resulted in a large increase in domain number, total condensed monolayer area, and a decrease in domain size. When protein and surfactant were present together, neutral lipid interactions with phase-separated monolayer regions proved dominant by increasing the

number of domains, increasing the total percentage of monolayer condensed domain coverage, and decreasing their size.

These results show that, during monolayer compression, individual components present in pulmonary surfactant can significantly alter the phase behavior of interfacial surfactant films, possibly providing a basis for a previously proposed interfacial film refinement mechanism. During refinement, the formation of a heterogeneous lipid phase may be required in order to interfacially exclude monolayer components which cannot sustain the high surface pressures required for lung surfactant activity. The lipid components that can sustain high surface pressures may exist separately in a phase devoid of the components that are leaving the membrane interface. If this is the case, components such as DPPC would form a phase within the membrane that is more condensed than the surrounding phase during compression. Results presented in Figs. 6.3-6.6 show that spread films of pulmonary surfactant are microstructured with a condensed phase surrounded by a more fluid phase (although the chemical composition of the more condensed phase is unknown). Though the measurements presented in this chapter do not directly address pulmonary surfactant components leaving the interface for bulk (and leaving behind a monolayer more capable of sustaining high surface pressure), the results do support the contention that, for refinement, monolayers of pulmonary surfactant may exhibit condensed phases. Moreover, fluorescence microscopy and isotherm measurements were made as close to an equilibrium situation as possible (slow compression rates). During compression in the lungs, pulmonary surfactant most likely is not in a state of equilibrium since the surfactant is undergoing rapid compression and decompression. With faster experimental compression rates *and* monolayer compression closer to collapse, lipid components leaving the interface for bulk may be more apparent.

REFERENCES

1.   Vieth, W. R. *Membrane Systems: Analysis and Design. Applications in Biotechnology, Biomedicine and Polymer Science*; Oxford University Press: Munich, 1988; pp 360.

2.   Carter, F. L. *Molecular Electronics*; Marcel Dekker: New York, 1987; Vol. II, pp 825.

3.   *Principles of Immobilization of Enzymes,* 2nd ed. (Kennedy, J. F., White, C. A., Eds.); John Wiley & Sons: Chichester, 1985; pp 147-207.

4.   McAlear, J. H. In *Molecular Electronics* (Carter, F.L. Ed.); Marcel Dekker: New York, 1987; Vol. II, pp 623-633.

5.   Ahlers, M., Blankenburg, R., Grainger, D. W., Meller, P., Ringsdorf, H., Salesse, C. (1989) *Thin Solid Films* 180, 93-98.

6.   Ahlers, M., Muller, W., Reichert, A., Ringsdorf, H., Venzmer, J. (1990) *Angew. Chem. Int. Ed. Engl.* 29, 1269-1285.

7.   Roberts, G. *Langmuir-Blodgett Films*; Plenum Press: New York, 1990; pp 425.

8.   Grainger, D. W., Maloney, K. M., Huang, X., Ahlers, M., Ringsdorf, H., Salesse, C., Herron, J. D., Hlady, V., Lim, K. In *Progress in Membrane Biotechnology* (Gomez-Fernandez, J. C., Chapman, D., Packer, L., Eds.); Birkhauser Verlag: Basel, 1991; pp 64-82.

9.   Cadenhead, D. A. In *Structure and Properties of Cell Membranes* (Benga, G. Ed.); CRC Press, Boca Raton, 1985; Vol. III, pp 21-62.

10. Ulman, A. *An Introduction to Ultrathin FIlms: From Langmuir-Blodgett to Self-Assembly*; Harcourt, Brace, Jovanovich: Boston, 1991, pp 414.

11. Jap, B. K., Zulauf, M., Scheybani, T., Hefti, A., Baumeister, W., Aebi, U. (1992) *Ultramicroscopy* 46, 45-84.

12. Newman, R. H., Leonard, K., Crumpton, M. J. (1991) *FEBS Lett.* 279, 21-24.

13. Newman, R., Tucker, A., Fergusen, C., Tsernoglou, D., Leonard, K., Crumpton, M. J. (1989) *J. Mol. Biol.* 206, 213-219.

14. Olofson, A., Kaveus, U., Hacksell, I., Thelestam, M., Hebert, H. (1990) *J. Mol. Biol.* 214, 299-306.

15. Ludwig, D. S., Ribi, H. O., Schoolnik, G. K., Kornberg, R. D. (1986) *Proc. Natl. Acad. Sci. USA* 83, 8585-8588.

16. Sato, A., Furuno, T., Toyoshima, C., Sasabe, H. (1993) *Biochim. Biophys. Acta.* 1162, 54-60.

17. Lebeau, L., Regnier, E., Schultz, P., Wang, J. C., Mioskowski, C., Oudet, P. (1990) *FEBS Lett.* 267, 38-42.

18. Yoshimura, H., Matsumoto, M., Endo, S., Nagayama, K. (1990) *Ultramicroscopy* 32, 265-274.

19. Ohnishi, S., Hara, M., Furuno, T., Okada, T., Sasabe, H. (1993) *Biophys. J.* 65, 573-577.

20. Akiba, T., Yoshimura, H., Namba, K. (1991) *Science* 252, 1544-1547.

21. Uzgiris, E. E., Kornberg, R. D. (1983) *Nature* 301, 125-129.

22. Uzgiris, E. E. (1986) *Biochem. Biophys. Res. Commun.* 134, 819-826.

23. Uzgiris, E. E. (1990) *Biochem. J.* 272, 45-49.

24. Edwards, A. M., Darst, S. A., Feaver, W. J., Thompson, N. E., Burgess, R. R., Kornberg, R. D. (1990) *Proc. Natl. Acad. Sci. USA* 87, 2122-2126.

25. Darst, S. A., Kubalek, E. W., Edwards, A. M., Kornberg, R. D. (1991) *J. Mol. Biol.* 221, 347-357.

26. Ribi, H. O., Reichard, P., Kornberg, R. D. (1987) *Biochemistry* 26, 7974-7979.

27. Darst, S. A., Ahlers, M., Meller, P. H., Kubalek, E. W., Blankenburg, R., Ribi, H. O., Ringsdorf, H., Kornberg, R. D. (1988) *Biophys. J.* 59, 387-396.

28. Robinson, J. P., Schmid, M. F., Morgan, D. G., Chiu, W. (1988) *J. Mol. Biol.* 200, 367-375.

29. Gaines, G. L. *Insoluble Monolayers at Liquid-Gas Interfaces*; Wiley (Interscience): New York, 1966; pp 386.

30. *Handbook of Monolayers* (Mingotaud, A.-F., Mingotaud, C., Patterson, L. K., Eds.); Academic Press: San Diego, CA, 1993; Vol. 1, pp 2726.

31. *The Enzymes*, 3rd ed. (Dennis, E. A., Ed.); Academic Press: New York, 1983; Vol. 16, pp 307-353.

32. Verger, R., Mieres, M. C. E., de Haas, G. H. (1972) *J. Biol. Chem.* 218, 4023-4034.

33. Souvignet, C., Pelosin, J.-M., Daniel, S., Chambaz, E. M., Ransac, S., Verger, R. (1991) *J. Biol. Chem.* 266, 40-44.

34. Blankenburg, R., Meller, P., Ringsdorf, H., Salesse, C. (1989) *Biochemistry* 28, 8214-8221.

35. Thompson, N. L., Poglitsch, C. L., Timbs, M. M., Pisarchick, M. L. (1993) *Acc. Chem. Res.* 26, 567-573.

36. Thompson, N. L., McConnell, H. M., Burghart, T. P. (1984) *Biophys. J.* 46, 739-747.

37. McConnell, H. M., Tamm, L. K., Weis, R. M. (1984) *Proc. Natl. Acad. Sci. USA* 81, 3249-3253.

38. Mohwald, H. (1990) *Annu. Rev. Phys. Chem.* 41, 441-476.

39. Albrecht, O., Gruler, H., Sackmann, E. (1978) *J. Phys. (Paris)* 39, 301-313.

40. Losche, M., Duwe, H.-P., Mohwald, H. (1988) *J. Colloid Interface Sci.* 126, 432-444.

41. Peters, R., Beck, K. (1983) *Proc. Natl. Acad. Sci. USA* 81, 3249-3253.

42. Grainger, D. W., Reichert, A., Ringsdorf, H., Salesse, C. (1989) *FEBS Lett.* 252, 79-85.

43. Grainger, D. W., Reichert, A., Ringsdorf, H., Salesse, C. (1990) *Biochim. Biophys. Acta* 1023, 365-379.

44. Grainger, D. W., Reichert, A., Ringsdorf, H., Salesse, C., Davies, D. E., Lloyd, J. B. (1990) *Biochim. Biophys. Acta* 1022, 146-154.

45. Langmuir, I. (1937) *J. Am. Chem. Soc.* 39, 1848-1906.

46. Langmuir, I., Schaefer, V. J., Wrinch, D. M. (1937) *Science* 85, 76-80.

47. Lehn, J.-M. (1990) *Angew. Chem. Int. Ed. Engl.* 29, 1304-1319.

48. Tanford, C. *The Hydrophobic Effect: Formation of Micelles and Biological Membranes*, 1st ed.; Wiley: New York, 1973; pp 200.

49. Israelachvili, J. N. *Intermolecular and Surface Forces*, 2nd ed.; Academic Press, Ltd.: San Diego, 1992; pp 450.

50. Haussling, L., Ringsdorf, H., Schmitt, F.-J., Knoll, W. (1991) *Langmuir* 7, 1837-1840.

51. Collinson, M., Bowden, E. F. (1992) *Langmuir* 8, 1247-1250.

52. Okahata, Y., Ebato, H. (1991) *Anal. Chem.* 63, 203-207.

53. Okahata, Y., Arriga, K., Tanaka, K. (1992) *Thin Solid Films* 210/211, 702.

54. Okahata, Y., Ebara, Y. (1992) *J. Chem. Soc. Chem. Commun.* 116-117.

55. Okahata, Y., Ebato, H. (1992) *Trends Anal. Chem.* 11, 344.

56. Ahlers, M., Grainger, D. W., Herron, J. N., Lim, K., Ringsdorf, H., Salesse, C. (1992) *Biophys. J.* 63, 823-838.

57. Andrade, J. D. In *Surface and Interfacial Aspects of Biomedical Polymers: Protein Adsorption* (Andrade, J.D. Ed.); Plenum Press: New York, 1985; Vol. 2, pp 1-75.

58. MacRitchie, F. (1978) *Adv. Protein Chem.* 32, 283-326.

59. Muller, W., Ringsdorf, H., Rump, E., Wildburg, G., Zhang, X., Angermaier, L., Knoll, W., Liley, M., Spinke, J. (1993) *Science* 262, 1706-1708.

60. Pieterson, W. A., Vidal, J. C., Volwerk, J. J., deHaas, G. H. (1974) *Biochemistry* 13, 1455-1460.

61. Jain, M. K., Berg, O. G. (1989) *Biochim. Biophys. Acta* 1002, 127-156.

62. Op den Kemp, J. A. F., de Gier, J., van Deenen, L. L. M. (1974) *Biochim. Biophys. Acta* 345, 253-256.

63. Yu, B.-Z., Jain, M. K. (1989) *Biochim. Biophys. Acta* 980, 15-22.

64. Jain, M. K., Yu, B., Kozubek, A. (1989) *Biochim. Biophys. Acta* 980, 23-32.

65. Apitz-Castro, R., Jain, M. K., de Haas, G. H. (1982) *Biochim. Biophys. Acta* 688, 349-356.

66. Burack, W. R., Yuan, Q., Biltonen, R. L. (1993) *Biochemistry* 32, 583-589.

67. Reichert, A., Ringsdorf, H., Wagenknecht, A. (1992) *Biochim. Biophys. Acta* 1106, 178-188.

68. Albrecht, O. (1989) *Thin Solid Films* 178, 93-101.

69. Meller, P. (1988) *Rev. Sci. Instrum.* 59, 2225-2231.

70. Verger, R., deHaas, G. H. (1973) *Chem. Phys. Lipids* 10, 127-136.

71. Lowry, O. H., Rosebrough, N. J., Farr, A. L., Randall, R. J. (1951) *J. Biol. Chem.* 193, 265-275.

72. Smith, P. K., Krohn, R. I., Hermanson, G. T., Mallia, A. K., Gartner, F. H., Provenzano, M. D., Fujimoto, E. K., Goeke, N. M., Olson, B. J., Klenk, D. C. (1985) *Anal. Biochem.* 150, 76-85.

73. Nargessi, R. D., Smith, D. S. (1986) *Methods Enzymol.* 122, 67-73.

74. Eklund, K. K., Vuorinen, J., Mikkola, J., Virtanen, J. A., Kinnunen, P. K. J. (1988) *Biochemistry* 27, 3433-3437.

75. Lugtigheid, R. B., Nicolaes, G. A. F., Veldhuizen, E. J. A., Slotboom, A. J., Verheij, H. M., deHaas, G. H. (1993) *Eur. J. Biochem.* 216, 519-525.

76. Yuan, Q., Biltonen, R. L. (1991) *Biophys. J.* 59, 590a.

77. Dennis, E. A. (1973) *Arch. Biochem. Biophys.* 158, 485-496.

78. It was incorrectly reported in ref. 67 that binary mixed (1:1) monolayers of C16Lyso and palmitic acid are fluid-like monolayers. They exhibit phase-

separated, anionic microstructures. Reichert, A., Ringsdorf, H., personal communication (1993).

79. Maloney, K. M., Grainger, D. W. (1993) *Chem. Phys. Lipids* 65, 31-42.

80. Burns, R. A. J., Donovan, J. M., Roberts, M. F. (1983) *Biochemistry* 22, 964-973.

81. Burns, R. A. J., Roberts, M. F. (1980) *Biochemistry* 19, 3100-3106.

82. Lewis, K. A., Bian, J., Roberts, M. F. (1990) *Biochemistry* 29, 9962-9970.

83. Metcalfe, L. D., Schmitz, A. A. (1961) *Anal. Chem.* 33, 363-364.

84. Demel, R. A., Geurts van Kessel, W. S. M., Zwall, R. F. A., Roelofsen, B., van Deenen, L. L. M. (1975) *Biochim. Biophys. Acta* 406, 97-107.

85. *Handbook of Biochemistry and Molecular Biology: Lipids, Carbohydrates and Steroids*, 3rd ed. (Fasman, G. D., Ed.); CRC Press: Cleveland, 1975; pp 495.

86. Dijkstra, B. W., Kolk, K. H., Hol, W. G. J., Drenth, J. (1981) *J. Mol. Biol.* 147, 97-123.

87. Scott, D. L., Otwinowski, Z., Gelb, M. H., Sigler, P. B. (1990) *Science* 250, 1563-1566.

88. White, S. P., Scott, D. L., Otwinowski, Z., Gelb, M. H., Sigler, P. B. (1990) *Science* 250, 1560-1563.

89. Cho, W., Tomasselli, A. G., Heinrikson, R. L., Kezdy, F. J. (1988) *J. Biol. Chem.* 263, 11237-11241.

90. Lehninger, A. L. *Principles of Biochemistry*; Worth Publishers: New York, 1982, pp 702.

91. Vogel, V., Mobius, D. (1988) *J. Colloid Interface Sci.* 126, 408-420.

92. Waite, M. *The Phospholipases*; Plenum Press: New York, 1978; Vol. 5, pp 332.

93. Kupferberg, J. P., Yokoyama, S., Kezdy, F. J. (1981) *J. Biol. Chem.* 256, 6274-6281.

94. Losche, M., Sackmann, E., Mohwald, H. (1983) *Ber. Bunsenges. Phys. Chem.* 87, 848-852.

95. Reichert, A., Ph.D. Thesis, University of Mainz, 1993.

96. Watkins, G. C. (1968) *Biochim. Biophys. Acta* 152, 293-306.

97. Hall, S. B., Venkitaraman, A. R., Whitsett, J. A., Holm, B. A., Notter, R. H. (1992) *Am. Rev. Respir. Dis.* 145, 24-30.

98. Bligh, E., Dyer, W. (1959) *Can. J. Biochem. Physiol.* 37, 911-917.

99. Hall, S. B., Wang, Z., Notter, R. H. (1994) *J. Lipid Res.* 35, 1386-1294.

100. Takahashi, A., Fujiwara, T. (1986) *Biochem. Biophys. Res. Commun.* 135, 527-532.

101. Bizzozero, O., Besio-Moreno, M., Pasquini, J. M., Soto, E. F., Gomez, C. J. (1982) *J. Chromatogr.* 227, 33-44.

102. Ames, B. M. (1966) *Methods Enzymol.* VIII, 115-118.

103. Kaplan, R. S., Pedersen, P. L. (1989) *Anal. Biochem.* 150, 97-104.

104. Searcy, R. L., Bergquist, L. M. (1960) *Clin. Chim. Acta* 5, 192-199.

105. Honig, D., Mobius, D. (1991) *J. Phys. Chem.* 95, 4590-4592.

106. Henon, S., Meunier, J. (1991) *Rev. Sci. Instrum.* 62, 936-939.

107. Harrick, N. J. *Internal Reflection Spectroscopy*; Interscience: New York, 1967; pp 327.

108. Yu, S.-H., Possmayer, F. (1986) *Biochem. J.* 236, 85-89.

109. Ward, M. D., Buttry, D. A. (1990) *Science* 249, 1000-1007.

110. Sauerbrey, G. (1959) *Z. Phyz.* 155, 206-222.

APPENDIX A

ATTEMPTS TO TWO-DIMENSIONALLY CRYSTALLIZE PLA$_2$ ON POLYMER MEMBRANES AT THE AIR-WATER INTERFACE

Several attempts to crystallize monomolecularly thin protein films have been successful through the use of monolayers at the air-liquid interface (see Table 1.1). Used as two-dimensional (2-D) scaffolds for protein nucleation and crystal growth, monolayer interfaces presented to protein-containing subphases have utilized both non-specific and highly specific binding properties to assemble proteins. Monolayers doped with protein receptors have been designed and prepared to present a specific binding surface for the protein [12,15,21,22]. In contrast, non-specific nucleating monolayer surfaces include polymer films that presumably induce protein crystallization through general electrostatic attraction [16,19]. Polymer films used in these cases are charged opposite to the protein. Polymer and protein charges are adjustable by varying monolayer chemistry and subphase pH. The air-Hg interface has also been used to crystallize ferritin two-dimensionally [18]. In this case, the high interfacial tension of the Hg-air interface (486.5 mN m^{-1}) is believed to play an important role in ferritin crystallization (through capillary forces).

In this study, poly(1-benzyl-L-histidine) (PBLH) monolayers were used as nucleating surfaces for potential 2-D PLA$_2$ crystallization. PBLH monolayers at the air-water interface have previosuly been shown to induce ferritin (Fig. A.1) and catalase 2-D crystallization [16,19]. 2-D protein crystallization in these cases is based on non-specific electrostatic interactions between the protein and monolayer. Since this method succeeded for several different proteins, and appeared to be a general method, PLA$_2$ crystallization on PBLH monolayers was attempted. Details concerning preparation of PBLH monolayers and the transfer of protein-polymer films is described in the experimental section (Chapter 2).

Before PLA$_2$ crystallization experiments were conducted, 2-D crystallization of ferritin to PBLH polymer monolayers was undertaken to ensure that the crystallization technique developed by Furuno and coworkers could be repeated [16,19]. As shown in Fig. A.1, ferritin arrays are clearly visible, and it was concluded that the technique was reproducible and attempts to crystallize PLA$_2$ then proceeded.
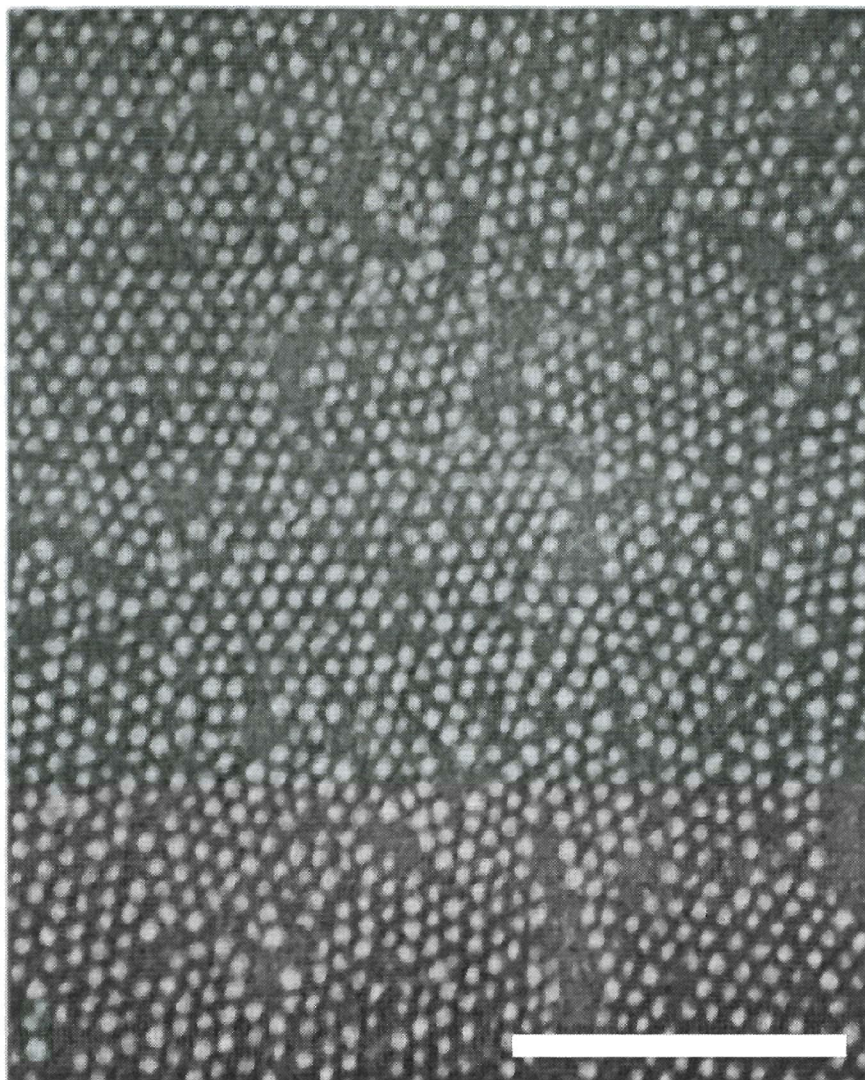
Fig. A.1 Scanning electron micrograph of 2-D ferritin crystals on PBLH monolayers. Scale bar = 150 nm.

Several experimental variables were adjusted to determine their effects on PLA_2 adsorption to PBLH monolayers. PBLH has an apparent interfacial pK near 7 (histidine). Since *N. naja naja* PLA_2's pI is near 5 [92], a monolayer subphase pH above 7 will keep the PBLH net positively charged and PLA_2 negatively charged. Therefore, monolayer subphase pH was varied to get the PBLH monolayer and PLA_2 oppositely charged and to drive crystallization electrostatically.

Though many experimental variables were adjusted, PLA$_2$ crystallization on PBLH monolayers was unsuccessful as determined by SEM. However, PLA$_2$ totally wetted PBLH monolayers as evidenced when PLA$_2$-adsorbed PBLH monolayers were removed from the air-buffer interface. When proteins do not adsorb to PBLH films, the polymer film appears dry when removed from the air-buffer interface. Since PLA$_2$ adsorbed to PBLH monolayers, it is believed that 2-D crystallization can be accomplished. The necessary conditions for 2-D crystallization, however, remain elusive.

pH variance had no observable effect on the experimental outcome. Crystallization experiments normally proceeded by spreading PBLH films over protein-containing buffer. Occasionally, protein was injected beneath the monolayer. Results obtained by both methods were identical. Calcium was included in the monolayer subphase in some experiments. Calcium seemed to make PBLH films stiff as compared to crystallization experiments where calcium was absent. Even with calcium in the subphase, PLA$_2$ crystallization was not afforded. Table A.1 summarizes the different subphase and film preparation conditions used in this study.

Imaging of PLA$_2$-coated monolayers by SEM was difficult. Since 2-D PLA$_2$ arrays were not observed, it was very difficult to image the PBLH-PLA$_2$ assembly since no surface structures were present to focus on. Since PLA$_2$ is a small protein (occupies a surface area of ~ 1800 Å^2), this also made imaging difficult. Moreover, the non-specific crystallization technique developed by Furuno and coworkers [16,19] works best with large, globular proteins such as ferritin. By contrast, PLA$_2$ is small ($M_r \approx 14,000$) and highly asymmetric. Future attempts to crystallize PLA$_2$ at monolayer surfaces should rely on methods utilizing non-hydrolyzable ligands that bind to PLA$_2$'s active site, or ligands that specifically interact with selected residues on PLA$_2$'s surface.

Table A.1 Conditions for Attempted PLA$_2$ 2-D Crystallization to PBLH
Monolayers at the Air-Buffer Interface[a]

Subphase	pH	[PLA$_2$] (μg/ml)	Incubation Time (hours)	Temp
Phosphate[b]	7.4	1.3	2	RT
Phosphate	4.2	1.3	2	RT
Phosphate	4.0	1.3	2	RT
Tris[c]	8.2	1.3	2	RT
Tris[d]	8.7	1.9	2.5	RT
Tris[d]	7.4	1.9	2.5	RT
Phosphate[e]	5.6	1.3	3.5	RT
Phosphate	5.6	2.6	2	RT
Tris[c]	9.3	1.3	2	RT
Phosphate[f]	5.6	1.3	2	RT

[a]PBLH monolayers were created by spreading 3 μl of 0.6 mg/ml PBLH solution. PLA$_2$ samples were stained with phosphotungstic acid [b]Phosphate buffer contains 20 mM NaCl, 20 mM phosphate. [c]Tris buffer contains 20 mM NaCl, 20 mM Tris. [d]Bee venom PLA$_2$. [e]Ca^{2+} was injected 1.5 hours after spreading the monolayer to give a final subphase [Ca^{2+}] of 0.5 mM. [f]5 mM phosphate subphase.

APPENDIX B

PLA$_2$ BINDING TO LANGMUIR-BLODGETT PHOSPHOLIPID FILMS AS MONITORED BY QUARTZ CRYSTAL MICROBALANCE METHODS

Mass sensing with quartz crystal microbalances (QCM) [109] has recently been used to monitor L-B film formation [52-54] and PLA$_2$-mediated hydrolysis of DPPE L-B films [54]. Operation of the QCM is based on the inverse piezoelectric effect. Application of a voltage across a quartz crystal induces crystal oscillation. The resonance frequency of the crystal oscillation is sensitive to several experimental parameters including mass adsorption to the crystal surface. By monitoring quartz crystal frequency changes versus time of adsorption, an adsorption isotherm can be measured (assuming the frequency change is solely due to mass transfer). Okahata reported that, during the initial stage of DPPE L-B film hydrolysis, a QCM frequency change occurred that corresponded to an increase in adsorbed PLA$_2$ [54]. This decrease in frequency continued, followed by an increase in resonance frequency. This was interpreted as DPPE hydrolysis products leaving the L-B film for the bulk aqueous phase. Since PLA$_2$ hydrolysis of L-B films could be followed by QCM, we attempted to look in more detail at PLA$_2$ adsorption to L-B films consisting of hydrolyzable and non-hydrolyzable substrate.

The lipid dimyristoylphosphomethanol (DMPM) has been used extensively as a PLA$_2$ substrate because pancreatic PLA$_2$ sources are known to exhibit enhanced activities towards negatively charged bilayer interfaces [61]. The goal of this research initiative was to ascertain the feasibility of using the QCM to study PLA$_2$ docking to tailored interfaces.

L-B film preparation:

A monolayer isotherm of DMPM is shown in Fig. B.1. This lipid derivative of DMPA shows condensed phase behavior when compressed on Ca^{2+}-containing subphases. Limiting molecular areas at high surface pressure corresponds to close packed lipid acyl chains.
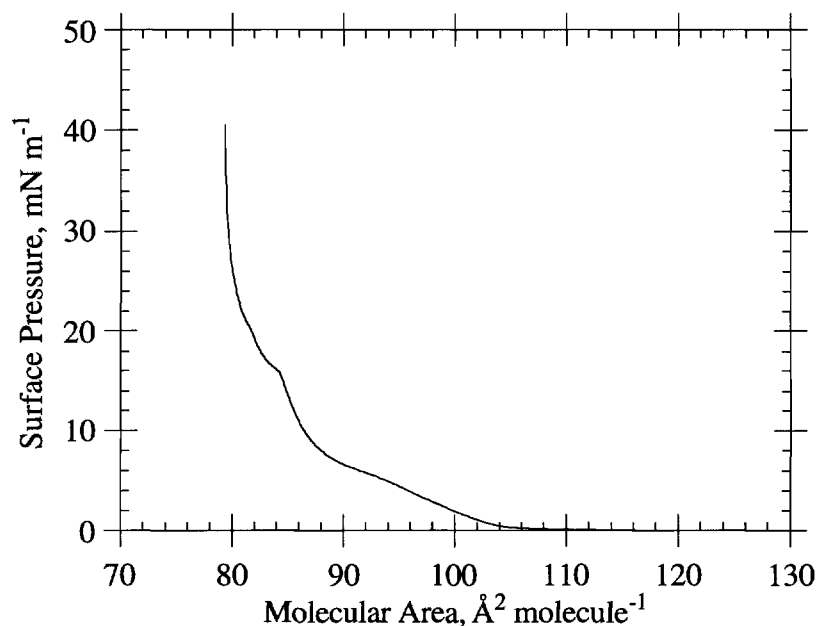
Fig. B.1 Monolayer compression isotherms of DMPM on 0.5 mM $CaCl_2$. T = 20°C; compression rate was 2 $Å^2$ molecule^{-1} minute^{-1}.

Since DMPM monolayers are negatively charged, calcium was added to the subphase to facilitate L-B film fabrication. The addition of divalent ions to negatively charged lipid monolayer subphases is a common technique to improve L-B film transfer of negatively charged lipids [7]. Here, 0.5 mM $CaCl_2$ subphases were employed. As shown in Fig. B.1, DMPM monolayers exhibit a condensed phase, as reflected by the steep increase in surface pressure above 20 mN m^{-1}. DMPM monolayers were compressed to 30 mN m^{-1} (pressures below and above 30 mN m^{-1} were also tried with similar results). L-B film deposition variables were adjusted to find the optimum deposition parameters. Despite several attempts, no more than 4 monolayers of DMPM could be transferred to hydrophobized QCM surfaces. Attempts to exceed 4 deposited monolayers resulted in poor film transfer as evidenced by QCM frequency shifts reflecting incomplete lipid adsorption. Film transfer ratios as obtained from monolayer area kinetics could not be used to ascertain film deposition because the Teflon holder used for the QCM was undoubtedly also covered with lipid during each monolayer deposition.
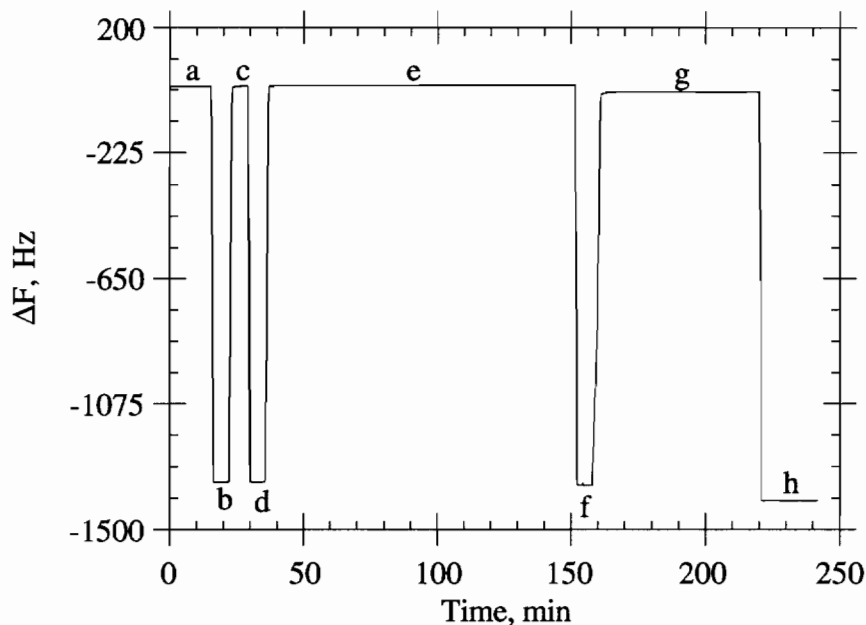
Fig. B.2 QCM resonant frequency versus time. Frequencies from a to d represent uncoated QCM surfaces and e to h represent frequencies during L-B film deposition.

QCM resonance frequencies versus L-B deposition time are shown in Fig. B.2. At point a, the QCM assembly (silicone-coated to render it hydrophobic) is located above a clean water surface. The QCM is then slowly dipped into buffer (0.5 mM $CaCl_2$), and a new resonance frequency is established due to a new crystal environment (point b). This procedure is then repeated; the QCM is moved from buffer to air (point b to c), air to buffer (point c to d) and then back to air (point d to e). The frequency of the QCM at points a, c, and e are nearly identical and represent a stable quartz crystal resonating in air. Similarly, points b and d represent the QCM frequency in buffer, showing similar stability. This procedure was routinely conducted to ensure the silicone-coated QCM was stable before L-B film deposition occurred. After the QCM is brought into the air (beginning of segment e), a monolayer of DMPM is spread and compressed to 40 mN m^{-1}. The time taken to spread and compress the DMPM monolayer is reflected by the length of segment e (approximately 120 minutes). Upon monolayer stabilization (end of segment e), the hydrophobized QCM is slowly (1 cm sec^{-1}) dipped through the monolayer interface and into the bulk buffer (point f). The frequency at point f is different than the frequency at points b and d. The difference in resonance frequency in the buffered subphase between points f and b (or d) is approximately 12 Hz. For a quartz crystal oscillating at 5 MHz, this

closely corresponds to DMPM monolayer coverage (see below). Similarly, when the QCM is drawn back into air (point g), the frequency change with respect to an uncoated QCM *in air* is about 22 Hz, indicating that the QCM is coated with a bilayer of DMPM.

Given the QCM surface area of 53.88 mm^2, a perfect monolayer of DMPM at 40 Å^2 molecule^{-1} corresponds to 140 ng. Using the Sauerbray eq. [110] for a 5 MHz oscillator:

$$\Delta F = (-2 F_o^2) / (A \sqrt{\rho_q \mu_q})$$
(B-1)

a 9.5 ng mass change corresponds to a frequency change of 1 Hz. For DMPM monolayers (140 ng), this means a ΔF of ~ 12 Hz. Fig. B.3 shows that the first layer induced a 12 Hz change, and the second layer yielded a 10 Hz change (total change of 22 Hz).

After preparing the L-B film and equilibrating the multilayer assembly to constant temperature, pancreatic PLA$_2$ (17 U) was introduced to the sample chamber. Following the QCM resonant frequency versus time yielded the data presented in Fig. B.3.
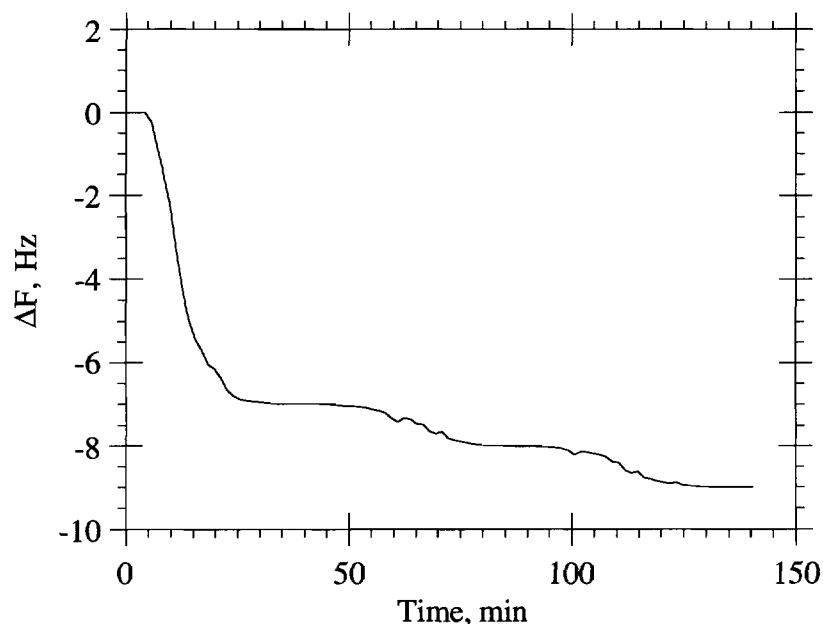

Fig. B.3 Quartz crystal microbalance frequency versus time. Pancreatic PLA$_2$ (17 U) was injected at t=10 min. Buffer: 0.5 mM CaCl$_2$.

An immediate decrease in frequency is apparent, corresponding to an increase in adsorbed PLA$_2$ (~ 85 ng). Control experiments were conducted to determine if this frequency

change was due to PLA$_2$ buffer (different from the buffer used to prepare the L-B films. Changes in resonance frequency in this case were nil, suggesting that the decrease in frequency is due to PLA$_2$ adsorption to L-B films on the quartz crystal. Observed frequency changes during DPPE L-B film hydrolysis, as reported by Okahata [54], were not observed with PLA$_2$/DMPM multilayered systems. Data presented by Okahata initially showed a frequency decrease (PLA$_2$ adsorption) followed by a frequency increase (hydrolyzed L-B film dissolution). Quantitative analysis of solution-dissolved lipid reaction products showed that the dissolved reaction products closely corresponded to what would be expected based on totally hydrolyzed DPPE L-B films. Alternatively, the frequency changes reported by Okahata could be explained by other processes that also affect QCM resonant frequency (in addition to mass changes). The "sharpness" of the shear plane parallel to the oscillating surface effects QCM frequencies. Viscosities of adsorbed layers alone affect resonant frequencies. It may be possible that PLA$_2$ alters the shear plane by contributing to the microviscosity in the vicinity of the multilayered surface. A more complete analysis of the situation would include an impedance analysis as suggested by Ward and Buttry [109].

Finally, a control experiment consisting of PLA$_2$ adsorption to hydrophobized QCM surfaces in the absence of L-B films resulted in large amounts of PLA$_2$ adsorption (Fig. B.4).
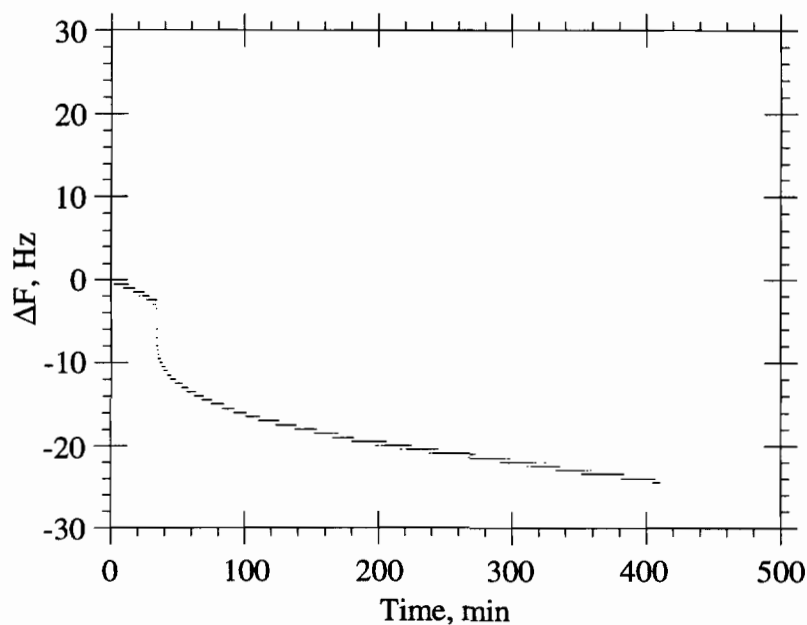

Fig. B.4 PLA$_2$ adsorption to silicone hydrophobized quartz crystal microbalance.

This control experiment shows that if any defects are present in the L-B assembly allowing PLA_2 to adsorb to the hydrophobized QCM surface, significant enzyme adsorption is likely. Unfortunately, this increase was larger than observed for PLA_2 adsorption to lipid-coated interfaces. One way around this problem is to hydrophobize the QCM surface with self-assembling alkylthiols (SAMs). Silicone treatment of quartz is not suitable for high quality control. Though SAMs cannot be easily removed (harsh oxidation conditions; "pirhanna" solution), they at least provide a well-characterized surface on which to build L-B films.

In summary, a QCM was used to monitor L-B film formation and was deemed successful in this regard, consistent with several accounts [52-55]. Detecting PLA_2 activity towards multilayered DMPM assemblies was found difficult due to the irreproducibility of L-B film preparation. Reproducible enzyme binding and hydrolysis is only possible with well-characterized L-B multilayers. It is proposed that future work in this area be conducted on QCM surfaces that are hydrophobized using self-assembled alkylthiols (or other suitable SAM-forming thiols) instead of silicone-treated QCM's, since PLA_2 appeared to adsorb to silicone surfaces to a larger extent than to L-B films of phospholipid substrates.

BIOGRAPHICAL SKETCH

Kevin M. Maloney was born in Manchester, NH, in 1968. He attended Worcester Polytechnic Institute in Worcester, MA, and in 1990 earned a Bachelor of Science degree in chemistry with a focus in physical chemistry. After four years in the Department of Chemistry, Biochemistry, and Molecular Biology of the Oregon Graduate Institute of Science & Technology, he received his Ph.D. in chemistry. Following graduation from OGI, Kevin moved to Southern California where he is a Research Fellow in Chemical Engineering at the California Institute of Technology in Pasadena. His research interests include protein self-assembly, membrane chemistry and membrane-related technologies.

Kevin participated in the National Science Foundation's Summer Institute in Japan, June–August 1993, at the Institute of Physical and Chemical Research (RIKEN), Japan. For academic achievements and community involvement, Kevin co-received OGI's first annual Student Achievement Award in May, 1994.

List of Publications:

Maloney, K. M., Korcakova, B., Grainger, D. W., Schief, W., Vogel, V. and Hall, S.B. Structured Domains In Interfacial Films Of Pulmonary Surfactant. Manuscript in preparation for submission to *Biophys. J.*

Maloney, K. M., Grandbois, M., Salesse, C. and Grainger, D. W. (1994) Phospholipase A_2 Hydrolysis of Asymmetric Phospholipid Monolayers at the Air–Water Interface. Accepted for publication in *Biochim. Biophys. Acta.*

Maloney, K. M., Grandbois, M., Salesse, C., Grainger, D. W. and Reichert, A. Phospholipase A_2 interactions with model monolayer membranes In *Proteins at Interfaces* (Horbett, T. and Brash, J., Eds.), ACS Symposium Series. Accepted for publication, February, 1995.

Maloney, K. M. and Grainger, D. W. (1993) Phase-separated anionic domains in ternary mixed lipid monolayers at the air–water interface. *Chem. Phys. Lipids* 65, 31–42.

112

Maloney, K. M. and Grainger, D. W. Biopolymer–Thin Film Interactions, *MRS Symp. Proc.* 292, 175–180, 1993.

Grainger, D. W., Maloney, K. M., Huang, X., Ahlers, M., Ringsdorf, H., Salesse, C., Herron, J. D., Hlady, V., and Lim, K. (1991) Binding, Interaction, and Organization of Proteins with Lipid Model Membranes In *Progress in Membrane Biotechnology* (Gomez–Fernandez, J. C., Chapman, D., and Parker, L., Eds.); Birkhauser Verlag, Basel, pp 64–82.